ANALYTICAL SOLUTIONS OF STEADY-STATE HEAT CONDUCTION IN MULTI-LAYER STACK PACKAGING

by

SAEED GHALAMBOR

Presented to the Faculty of the Graduate School of

The University of Texas at Arlington in Partial Fulfillment

of the Requirements

for the Degree of

DOCTOR OF PHILOSOPHY

THE UNIVERSITY OF TEXAS AT ARLINGTON

August 2014

Acknowledgements

I would like to thank my committee chair Professor Agonafer, for his patience and time, not to mention his continual support during the entire course of this dissertation. I specially would like to thank committee co-chair Professor Haji-Sheikh for his continuous guidance and persistent help in this dissertation. I would also like to express my gratitude to the committee members, Professor Lawrence, Professor Nomura, and Professor Celik Butler for their invaluable time and support. Thank you all for your support in this research.

August 1, 2014

Abstract

ANALYTICAL SOLUTIONS OF STEADY-STATE HEAT CONDUCTION

IN MULTI-LAYER STACK PACKAGING

Saeed Ghalambor, PhD

The University of Texas at Arlington, 2014

Supervising Professor: Dereje Agonafer

Analytical models that can be utilized in modeling the steady-state temperature solutions of planar and 3D packaged integrated circuits are discussed. This mathematically-driven model will include solutions for uniform and non-uniform footprint die stack systems as well as planar flip chip packages. These analytically obtained temperature solutions will include the contribution of thermal resistance for both cases as well as perfect contact scenarios. The acquired solution will accommodate any kind of boundary conditions (first, second and third kind) on the top and bottom surfaces of the stack system with the sides being adiabatic. Furthermore, the algorithm developed will consider volumetric heat generation as well as heat source at any cross section within the model.

Finally, the diffusion equation for heterogeneous layers is solved using the Galerkin-based integral approach. The latest development pertains to the analytical solutions of the steady-state heat conduction in stacked dies of an electronic chipset with or without TSV (Through Silicon Via) technology. TSVs are used as interconnections between different dies in vertical layers. Furthermore, the effect of thermal conductance between the constituents of the layers is considered.

Table of Contents

List of Tables

List of Illustrations

Nomenclature

a, b	dimensions of body 1
c, d	dimensions of body 2
[A]	vector of A_m coefficients
A_{mn}	unknown coefficients
Bi	Biot number hc/k_2
B_{mn}	constants in Fourier series
C_{mn}	constants in Fourier series
D_{mn}	constants in Fourier series
j	index
k_j	thermal conductivity in Layer j, $W/m \cdot K$
m, n	indices
q_0	heat flux at y=0, W/m^2
q_w	input heat flux, W/m^2
R	contact resistance, $m^2 K/W$
T_0	temperature at y=0, K
T_j	temperature in Layer j, K
x, y, z	coordinates in Layer 1, m

Greek

β_{mn}	elements of matrix |B| and vector $\|B_0\|$
|B|	matrix having β_{mn} elements
$\|B_0\|$	vector of β_{m0} coefficients

γ_{mn}	eigenvalues
η	coordinate parallel to y-direction, in Layer 2
ξ	coordinate parallel to x-direction, in Layer 2
ζ	coordinate parallel to z-direction, in Layer 2
ε	spacing between y and η axes in Figure 4-1
η	coordinate parallel to y-direction
θ_j	physical temperature, K
θ_∞	temperature of surroundings, K
ξ	coordinate parallel to x-direction
ω	relaxation factor
μ	micro, unit length
θ	auxiliary temperature
$\emptyset$	boundary function
ψ	vector matrix
ϕ	potential function

Subscripts

w	wall condition at $y=b$
a, b	dimensions
A_n,	constants in Fourier series
Bi	Biot number hc/k_2
B_n C_n,	constants in Fourier series
k_j	thermal conductivity in Layer j, $W/m \cdot K$
m, n	indices

q_0	heat flux at y=0, W/m^2
q_w	input wall heat flux, W/m^2
T_0	reduced temperature at y=0, C
T_j	reduced temperature in Layer j, c
x, y, z	coordinates, m
V	volume, m^3
C	thermal contact conductance W/m^2K
a_{ij}	elements of matrix A
b_{ij}	element of matrix B
c_P	specific heat $kJ/kg.K$
d_n	coefficients
f_j	basis functions
H	auxiliary function
L	thickness
T	temperature
U	conductance function
R	thermal resistance m^2K/W
w	wall condition at $y=b$
i, j, k, l, n, m, o, p	indices
m	main domain
e	inclusion domain

Chapter 1

Introduction

The semiconductor industry has consistently followed a trajectory of miniaturization that enables design engineers to achieve greater levels of innovation in the same or smaller dies. This trajectory has also allowed them to use less real estate by stacking the dies vertically. With this architectural achievement come challenges such as cooling, as the devices must operate under specified junction temperatures. Therefore, the thermal behavior of 3D stack packaging has recently become the center of attention in the electronics industry. The accumulation of excessive heat within the stack is a challenge that has caused thermal engineers to focus on the issue of extracting this heat from the system. Thus, one important aspect of design is the ability to obtain a robust analytical temperature solution of the multi-layer stack packages beforehand in order to sustain the reliability of the 3D stack packages. This study addresses the analytical formulation and governing equations that pertain to such systems by developing a Mathematica code to obtain analytical solutions of temperature distribution in multi-layer bodies.

Small, high-speed, and multi-functional computers and other electronic devices have been enabled by high integration technologies that have come to reality by the miniaturization through the process of scaling which uses a very fine pattern. However, an upper limit in the progress of such miniaturization has come into sight. The process of miniaturization will be technologically limited due to the increase of leak current which generates heat in transistors, and signal delay time caused by wiring. 3D packaging technology is one of the technologies expected to make a breakthrough such miniaturization on a 2D surface, which will enable high density integration that does not

depend on miniaturization on 2D surfaces. By stacking chips vertically, which would conventionally be set out on a plane, it will be possible to produce components with the same functionality as that of the components produced by conventional methods, but with a smaller footprint. A key 3D key technology is electrical packaging technology, which means that it is vital to connect the stacked chips electrically. Conventional 3D packaging technology uses wire bonding with fine metal lead wires. Recently, novel technologies have been developed to replace wire bonding. For example, wireless connection for data communication, which will reduce the space needed for wiring, has been proposed [1-4]. Another example is through-silicon via packaging technology [5-7] (hereinafter, referred to as TSV technology), which uses through-holes in silicon substrate for electrical connection. By using TSVs, it is possible to save the space that would be necessary for bonding wires and to make wiring lengths shorter. TSV technology is moving further ahead of other novel 3D packaging technologies mentioned above towards the production of commercially viable components [8, 9].

In this research the mathematical modeling for both technologies are discussed.

One major concern about 3D packaging is the thermal design. As the chips are being stacked on top of one another, overall stack package will have highly non-uniform heat distribution with higher heat density per foot print. Therefore, one must find ways to minimize the thermal resistance from electronic device junction to the ambient air. One way to reduce R_{ja} is to reduce R_{cs}, the contact resistance between the electronic device case and the ambient-cooled, finned heat sinks or the liquid-cooled cold plates. Several factors impact R_{cs}, including surface flatness, surface roughness, contact force or clamping pressure, surface cleanliness, and interface materials. Many technologies and techniques can optimize the thermal path from the electronic device junction to the heat sink. It is important to minimize the thermal resistance to maintain the electronic device

temperature below its maximum rated value and increase the end product reliability. Therefore, the inclusion of thermal contact resistance in the calculation of temperature fields becomes crucial. In the first chapter of this research, consideration is given to the derivation and development of steady-state heat conduction solutions in multi-layer bodies with uniform footprint. The study will reveal the effect of different boundary conditions on the top or bottom surfaces of the multi-layer stack, and changes required to obtain the temperature solutions in each case is discussed accordingly.

Chapter 3 will include the effect of thermal resistance in the existing solution obtained in chapter 2.

In chapter 4 and 5 the consideration is given to a multi-layer stack package consisting of two different footprints.

The solutions for steady-state heat conduction of non-uniform footprint will be solved using classical approach (Chapter 4) and by means of an iterative inverse methodology (Chapter 5).

Finally, Chapter 5 will consider the determination of steady-state heat conduction in heterogeneous material which does not possess closed- form solutions. Chapter 5 is dedicated to the TSV technology mentioned earlier with appearance of through silicon vias into the silicon dies. The latter study includes the Galerkin-based integral techniques to obtain solutions of steady-state heat conduction and consequently, will lead to determination of effective thermal conductivity in a Silicon-Copper die layer.

This study complements work on transient conduction in multi-dimensional layered materials by Haji-Sheikh and Beck [10]. One-dimensional orthogonal solutions of composite medium were presented in [11] that described the generalized Sturn-Liouville procedure for composite and anisotropic domain in transient heat conduction problems.

Various mathematical details are in [12,13]. Dowding et al. [14] presented a mixture of experimental and numerical study of a two-dimensional, two-layer solution with prescribed heat flux over all surfaces. Computation of temperature solution in multi-layer stack packages exhibits many features that are not common when computing the temperature solutions in homogeneous material due to a mixture of real and imaginary eigenvalues. Steady-state solutions complement transient solution, however in some cases transient solutions can enhance the accuracy of steady-state solutions [15-17]. This study modifies the existing solutions of steady-state heat conduction in two-layer bodies [18]. Then, extends the solutions to N-layer for electronic applications and include the effect of thermal conductance to the existing solutions. Also, the study further investigates the solutions for non-uniform die footprints [19]. Study conducted by A. Kaisare et al. [20] uses an iteration technique to obtain the temperature solutions to a non-uniform footprint system by guessing the heat flux at the interface of the two –layer stack. However, in this research the procedure takes the prescribed heat flux and solves the temperature solutions for each layer using inverse techniques and classical series solution. There are also numerous publications on multi-layer bodies such as M.M. Yovanovich [21] in 1980 that uses finite difference approach and matrices to obtain temperature solutions in multi-layer bodies. The procedure of aforementioned method will lead to inversion of large matrices and is very CPU intensive compared to the methodologies used in this research which is mostly integral-based and closed-form solutions.

Many engineering systems often include heterogeneous materials such as composite parts, integrated electronics packages, and other solid bodies with inclusions of secondary materials. The secondary material can be a fiber, solder ball, or a layer of a different material such as TSVs (Through silicon Via) in electronic packaging.

Zuzovski and Brenner [22] compared the work of Rayleigh and Maxwell for computation of effective thermal conductivity in an infinite domain with periodically arranged spheres. Sangani and Acrivos [23] modified the method of Zuzovski and Brenner to solve for effective thermal conductivity of a periodic array with inline and staggered arrangement of spheres also in an infinite domain. An accurate computation of temperature in a three-dimensional heterogeneous region is generally time consuming and cumbersome. For this reason, it is common practice to select average thermophysical properties to predict temperature and heat flux in heterogeneous bodies. Various properties of the medium are needed to determine the thermal conductivity of a heterogeneous medium; these include the statistical distribution of constituents, volume fraction, and the microstructure characteristics such as orientation, size, and connectivity of individual constituents [24][. Since it is difficult to take into account all available information, the common theoretical approach is to define lower and upper bounds for effective properties [25]. An extensive survey related to average properties is given by Hashin [26]. A study done by Y.M. Lee in 1994 describes the effect of elliptical inclusion in a matrix domain for determination of thermal conductivity in multidimensional bodies [27]. In this research the effect of cylindrical inclusion (TSVs) into the matrix (Silicon die) is considered and the effective thermal conductivity was computed for the composite layer.

Furthermore, the contribution of thermal heat conductance between the constituents was considered.

Chapter 2

Mathematical Formulations and Solution Procedure for Thermal Conduction in Multi-Layer Stack Packages with Uniform Footprint

The study of steady-state temperature solution in a stack of multi-layered orthotropic bodies with uniform profiles is the subject of this chapter. A stacked system is a body with layers of different materials as shown in Figure 2-1. The exact series solution of temperature fields in three multi-dimensional regions receives primary consideration. The mathematical formulation in this chapter does not include the contribution of thermal contact resistance at the interface between layers. The contribution and addition of thermal resistance into the current derivation will be discussed in detail in chapter 3.

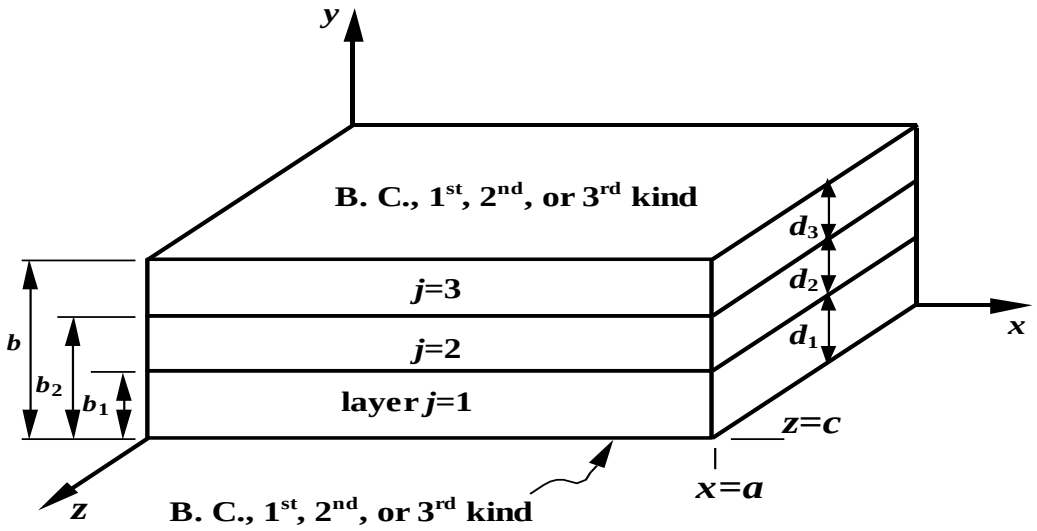

Figure 2-1 Schematic of a multi-layer body.

2.1 Steady State Energy Equation

The steady state energy equation for orthotropic layer *j* within a stack of many layers is

$$k_{x,j}\frac{\partial^2 T_j}{\partial x^2}+k_{y,j}\frac{\partial^2 T_j}{\partial y^2}+k_{z,j}\frac{\partial^2 T_j}{\partial z^2}=0,\ \text{in Region } j \qquad (2\text{-}1)$$

For $j=1, 2, \cdots, N$

subject to the boundary conditions to be specified. The solution for layer *j* using the method of separation of variables has the form

$$T_j(x,y,z)=X_j(x)Y_j(y)Z_j(z),\ \text{in Region } j \qquad (2\text{-}2)$$

For $j=1, 2, \cdots, N$

To satisfy the compatibility condition at each interface between adjacent layers *j* and *j*+1, it is required to have $X_j=X_{j+1}$ and $Z_j=Z_{j+1}$. After substitution of T_j from Eq. (2-2) in Eq. (2-1), the result is

$$k_{x,j}\frac{X_j''}{X_j}+k_{y,j}\frac{Y_j''}{Y_j}+k_{z,j}\frac{Z_j''}{Z_j}=0,\ \text{in Region } j \qquad (2\text{-}3)$$

For $j=1, 2, \cdots, N$

Preliminary consideration is given to the case of having a non-homogeneous boundary condition to be located over an outer surface perpendicular to the *y*-axis. Two cases of having the non-homogeneous boundary condition over *y*=0 surface and y=b surface are presented separately.

2.2 Non-Homogeneous Boundary Condition Over *y*=0 Surface.

It is possible to have boundary conditions of the first, second, or third kind over a surface perpendicular to the *y*-axis. However, only the boundary conditions of the first or second kinds are considered for *x*- and *z*-directions. Accordingly, the functions X_j and Z_j, as given in Eq. (2-2), must satisfy the conditions:

$$X_1''/X_1=X_2''/X_2=\cdots=X_N''/X_N=X''/X=-\beta^2 \qquad (2\text{-}4a)$$

$$Z_1''/Z_1 = Z_2''/Z_2 = \cdots = Z_N''/Z_N = Z''/Z = -\nu^2 \tag{2-4b}$$

where β and ν, are eigenvalues for homogeneous boundary conditions in *x* and *z* directions, respectively. For specified eigenvalues β_m and ν_n, the solutions for X_m and Z_n functions are

$$X_m = D_1 \cos(\beta_m x) + D_2 \sin(\beta_m x) \tag{2-5a}$$

$$Z_n = E_1 \cos(\nu_n z) + E_2 \sin(\nu_n z) \tag{2-5b}$$

and they are to remain the same for all layers.

A differential equation for Y_j is obtainable after substitution for $X''/X = X_m''/X_m = -\beta_m^2$ and $Z''/Z = Z_n''/Z_n = -\nu_n^2$ in Eq. (2-3) to get,

$$-k_{x,j}\beta_m^2 + k_{y,j}Y_j''/Y_j - k_{z,j}\nu_n^2 = 0 \tag{2-6}$$

that becomes

$$\frac{Y_j''}{Y_j} = \frac{k_{x,j}}{k_{y,j}}\beta_m^2 + \frac{k_{z,j}}{k_{y,j}}\nu_n^2 = \gamma_{j,mn}^2 \tag{2-7}$$

It is to be noted that for steady state conduction in isotropic layers $\gamma_{j,mn} = \gamma_{mn}$, remains the same for all layers. For this case, the homogeneous boundary condition is located at $z = b_N = b$ and the appropriate solution form of Y_j, as given in [12] and in [18], for a specified β_m and ν_n, is

$$Y_{j,mn} = A_{j,mn}\cosh[\gamma_{j,mn}(b_j - y)] + B_{j,mn}\sinh[\gamma_{j,mn}(b_j - y)] \tag{2-8}$$

This would provide temperature solutions with the forms

$$T_j = \sum_{m=1}^{\infty}\sum_{n=1}^{\infty} C_{mn}\{A_{j,mn}\cosh[\gamma_{j,mn}(b_j - y)] + B_{j,mn}\sinh[\gamma_{j,mn}(b_j - y)]\}X_m(x)Z_n(z) \text{ for } j = 1, 2, \cdots, N \quad (2\text{-}9)$$

This solution form presented for T_j leads to a relatively simple method for finding the coefficients $A_{j,mn}$ and $B_{j,mn}$. Having the homogeneous boundary condition located at $z = b_N = b$, the functional form of temperature for the layer *j=N* is

$$T_N = \sum_{m=1}^{\infty}\sum_{n=1}^{\infty} C_{mn}\{A_{N,mn}\cosh[\gamma_{N,mn}(b - y)] + B_{N,mn}\sinh[\gamma_{N,mn}(b - y)]X_m(x)Z_n(z)\} \quad (2\text{-}10)$$

wherein $A_{N,mn} = 0$ and $B_{N,mn} = 1$ for the boundary condition of the first kind while $A_{N,mn} = 1$ and $B_{N,mn} = 0$ for the boundary condition of the second kind. For the boundary condition of the third kind, the condition $-k_{y,N}(\partial Y_{N,mn}/\partial y) = hY_{N,mn}$ at $y = b$, after arbitrarily setting $A_{N,mn} = 1$, produces $B_{N,mn} = h/(\gamma_N k_{y,N})$.

Next, the coefficients $A_{j,mn}$ and $B_{j,mn}$ for other layers, also become deterministic once these parameter are known for the neighboring (*j*+1)th layer. Accordingly, the compatibility condition for heat flux

$$k_{y,j}\partial T_j/\partial y\big|_{y=b_j} = k_{y,j+1}\partial T_{j+1}/\partial y\big|_{y=b_j}, \quad (2\text{-}11a)$$

at the interface between layer *j* and the layer *j*+1, produces the coefficient

$$B_{j,mn} = \frac{\gamma_{j+1,mn}k_{y,j+1}}{\gamma_{j,mn}k_{y,j}}\left[A_{j+1,mn}\sinh(\gamma_{j+1,mn}d_{j+1}) + B_{j+1,mn}\cosh(\gamma_{j+1,mn}d_{j+1})\right] \quad (2\text{-}11b)$$

where d_{j+1} is the thickness of the layer *j*+1, as shown in Figure 2-1. The other compatibility condition

$$-k_{y,j}\partial T_j/\partial y\big|_{y=b_j} = (T_j - T_{j+1})\big|_{y=b_j}/R_j \tag{2-12a}$$

provides the coefficient

$$\begin{aligned} A_{j,mn} = {} & A_{j+1,mn}\left[\cosh(\gamma_{j+1,mn}d_{j+1}) + \gamma_{j+1,mn}R_j k_{y,j+1}\sinh(\gamma_{j+1,mn}d_{j+1})\right] \\ & + B_{j+1,mn}\left[\sinh(\gamma_{j+1,mn}d_{j+1}) + \gamma_{j+1,mn}R_j k_{y,j+1}\cosh(\gamma_{j+1,mn}d_{j+1})\right] \end{aligned} \tag{2-12b}$$

where R_j is the contact resistance between the layer *j* and the layer *j*+1; it assumes a zero value if these two bodies are in perfect contact. Beginning with layer *N*, these two recursive relations produce the values of $A_{j,mn}$ and $B_{j,mn}$ within the temperature solution T_j, as given by Eq. (2-9), in a descending order for all layers.

The remaining unknown is the coefficient C_{mn} to be determined from the non-homogeneous boundary condition at *y*=0. As an illustration, for a boundary condition of the first kind, when $T_1 = f(x,z)$ at *y*=0, Eq. (2-9) leads to the relation

$$f(x,z) = \sum_{m=1}^{\infty}\sum_{n=1}^{\infty} C_{mn}\left[A_{1,mn}\cosh(\gamma_{1,mn}b_1) + B_{1,mn}\sinh(\gamma_{1,mn}b_1)\right]X_m(x)Z_n(z) \tag{2-13}$$

and then the orthogonality conditions in *x*- and *z*-directions produce

$$C_{mn} = \frac{\int_{z=0}^{c}\int_{x=0}^{a} f(x,z)X_m(x)Z_n(z)dxdz}{\left[A_{1,mn}\cosh(\gamma_{1,mn}d_1) + B_{1,mn}\sinh(\gamma_{1,mn}d_1)\right]N_{x,m}N_{z,n}} \tag{2-14a}$$

where

$$N_{x,m} = \int_{x=0}^{a} [X_m(x)]^2 dx \tag{2-14b}$$

and

$$N_{z,n} = \int_{z=0}^{c} [Z_n(x)]^2 dx \tag{2-14c}$$

Some modifications are needed when $\beta_1 = \nu_1 = 0$ that would make $\gamma_{1,1} = 0$. For this special case, the modified functional forms of Y_j are obtainable beginning with

$$T_N = C_{00}[A_{N,00} + B_{N,00}(1 - y/b)] \tag{2-15}$$

As before, $A_{N,00} = 0$ and $B_{N,00} = 1$ for the boundary condition of the first kind, $A_{N,00} = 1$ and $B_{N,mn} = 0$ for the boundary condition of the second kind, while $A_{N,mn} = 1$ and $B_{N,00} = hb/k_{y,N}$, for the boundary condition of the third kind. Further discussions related to this special case are within the next numerical example.

2.3 Non-Homogeneous Condition Over *y*=*b* Surface

Minor modifications of the previous case are needed when the homogeneous boundary condition is located at *y*=0 and the non-homogeneous boundary condition is located at $y = b$. For this case, Eq. (2-9) takes the form

$$T_j = \sum_{m=1}^{\infty} \sum_{n=1}^{\infty} C_{mn} \{A_{j,mn} \cosh[\gamma_{j,mn}(y - b_{j-1})] + B_{j,mn} \sinh[\gamma_{j,mn}(y - b_{j-1})] X_m(x) Z_n(z)\} \tag{2-16}$$

While the homogeneous boundary condition at $y = b_0 = 0$ produces the functional form of temperature for layer 1 as

$$T_1 = \sum_{m=1}^{\infty} \sum_{n=1}^{\infty} C_{mn}\left[A_{1,mn}\cosh(\gamma_{1,mn}y) + B_{1,mn}\sinh(\gamma_{1,mn}y)\right]X_m(x)Z_n(z) \tag{2-17}$$

since $b_0 = 0$. Then, the values of coefficients $A_{j,mn}$ and $B_{j,mn}$ are obtainable in ascending order from the modified forms of Eq. (2-11b) and Eq. (2-12b) as

$$B_{j+1,mn} = \frac{\gamma_{j,mn}k_{y,j}}{\gamma_{j+1,mn}k_{y,j+1}}\left[A_{j,mn}\sinh(\gamma_{j,mn}d_j) + B_{j,mn}\cosh(\gamma_{j,mn}d_j)\right] \tag{2-18a}$$

and

$$\begin{aligned} A_{j+1,mn} = {} & A_{j,mn}\left[\cosh(\gamma_{j,mn}d_j) + \gamma_{j,mn}R_j k_{y,j}\sinh(\gamma_{j,mn}d_j)\right] \\ & + B_{j,mn}\left[\sinh(\gamma_{j,mn}d_j) + \gamma_{j,mn}R_j k_{y,j}\cosh(\gamma_{j,mn}d_j)\right] \end{aligned} \tag{2-18b}$$

The forms of coefficients $A_{j,mn}$ and $B_{j,mn}$ within function $Y_{j,mn}$, for *j*=1 and 2, and for insertion into

$$Y_1 = A_{1,mn}\cosh(\gamma_{1,mn}y) + B_{1,mn}\sinh(\gamma_{1,mn}y)$$

$$Y_2 = A_{2,mn}\cosh[\gamma_{2,mn}(y-b_1)] + B_{2,mn}\sinh[\gamma_{j,mn}(y-b_{j-1})],$$

are in Table 1. Once the coefficients $A_{j,mn}$ and $B_{j,mn}$ for the layer *N* are known, the coefficient C_{mn} can be determined from the non-homogeneous boundary condition at *y=b*. As an illustration, for a boundary condition of the first kind, $T_1(x,b,z) = f(x,z)$ at *y=b* and then the coefficient C_{mn} becomes

$$C_{mn} = \frac{\int_{z=0}^{c}\int_{x=0}^{a} f(x,z)X_m(x)Z_n(z)dxdz}{\left[A_{N,mn}\cosh(\gamma_{N,mn}d_N) + B_{N,mn}\sinh(\gamma_{N,mn}d_N)\right]N_m N_n} \tag{2-19}$$

for insertion in Eq. (2-16).

Numerical Example.

Consideration is given to a body, for which $a = 2,\ b = 3,\ c = 2$, while having three isotropic layers with $b_1 = b_2 = b_3 = 1,\ k_j = k_{x.j} = k_{y,j} = k_{z.j},\ k_1 = 1,\ k_2 = 2,$ and $k_3 = 5$, as shown in Figure 2-1. The boundaries at $x = 0$, $x = a$, $z = 0$, and $z = c$ are insulated while there is a zero temperature at $y = b$. Over the $y = 0$ surface, there is a surface heat flux q_1 within the areas. Next, the aforementioned procedures were used for determination of temperature field.

Solution: For boundary conditions of the second kind, the eigenvalues are $\beta_m = (m-1)\pi / a$ with $m = 1, 2, \cdots$ and $\nu_n = (n-1)\pi / c$ with $n = 1, 2,$ while the corresponding eigenfunctions are $X_m(x) = \cos[(m-1)\pi x / a]$ and $Z_n(z) = \cos[(n-1)\pi z / c]$. For each isotropic layer, $k_{x,j} = k_{y,j} = k_{z,j} = k_j$ and this causes Eq. (2-7) to become

$$\frac{Y_j''}{Y_j} = \beta_m^2 + \nu_n^2 = \gamma_{mn}^2 \tag{2-20a}$$

while Eq. (2-10) reduces to

$$T_3 = \sum_{m=1}^{\infty} \sum_{m=1}^{\infty} C_{mn} \sinh[\gamma_{mn}(b-y)] X_m(x) Z_n(z) \tag{2-20b}$$

since $A_{3,mn} = 0$ and $B_{3,mn} = 1$. In the presence of perfect contact between the layers, Eq. (2-11b) and Eq. (2-12b) provide the constants $A_{2,mn} = \sinh(\gamma_{mn} d_3)$ and $B_{2,mn} = (k_3 / k_2)\cosh(\gamma_{mn} d_3)$, which makes

$$T_2 = \sum_{m=1}^{\infty} \sum_{m=1}^{\infty} C_{mn} \{\sinh(\gamma_{mn} d_3) \cosh[\gamma_{mn}(b_2 - y)] + (k_3 / k_2) \cosh(\gamma_{mn} d_3) \sinh[\gamma_{mn}(b_2 - y)]\} X_m(x) Z_n(z) \quad \text{(2-20c)}$$

Next, when *j*=1, Eq. (2-11b) yields

$$A_{1,mn} = \sinh(\gamma_{mn} d_3) \cosh(\gamma_{mn} d_2) + (k_3 / k_2) \cosh(\gamma_{mn} d_3) \sinh(\gamma_{mn} d_2)$$

and Eq. (2-12b) yields

$$B_{1,mn} = (k_2 / k_1)[\sinh(\gamma_{mn} d_3) \sinh(\gamma_{mn} d_2) + (k_3 / k_2) \cosh(\gamma_{mn} d_3) \cosh(\gamma_{mn} d_2)]$$

for insertion in equation

$$T_1 = \sum_{m=1}^{\infty} \sum_{m=1}^{\infty} C_{mn} \{A_{1,mn} \cosh[\gamma_{mn}(b_1 - y)] + B_{1,mn} \sinh[\gamma_{mn}(b_1 - y)]\} X_m(x) Z_n(z) \quad \text{(2-20d)}$$

Since $B_{N,mn}$ was selected arbitrarily, one can replace it to become

$1/\cosh(\gamma_{mn} d_3)$ for numerical determination of temperature. This would replace C_{mn} to become $C_{mn} / \cosh(\gamma_{mn} d_3)$ and the replaced forms of the temperature solutions are:

$$T_3 = \sum_{m=1}^{\infty} \sum_{n=1}^{\infty} C_{mn} \frac{\sinh[\gamma_{mn}(b - y)]}{\cosh(\gamma_{mn} d_3)} X_m(x) Z_n(z), \quad \text{(2-21a)}$$

$$T_2 = \sum_{m=1}^{\infty} \sum_{n=1}^{\infty} C_{mn} \{\tanh(\gamma_{mn} d_3) \cosh[\gamma_{mn}(b_2 - y)] + (k_3 / k_2) \sinh[\gamma_{mn}(b_2 - y)]\} X_m(x) Z_n(z), \quad \text{(2-21b)}$$

while

$$A_{1,mn} = \tanh(\gamma_{mn} d_3) \cosh(\gamma_{mn} d_2) + (k_3 / k_2) \sinh(\gamma_{mn} d_2)$$

and

$$B_{1,mn} = (k_2 / k_1)[\tanh(\gamma_{mn} d_3)\sinh(\gamma_{mn} d_2) + (k_3 / k_2)\cosh(\gamma_{mn} d_2)].$$

for insertion in Eq. (2-20d). Finally, the coefficient C_{mn} is computed from the definition of input heat flux

$$\begin{aligned} q_1 &= -k_1\left(\frac{\partial T_1}{\partial y}\right)_{y=0} \\ &= \sum_{m=1}^{\infty}\sum_{n=1}^{\infty} C_{mn} k_1 \left\{A_{1,mn}\sinh(\gamma_{mn} b_1) + B_{1,mn}\cosh(\gamma_{mn} b_1)\right\}\gamma_{mn} X_m(x) Z_n(z) \end{aligned} \tag{2-22}$$

with $X_m(x) = \cos[(m-1)\pi x / a]$ and $Z_n(z) = \cos[(n-1)\pi z / c]$ whose orthogonality conditions provide

$$C_{mn} = \frac{\int_{z=0}^{c}\int_{x=0}^{a} q(x,z) X_m(x) Z_n(z) dx dz}{\gamma_{mn} k_1 \left[A_{1,mn}\sinh(\gamma_{mn} d_1) + B_{1,mn}\cosh(\gamma_{N,mn} d_1)\right] N_{x,m} N_{z,n}} \tag{2-23}$$

As stated earlier, when *m*=*n*=1, the above relations should be modified and they become

$$Y_{3,11} = A_{3,11} + B_{3,11}(b_3 - y) \text{ with } A_{3,11} = 0 \text{ and } B_{3,11} = 1,$$

$$Y_{2,11} = A_{2,11} + B_{2,11}(b_2 - y) \text{ with } A_{2,11} = b_3 - b_2 = d_3 \text{ and } B_{2,11} = k_3 / k_2$$

$$Y_{1,11} = A_{1,11} + B_{1,11}(b_1 - y) \text{ with } A_{1,11} = d_3 + d_2 k_3 / k_2 \text{ and } B_{1,11} = (k_3 / k_2)(k_2 / k_1)$$

It is to be noted that when the wall heat flux at y=0 is uniform, the temperature solution in region 1 takes the form

$$T_1 = C_{11}[d_3 + d_2 k_3 / k_2 + (k_3 / k_1)(b_1 - y)]$$

where $C_{11} = q / k_3$. When the heat flux has a uniform value within $0 \le x \le a_1 = 1$ and $0 \le z \le c_1 = 1$ while having a zero value elsewhere, the dimensionless surface

temperature $k_1T/(qd_1)$ values are computed and they are plotted in Figure 2-2. The solutions are numerically well behaved for practical applications. Clearly, when $a_1 = c_1 = 2$, the problem becomes one-dimensional and the computed value of dimensionless temperature at location $(0, 0, 0)$ using a single term is $k_1T(0,0,0)/(q_1b_1) = 1.7$. The series convergence characteristics suggest that more terms are needed as the problem becomes three-dimensional; e.g., when $y = 0$, more than 100 terms in each direction is needed to get five accurate digits. As a test case, for $a_1 = c_1 = 1.5$, 1.0, and 0.5, using 150 terms in *x*-direction and *z*-direction produced $k_1T(0,0,0)/(q_1b_1) = 1.30503$, 0.92787, and 0.50700 with error within the last digit, respectively. However, the error exponentially decays when *y*>0. For example, when $a_1 = c_1 = 1.5$, the computed dimensionless temperature is $k_1T(0,1,0)/(q_1b_1) = 0.072831194$, using 10 terms. The exact value of this temperature is 0.07283119526.

2.4 Volumetric Heat Source at Interior Locations

In this section, consideration is given to determination of temperature in a multi-layer body in the presence of volumetric heat source. The boundary conditions on all surfaces are homogeneous. The effect of non-homogeneous boundary conditions is in the earlier sections. The governing Poisson's equation in layer *j* is

$$k_{x,j}\frac{\partial^2 T_j}{\partial x^2} + k_{y,j}\frac{\partial^2 T_j}{\partial y^2} + k_{z,j}\frac{\partial^2 T_j}{\partial z^2} + g(x,y,z) = 0 \qquad (2\text{-}24)$$

where $g_j(x,y,z)$ describes the effect of a volumetric heat source in the layer *j*. The basic steps to acquire a solution are similar to those discussed earlier but with modifications presented below.

It is possible to propose a solution of the form

$$T_j = \sum_{m=1}^{\infty} \sum_{n=1}^{\infty} \sum_{p=1}^{\infty} C_{mn} X_m(x) Y_{j,p}(y) Z_n(z) \text{ for } j = 1, 2, \cdots, N \qquad (2\text{-}25)$$

where the functions $X_m(x)$, $X_m(x)$, $X_m(x)$ satisfy the differential equations

$$X''/X = -\beta^2 \qquad (2\text{-}26a)$$

$$Y_j''/Y_j = -\gamma^2 \qquad (2\text{-}26b)$$

$$Z''/Z = -\nu^2 \qquad (2\text{-}26c)$$

In this application, it is possible to select $\gamma_j = \gamma$ that remains the same in all layers. This makes the $Y_j(y)$ function have the same functional form as that in Eq. (2-26c), except $\gamma_j = \gamma$ for this application, unconditionally. This makes the $Y_j(y)$ function the same as that in an earlier section when all layers are isotropic. The functions $X(x)$ and $Z(z)$ remain the same as those presented in an earlier section, see Eqs. (2-5a,b). Next, the substitution of T_j from Eq. (2-24) into Eq. (2-25) produces the relation

$$\sum_{m=1}^{\infty} \sum_{n=1}^{\infty} \sum_{p=1}^{\infty} C_{mnp}(k_{x,j}\beta_m^2 + k_{y,j}\gamma_p^2 + k_{z,j}\nu^2) \times X_m(x) Y_{j,p}(y) Z_n(z) = g_j(x,y,z) \qquad (2\text{-}27)$$

The coefficient C_{mnp} is obtainable after application of the classical orthogonality conditions,

$$C_{mnp} = \frac{1}{N_{x,m} N_{y,p} N_{z,n}} \int_{x=0}^{a} \int_{z=0}^{c} \sum_{j=1}^{N} \int_{y=0}^{b_j} \frac{k_{y,j} g_j(x,y,z) X_m(\beta_m x) Y_{j,p}(\gamma_p y) Z_n(\nu_n z)}{(k_{x,j}\beta_m^2 + k_{y,j}\gamma_p^2 + k_{z,j}\nu^2)} dxdydz \tag{2-28a}$$

within

$$N_{y,mn} = \sum_{j=1}^{N} \int_{y=0}^{b_j} k_{y,j} [Y_{1,mn}(\gamma_{j,mn} y)]^2 dy \tag{2-28b}$$

while the other norms are obtainable using Eqs. (2-14b, c).

In proceeding chapters the numerical examples of this type are illustrated.

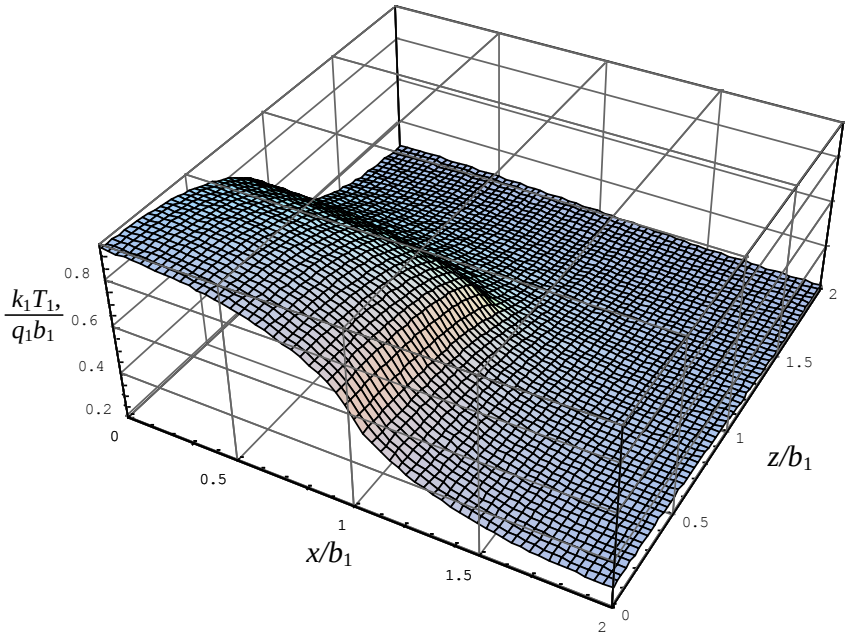

Figure 2-2 The surface temperature at $y = 0$ for example 1 when $a_1 = c_1 = 1$.

Chapter 3

Analytical Thermal Solution in Multi-layer Stack Package with Non-uniform Power Distribution and Contact Resistance

The use of one-dimensional orthogonal expansion for thermal conduction in composite media is described in [28]. A Sturm-Liouville procedure for solving transient heat conduction problems for composite and anisotropic domains is outlined in [29]. Various studies of transient conduction in multi-layer bodies are in [30-35]. This research work modifies the solution of steady-state conduction in two-layered bodies reported in [36] for electronic cooling applications. An iterative solution of temperature field in multi-layer bodies with different form factors is in [37, 38].

In this chapter, the mathematical procedures focus on studying steady-state temperature solutions in a stack of multi-layered isotropic and orthotropic bodies with uniform rectangular profiles. An important feature that is included in the model is a non-uniform power distribution. A stacked system is a body with many layers of different materials, as shown by the three layers in Fig. 3-1. The study primarily considers the exact series solution of a temperature field in a three multi-dimensional region. The mathematical formulation includes the contribution of thermal contact resistance at the interface between layers. This resistance vanishes in the presence of perfect thermal contact.

3.1 Governing Steady State Equations

The steady state equation selected for this study is the classical Poisson's equation, which becomes the Laplace equation in the absence of a volumetric heat source. We consider the solution of the energy equation in a stack of *N* layers. Then the governing equation for the orthotropic layer *j* within this multi-layer stack is

$$k_{x,j}\frac{\partial^2 T_j}{\partial x^2}+k_{y,j}\frac{\partial^2 T_j}{\partial y^2}+k_{z,j}\frac{\partial^2 T_j}{\partial z^2}+g_j = 0 \text{ in Region } j \qquad (3\text{-}1)$$

$$\text{For } j=1, 2, \cdots, N$$

where $T_j = T_j(x, y, z)$ is the temperature in layer *j* and $g_j = g_j(x, y, z)$ is the volumetric heat source. The solution for layer *j* using the method of separation of variables is

$$T_j(x, y, z) = X_j(x)Y_j(y)Z_j(z) \text{ in plate } j \qquad (3\text{-}2)$$

$$\text{for } j=1, 2, \cdots, N$$

For the first case, we select the non-homogeneous boundary condition over an outer surface perpendicular to the *y*-axis at *y* = 0. Additionally, we modify the acquired solution when the non-homogeneous boundary condition is located over the surface at *y* = *b*. These two solutions apply to the systems when the released power is over an external surface. In the presence of released energy within interior locations, we use Poisson's equation in a later section.

3.2 Non-Homogeneous Boundary Conditions

First, we select a specified non-homogeneous boundary condition over a surface normal to the *y*-axis at *y* = 0. An examination of the compatibility conditions between adjacent layers *j* and *j*+1leads to the required conditions of $X_j = X_{j+1}$ and $Z_j = Z_{j+1}$. Then, the substitution of T_j from Eq. (3-2) into Eq. (3-1) produces the relation

$$k_{x,j}\frac{X_j''}{X_j}+k_{y,j}\frac{Y_j''}{Y_j}+k_{z,j}\frac{Z_j''}{Z_j} = 0 \text{ in Region } j \qquad (3\text{-}3)$$

for $j=1, 2, \cdots, N$

As stated earlier, the plates cannot have the boundary condition of the third kind in the *x* and z directions. Accordingly, the functions X_j and Z_j, as given in Eq. (3-2), must satisfy the following conditions:

$$X_1''/X_1 = X_2''/X_2 = \cdots = X_N''/X_N = X''/X = -\beta^2 \tag{3-4a}$$

and

$$Z_1''/Z_1 = Z_2''/Z_2 = \cdots = Z_N''/Z_N = Z''/Z = -\nu^2 \tag{3-4b}$$

where β and ν are the eigenvalues and depend on the types of homogeneous boundary conditions in the *x* and *z* directions, respectively. Therefore, according to Eq. (3-4a) and Eq. (3-4b), for eigenvalues β_m and ν_n, the solutions for the functions X_m and Z_n are

$$X_m = D_1 \cos(\beta_m x) + D_2 \sin(\beta_m x) \tag{3-5a}$$

and

$$Z_n = E_1 \cos(\nu_n z) + E_2 \sin(\nu_n z) \tag{3-5b}$$

The solutions are to remain the same for all layers.

To obtain the functional form of $Y_j(y)$, we substitute

$X''/X = X_m''/X_m = -\beta_m^2$ and $Z''/Z = Z_n''/Z_n = -\nu_n^2$ into Eq. (3-3),which yields the relation

$$-k_{x,j}\beta_m^2 + k_{y,j}Y_j''/Y_j - k_{z,j}\nu_n^2 = 0 \tag{3-6}$$

This relation becomes

$$\frac{Y_j''}{Y_j} = \frac{k_{x,j}}{k_{y,j}}\beta_m^2 + \frac{k_{z,j}}{k_{y,j}}\nu_n^2 = \gamma_{j,mn}^2 \tag{3-7}$$

For the steady-state conduction in isotropic layers, $\gamma_{j,mn} = \gamma_{mn}$ is constant for all layers. With the homogeneous boundary condition located at $z = b_N = b$, the appropriate solution for the function Y_j, as given in [18], is

$$Y_{j,mn} = A_{j,mn}\cosh[\gamma_{j,mn}(b_j - y)] + B_{j,mn}\sinh[\gamma_{j,mn}(b_j - y)] \tag{3-8}$$

This produces the following temperature solutions:

$$\begin{aligned} T_j = \sum_{m=1}^{\infty}\sum_{n=1}^{\infty} C_{mn}\{&A_{j,mn}\cosh[\gamma_{j,mn}(b_j - y)] \\ &+ B_{j,mn}\sinh[\gamma_{j,mn}(b_j - y)]\}X_m(x)Z_n(z) \quad \text{for } j = 1, 2, \cdots, N \end{aligned} \tag{3-9}$$

This solution form presented for T_j eliminates the need for matrix inversions and leads to a relatively simple recursive method for finding the coefficients $A_{j,mn}$ and $B_{j,mn}$.

The next task is to develop a method for determining the coefficients $A_{j,mn}$ and $B_{j,mn}$. The functional form of the temperature solution for layer *j* = *N* at its homogeneous boundary condition, which is located at $z = b_N = b$, is

$$\begin{aligned} T_N = \sum_{m=1}^{\infty}\sum_{n=1}^{\infty} C_{mn}\{&A_{N,mn}\cosh[\gamma_{N,mn}(b - y)] \\ &+ B_{N,mn}\sinh[\gamma_{N,mn}(b - y)]X_m(x)Z_n(z)\} \end{aligned} \tag{3-10}$$

Clearly, this relation leads to the values of $A_{N,mn} = 0$ and $B_{N,mn} = 1$ for the boundary condition of the first kind and $A_{N,mn} = 1$ and $B_{N,mn} = 0$ for the boundary condition of the second kind. Additionally, the use of a homogeneous boundary condition

of the third kind leads to the relations $-k_{y,N}(\partial Y_{N,mn}/\partial y) = hY_{N,mn}$ at $y = b$. After arbitrarily setting $A_{N,mn} = 1$, it produces $B_{N,mn} = h/(\gamma_N k_{y,N})$. Once these two coefficients are determined, the coefficients $A_{j,mn}$ and $B_{j,mn}$ for the other layers become deterministic through recursive relations because these parameters are known for the neighboring layer of (*j*+1). Accordingly, the process begins by setting *j*+1 = *N*. The compatibility condition for heat flux is

$$k_{y,j}\partial T_j/\partial y\big|_{y=b_j} = k_{y,j+1}\partial T_{j+1}/\partial y\big|_{y=b_j} \tag{3-11a}$$

at the interface between layer *j* and layer *j*+1. After the substitution for temperature, it produces the coefficient $B_{j,mn}$ as

$$B_{j,mn} = \frac{\gamma_{j+1,mn}k_{y,j+1}}{\gamma_{j,mn}k_{y,j}}\left[A_{j+1,mn}\sinh(\gamma_{j+1,mn}d_{j+1}) + B_{j+1,mn}\cosh(\gamma_{j+1,mn}d_{j+1})\right] \tag{3-11b}$$

where d_{j+1} is the thickness of layer *j*+1, as shown in Figure 3-1. The other compatibility condition

$$-k_{y,j}\partial T_j/\partial y\big|_{y=b_j} = (T_j - T_{j+1})\big|_{y=b_j}/R_j \tag{3-12a}$$

provides the coefficient $A_{j,mn}$ as

$$\begin{aligned} A_{j,mn} = {} & A_{j+1,mn}\left[\cosh(\gamma_{j+1,mn}d_{j+1}) + \gamma_{j+1,mn}R_j k_{y,j+1}\sinh(\gamma_{j+1,mn}d_{j+1})\right] \\ & + B_{j+1,mn}\left[\sinh(\gamma_{j+1,mn}d_{j+1}) + \gamma_{j+1,mn}R_j k_{y,j+1}\cosh(\gamma_{j+1,mn}d_{j+1})\right] \end{aligned} \tag{3-12b}$$

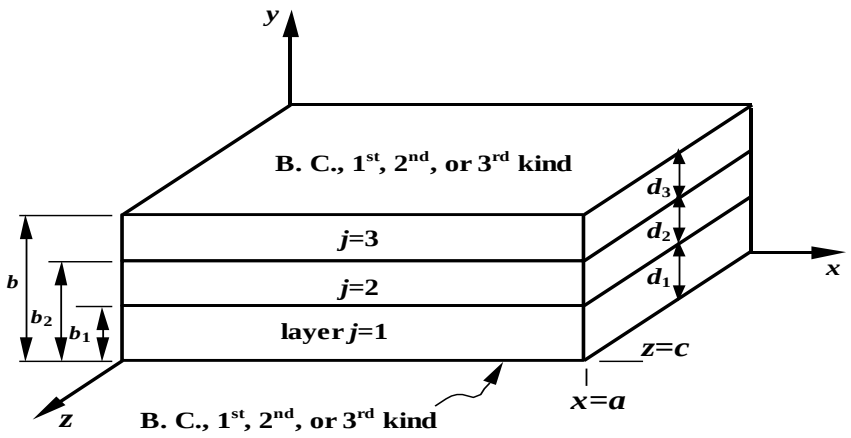

Figure 3-1 Schematic of a multi-layer body.

The parameter R_j in Eq. (3-12a) is the contact resistance between layer *j* and layer *j*+1.The parameter assumes a value of zero if these two layers are in perfect contact. Then the process of determining the coefficients $A_{j,mn}$ and $B_{j,mn}$ begins. When *j* = *N*-1.Eq. (3-12b), the recursive relations produce the value of $A_{j,mn}$, and Eq. (-11b) produces the value of $B_{j,mn}$in a descending order for all layers. Finally, the insertion of $A_{j,mn}$ and $B_{j,mn}$ into Eq. (3-9) provides the temperature solution T_j .

The remaining unknown in Eq. (3-9) is the coefficient C_{mn}, which is determined from the non-homogeneous boundary condition at *y* = 0. As an illustration, for a boundary condition of the first kind, when $T_1 = f(x,z)$ at *y* = 0, Eq. (3-9) leads to the relation

$$f(x,z) = \sum_{m=1}^{\infty}\sum_{n=1}^{\infty} C_{mn}\left[A_{1,mn}\cosh(\gamma_{1,mn}b_1) + B_{1,mn}\sinh(\gamma_{1,mn}b_1)\right]X_m(x)Z_n(z) \tag{3-13}$$

Then the orthogonality conditions in the *x*- and *z*-directions produce

$$C_{mn} = \frac{\int_{z=0}^{c}\int_{x=0}^{a} f(x,z)X_m(x)Z_n(z)dxdz}{\left[A_{1,mn}\cosh(\gamma_{1,mn}d_1)+ B_{1,mn}\sinh(\gamma_{1,mn}d_1)\right]N_{x,m}N_{z,n}} \quad \text{(3-14a)}$$

where

$$N_{x,m} = \int_{x=0}^{a} [X_m(x)]^2 dx \quad \text{(3-14b)}$$

and

$$N_{z,n} = \int_{z=0}^{c} [Z_n(x)]^2 dx \quad \text{(3-14c)}$$

In some applications, modifications become necessary when $\beta_1 = \nu_1 = 0$. For this condition, $\gamma_{1,mn} = \gamma_{1,11} = 0$, and a modified functional form of Y_j becomes

$$T_N = C_{00}[A_{N,00} + B_{N,00}(1 - y/b)] \quad \text{(3-15)}$$

As before, $A_{N,00} = 0$ and $B_{N,00} = 1$ for the boundary condition of the first kind, $A_{N,00} = 1$ and $B_{N,mn} = 0$ for the boundary condition of the second kind, and $A_{N,mn} = 1$ and $B_{N,00} = hb/k_{y,N}$ for the boundary condition of the third kind.

Minor modifications are needed when the homogeneous boundary condition is located at $y = 0$ while the non-homogeneous boundary condition is located at $y = b$. For this case, Eq. (3-9) takes the form

$$T_j = \sum_{m=1}^{\infty}\sum_{n=1}^{\infty} C_{mn}\{A_{j,mn}\cosh[\gamma_{j,mn}(y - b_{j-1})] + B_{j,mn}\sinh[\gamma_{j,mn}(y - b_{j-1})]X_m(x)Z_n(z)\} \quad \text{(3-16)}$$

and the homogeneous boundary condition at $y = b_0 = 0$ produces the functional form of temperature for layer 1 as

$$T_1 = \sum_{m=1}^{\infty} \sum_{n=1}^{\infty} C_{mn}\left[A_{1,mn}\cosh(\gamma_{1,mn}y) + B_{1,mn}\sinh(\gamma_{1,mn}y)\right]X_m(x)Z_n(z) \qquad (3\text{-}17)$$

because $b_0 = 0$. In this case, the values of coefficients $A_{j,mn}$ and $B_{j,mn}$ can be obtained in ascending order from the modified forms of Eq. (3-11b) and Eq. (3-12b) as

$$B_{j+1,mn} = \frac{\gamma_{j,mn}k_{y,j}}{\gamma_{j+1,mn}k_{y,j+1}}\left[A_{j,mn}\sinh(\gamma_{j,mn}d_j) + B_{j,mn}\cosh(\gamma_{j,mn}d_j)\right] \qquad (3\text{-}18a)$$

and

$$\begin{aligned} A_{j+1,mn} = {} & A_{j,mn}\left[\cosh(\gamma_{j,mn}d_j) + \gamma_{j,mn}R_j k_{y,j}\sinh(\gamma_{j,mn}d_j)\right] \\ & + B_{j,mn}\left[\sinh(\gamma_{j,mn}d_j) + \gamma_{j,mn}R_j k_{y,j}\cosh(\gamma_{j,mn}d_j)\right] \end{aligned} \qquad (3\text{-}18b)$$

Once the coefficients $A_{j,mn}$ and $B_{j,mn}$ for layer *N* are known, the coefficient C_{mn} can be determined from the non-homogeneous boundary condition at *y* = *b*. As an illustration, for a boundary condition of the first kind, $T_1(x,b,z) = f(x,z)$ at *y* = *b*. Then the coefficient C_{mn} becomes

$$C_{mn} = \frac{\int_{z=0}^{c}\int_{x=0}^{a} f(x,z)X_m(x)Z_n(z)dxdz}{\left[A_{N,mn}\cosh(\gamma_{N,mn}d_N) + B_{N,mn}\sinh(\gamma_{N,mn}d_N)\right]N_m N_n} \qquad (3\text{-}19)$$

and can be inserted into Eq. (3-16).

3.3 Volumetric Heat Source at Interior Locations

In this section, we consider the determination of temperature in a multi-layer body in the presence of a volumetric heat source. The boundary conditions on all

surfaces are homogeneous. Earlier sections described the effects of non-homogeneous boundary conditions. The governing Poisson's equation in the homogeneous layer *j* is

$$k_j\left(\frac{\partial^2 T_j}{\partial x^2}+\frac{\partial^2 T_j}{\partial y^2}+\frac{\partial^2 T_j}{\partial z^2}\right)+g(x,y,z)=0 \qquad (3\text{-}20)$$

where $g_j(x,y,z)$ describes the effect of a volumetric heat source in layer *j*. The basic steps to acquiring a solution are similar to those discussed earlier but contain the modifications presented below.

We can propose a solution of the form

$$T_j=\sum_{m=1}^{\infty}\sum_{n=1}^{\infty}\sum_{p=1}^{\infty} C_{mn}X_m(x)Y_{j,p}(y)Z_n(z) \text{ for } j=1,2,\cdots,N \qquad (3\text{-}21)$$

where the functions $X_m(x)$, $Y_{j,p}(x)$, and $Z_n(x)$ satisfy the differential equations

$$X''/X=-\beta^2 \qquad (3\text{-}22a)$$

$$Y_j''/Y_j=-\gamma^2 \qquad (3\text{-}22b)$$

$$Z''/Z=-\nu^2 \qquad (3\text{-}22c)$$

The functions $X(x)$ and $Z(z)$ remain the same as those in Eq. (3-5a) and Eq. (3-5b). However, in this application, $\gamma_j=\gamma$, and it remains the same in all layers. This causes the function $Y_j(y)$ to have the functional form

$$Y_{j,p}(y)=A_{j,mn}\cos[\gamma_p(y-b_{j-1})]+B_{j,p}\sin[\gamma_{j,p}(y-b_{j-1})] \qquad (3\text{-}23)$$

The coefficients $A_{j,mn}$ and $B_{j,mn}$ can be obtained from the recursive relations

$$B_{j+1,mn}=\frac{\gamma_{j,mn}k_j}{\gamma_{j+1,mn}k_{j+1}}\left[-A_{j,mn}\sin(\gamma_{j,mn}d_j)+B_{j,mn}\cos(\gamma_{j,mn}d_j)\right] \qquad (3\text{-}24a)$$

and

$$A_{j+1,mn} = A_{j,mn}\left[\cos(\gamma_{j,mn} d_j) - \gamma_{mn} R_j k_j \sin(\gamma_{j,mn} d_j)\right] + B_{j,mn}\left[\sin(\gamma_{j,mn} d_j) + \gamma_{mn} R_j k_j \cos(\gamma_{j,mn} d_j)\right] \tag{3-24b}$$

These two relations satisfy the compatibility conditions given in Eq. (3-12a) and Eq. (3-11a), respectively.

Next, the substitution of T_j from Eq. (3-21) into Eq. (3-20) produces the relation

$$\sum_{m=1}^{\infty}\sum_{n=1}^{\infty}\sum_{p=1}^{\infty} C_{mnp} k_j (\beta_m^2 + \gamma_p^2 + \nu^2) \times X_m(x) Y_{j,p}(y) Z_n(z) = g_j(x,y,z) \tag{3-25}$$

The coefficient C_{mnp} can be derived by applying classical orthogonality conditions. The orthogonality conditions for the *x*-direction and *z*-direction are described in Eq. (3-14b) and Eq. (3-14c). The orthogonality condition for the *y*-direction is in Appendix A. These orthogonality conditions yield the coefficient C_{mnp} for insertion into Eq. (3-21); that is,

$$C_{mnp} = \frac{1}{N_{x,m} N_{y,p} N_{z,n}} \int_{x=0}^{a} \int_{z=0}^{c} \sum_{j=1}^{N} \int_{y=0}^{b_j} \frac{g_j(x,y,z) X_m(\beta_m x) Y_{j,p}(\gamma_p y) Z_n(\nu_n z)}{(\beta_m^2 + \gamma_p^2 + \nu^2)} dxdydz \tag{3-26a}$$

where

$$N_{y,mn} = \sum_{j=1}^{N} \int_{y=0}^{b_j} k_{y,j} [Y_{1,mn}(\gamma_{j,mn} y)]^2 dy \tag{3-26b}$$

The other norms can be obtained using Eq. (3-14b) and Eq.(3-14c).

Numerical Examples and Discussions

Numerical examples are selected to illustrate the application of this methodology to select situations in electronic cooling applications.

Example 1. This example is selected to illustrate the numerical procedures that would directly produce the Fourier coefficients through recursive relations. It shows the accuracy of this series solution for selected eigenvalues of reasonable size, as described in [39, 40]. For this example, we select a five-layer body similar to the three-layer body depicted in Figure 3-1. In this body, a = 10 *mm*, b_1 = 0.625 *mm*, b_2 = 0.650 *mm*, b_3 = 1.275 *mm*, b_4 = 1.3 *mm*, b_5 = 1.925 *mm*, and c = 10*mm.* The selected thermal conductivities arek_1 = 100 *W/m·K*, k_2 = 4 *W/m·K*, k_3 = 100 *W/m·K*, k_4 = 4 *W/m·K*, and k_5 = 100 *W/m·K*. The layers have a convective surface at $y = b_5$ with h = 10,000 $W/m^2 \cdot K$, while all other surfaces are insulated. To simplify this presentation, we hypothesize that there are two volumetric heat sources: the first one in layer 1 with $g_1 = 2.56\times10^8$ W/m^3 and the second one in layer 5 with $g_5 = 5.76\times10^8$ W/m^3. Furthermore, the contact resistance within a unit area between layers in one-dimensional space is $R_j = 5\times10^{-6}$ $m^2 \cdot K/W$ for j = 1 to 4.

Using the procedures described earlier, we compute the temperature when the energy released in layers 1 and 5 are within x = 0 to $a/2$ and z = 0 to $c/2$ while y = 0 to b_1 in layer 1 and $y = b_4$ to b_5 in layer 5 as shown in Figure 3-2(a). We calculate the temperature using five eigenvalues in the x- and z-directions while selecting twenty eigenvalues for the y-direction. The acquired temperature values for $\theta_1(x,0,z) = T_1(x,0,z) - T_\infty$ are plotted in Figure 3-2(b). Additionally, the temperature variation $T_j(a/2, y, c/2) - T_\infty$ is plotted in Figure 3-3. To verify the accuracy of these data, we provide a sample for temperature $T_j(a/2, y, c/2)$ at different y locations in

Table 3-1 At these locations, it is possible to produce an exact solution. The superposition method indicates that these values can also be derived from a one-dimensional exact solution divided by four. Designating this auxiliary temperature as $\theta_j(y) = T_j^*(y) - T_\infty$, a one-dimensional steady-state solution clearly shows that

$$\begin{aligned}\theta_5^*(y) &= T_5^* - T_\infty \\ &= \frac{g_1 d_1 + g_5 d_5}{h} + \frac{g_5[d_5^2 - (y - b_4)^2]}{2k_5} + \frac{g_1 d_1[d_5 - (y - b_4)]}{k_5}\end{aligned}$$

Then the temperature when $y = b_4$ is

$$\theta_5^*(b_4) = \frac{g_1 d_1 + g_5 d_5}{h} + \frac{g_5 d_5^2}{2k_5} + \frac{g_1 d_1 d_5}{k_5}$$

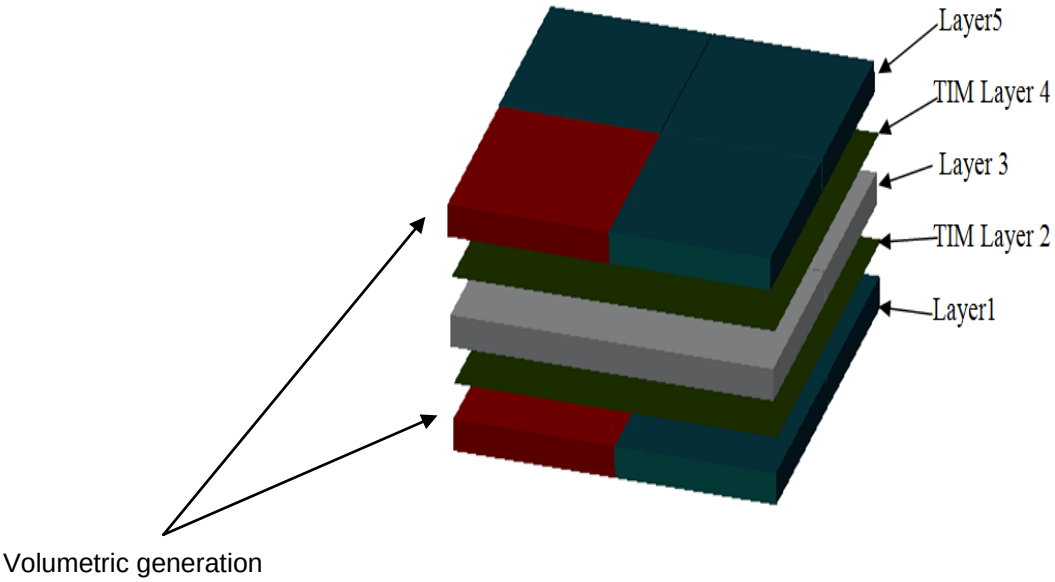

(a)

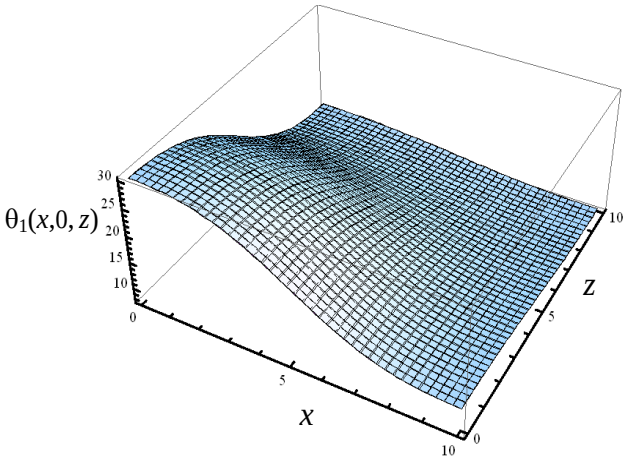

(b)

Figure 3-2 (a) The five-layer 3D stack, and (b) the surface temperature

$\theta_1(x,0,z) = T_1(x,0,z) - T_\infty$ as a function of x and z

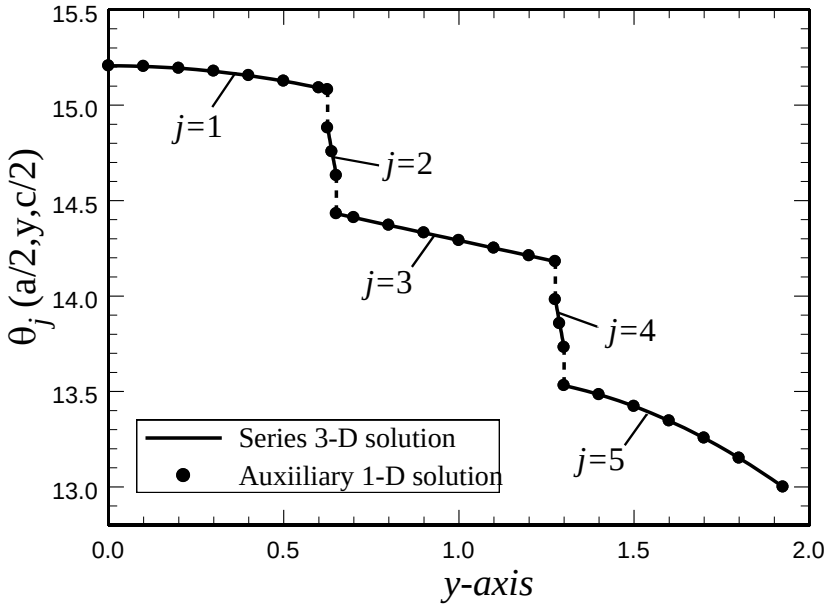

Figure 3-3 The computed temperature $\theta_j(a/2,0,c/2) = T_j(a/2,0,c/2) - T_\infty$ for a five-layer body in Example 1 and a comparison with $\theta_j^*(a/2,0,c/2)/4$.

Table 3-1 A comparison of $\theta_j\left(\frac{a}{2}, y, \frac{c}{2}\right)$ with the results from the exact solution using $\theta_j^*(y)/4$.

Layer *j*	Location *y*	$\theta_j\left(\frac{a}{2}, y, \frac{c}{2}\right)$	$\frac{1}{4}\theta_j^*(y)$
J = 1	0	15.2063	15.2063
	b_1	15.0813	15.0813
J = 2	b_1	14.8813	14.8813
	b_2	14.6313	14.6313
J = 3	b_2	14.4313	14.4313
	b_3	14.1813	14.1813
J = 4	b_3	13.9814	13.9813
	b_4	13.7314	13.7313
J = 5	b_4	13.5312	13.5313
	b_5	13.0	13.0

Applying the classical resistant networks produces the following temperature values

$$\theta_4^*(b_4) = \theta_5^*(b_4) + g_1 d_1 R_4 ,$$

$$\theta_1^*(b_1) = \theta_4^*(b_4) + g_1 d_1 \left(\frac{d_4}{k_4} + R_3 + \frac{d_3}{k_3} + R_2 + \frac{d_2}{k_2} + R_1 \right),$$

Finally, we obtain

$$\theta_1^*(y) = \theta_1^*(b_1) + \frac{g_1 b_1^2}{2k} \left[1 - \left(\frac{y}{b_1} \right)^2 \right]$$

We compute these temperatures at specified locations, and we present the values of $\theta_j^*(y)/4$ in Table 3-1 to compare them with the series solutions and selected data for $\theta_j^*(y)/4$ values are plotted in Figure 3-3 using circular symbols. The data show that a series solution of reasonable size would produce sufficiently accurate results.

Numerical Example 2. For this example, we consider a 3D package that consists of five layers (N = 5). The lateral dimensions are $a = 10\ (mm)$ and $b = 10\ (mm)$. This device could be considered a 3D stack package of low density that consists of three layers of silicon joined by two layers of thermal interface material (TIM). The silicon layers 1, 3, and 5 have the same thickness (that is, $d1 = d2 = d3 = 0.625\ (mm)$. See Figure 3-4(a).

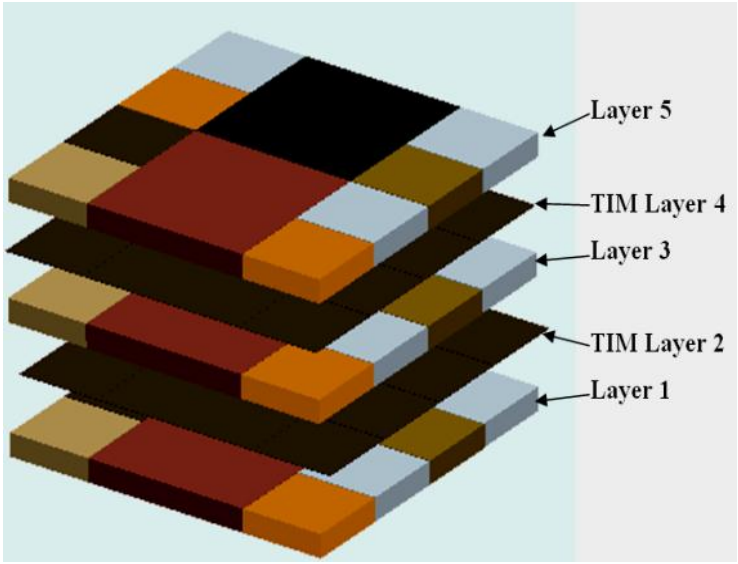

(a)

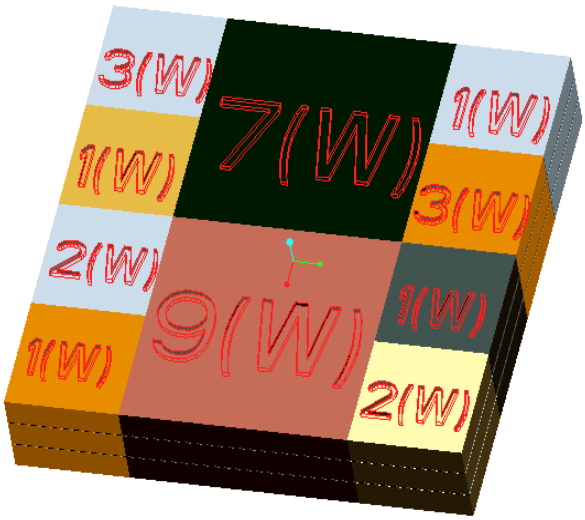

(b)

Figure 3-4 (a) The five-layer 3D stack, and (b) the wattage of each volumetric source

The TIM layers 2 and 4 have a thickness of $d2 = d4 = 0.05\ (mm)$. The TIM layers have a thermal conductivity of $k2 = k4 = 4\ (W/m.K)$, whereas the silicon layers

have a thermal conductivity of $k1 = k3 = k5 = 100\ (W/m.K)$. The top surface of the stack package is exposed to the boundary condition of the third kind, where $h = 10000(W/m^2K)$. Ten functional blocks exist at each layer, and each one dissipates differently. However, every layer has the same configuration with respect to volumetric heat generation (in this case, the functional blocks). The wattage of each volumetric source is depicted in Figure 3-4(b). The ambient temperature is $T_\infty = 23℃$. We use the procedure described in Section 3.2 to acquire analytical solutions and the commercially available software ANSYS as a comparison tool to determine the temperature field for the given configuration.

Solution/Discussion for Example 1:

We perform a steady-state thermal analysis to determine the thermal response under applied steady-state loads. In this analysis, temperature and heat flow rates are usually the items of interest, although heat flux can be reported as well in ANSYS Workbench.

The general governing thermal equation is as follows:

$$[C(T)].\{\dot{T}\} + [K(T)].\{T\} = \{Q(t,T)\}$$

Where t is time and $\{T\}$ is the temperature. $[C]$ is the specific heat (thermal capacitance) matrix, $[K]$ is the conductivity matrix, and $\{Q\}$ is the heat flow rate vector.

In steady-state analysis, all time-dependent terms vanish. However, this does not mean that non-linearities are ignored.

For steady-state thermal analysis in ANSYS, the temperature matrix {T} is solved without time dependent terms, as shown below;

$$[K(T)].\{T\} = \{Q(T)\}$$

The thermal conductivity matrix [K] can be constant or temperature-dependent. In this case, we have a constant conductivity matrix. Similarly, {Q} can be constant or time-dependent.

For a steady-state solution, the coefficient of heat transfer (h) can be input as the convective boundary conditions. Fourier's Law provides the basis for the latter equation. That is, heat flows in the solid in the basis of the [K] matrix. Heat flow, heat flux, and convection are treated as the boundary conditions on the system {Q}. Note that if we need to solve conjugate heat transfer, we should use ANSYS CFD because ANSYS Workbench is not capable of solving conjugate problems.

In our example, we use the data provided as an input. We model the package in Pro/E and import it to ANSYS Workbench for thermal analysis. We mesh the model as shown in Figure 3-5(a). The resulting temperature contour and total heat flux are shown in Figure 3-5(b) and Figure 3-6, respectively. Figure 3-7 shows the analytical temperature distribution in the first layer obtained from Mathematica. Figure 3-8 compares the analytically and numerically derived temperature solutions for some randomly selected points from each layer.

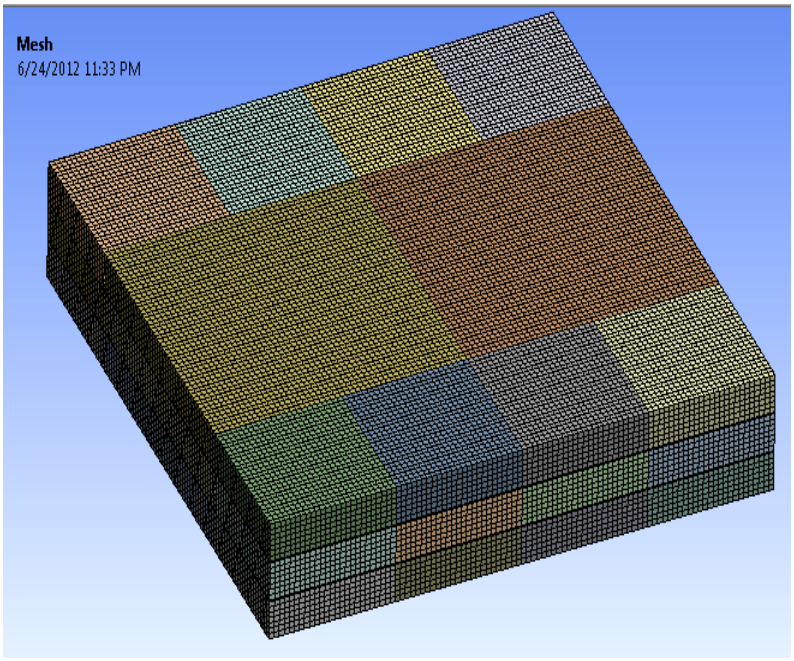

(a)

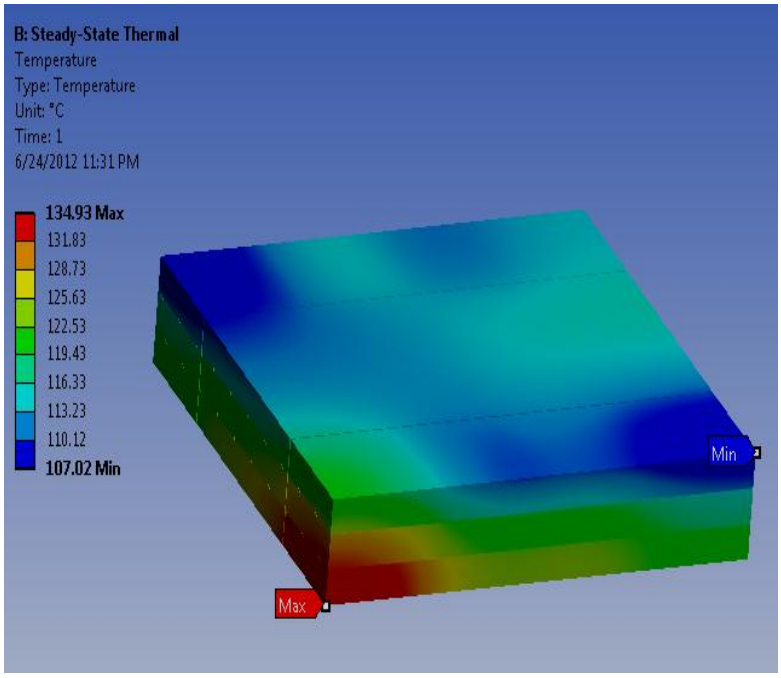

(b)

Figure 3-5 (a) The mesh of the model, and (b) the temperature contours.

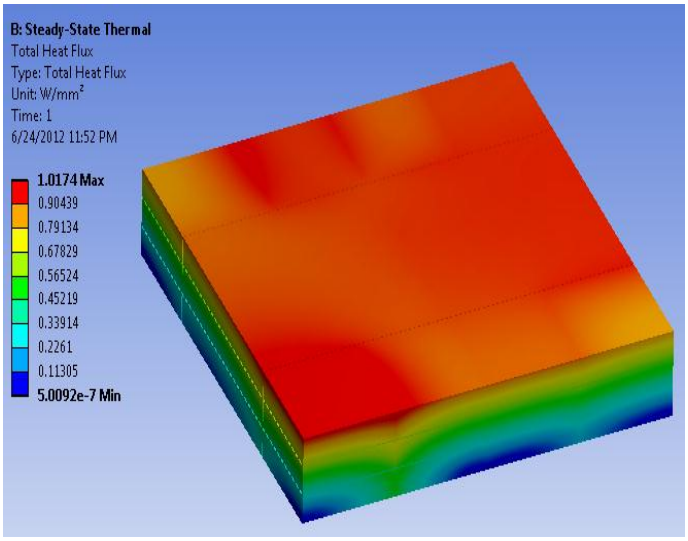

Figure 3-6 The total heat flux of the package.

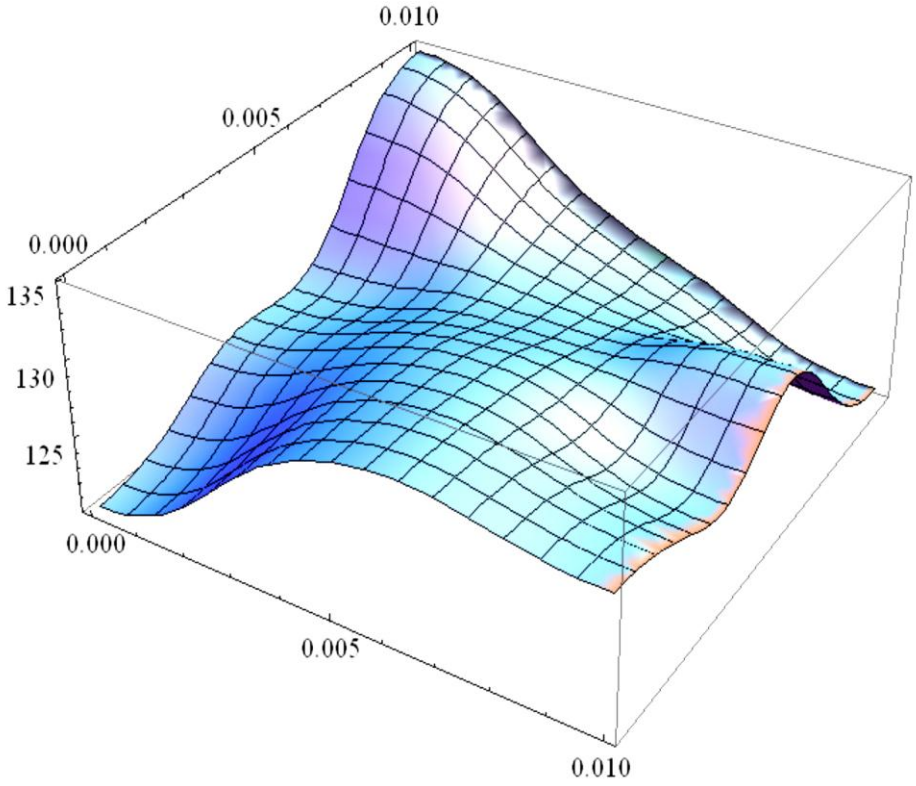

Figure 3-7 The analytically obtained temperature profile for the first layer.

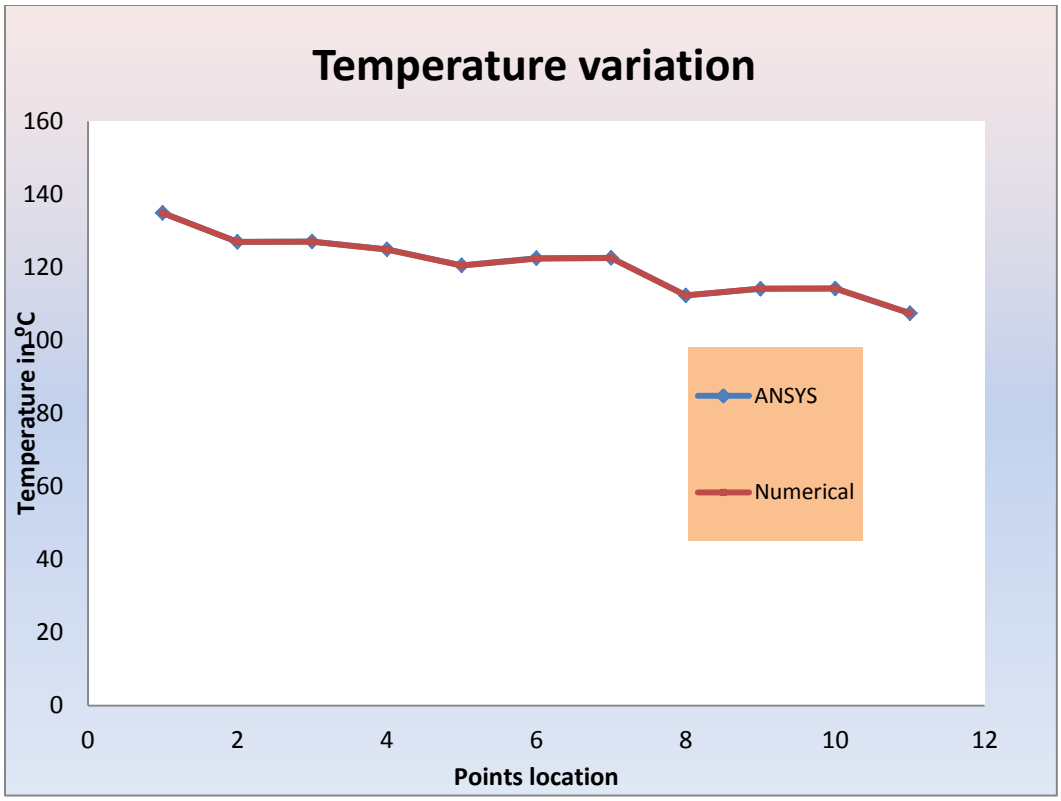

Figure 3-8 Comparison of the numerically and analytically derived temperature solutions.

Numerical Example 3. In this example, we consider a five-layer stack of silicon material, as shown in Figure 3-9. Each layer consists of four functional units. Each unit dissipates differently, as depicted in Figure 3-10. The overall dimensions of the stack package area $= b = 10(mm)$ and $d1 = d2 = d3 = d4 = d5 = 0.625\ (mm)$. The contact resistance between each layer is emphasized (that is, $R1 = R2 = R3 = R4 = 2\ (K/Wmm^2)$. The thermal conductivity of each layer is $k1 = k2 = k3 = k4 = k5 = 100(W/mK)$. The top surface of the stack experiences a convection value of $h = 10000(W/m^2K)$, while the four sides of the stack are assumed to be insulated.

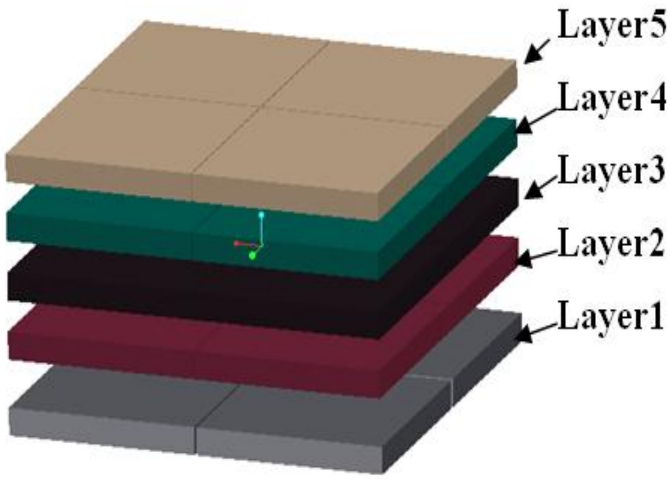

Figure 3-9 A five-layer stack of silicon material

Four different functional blocks

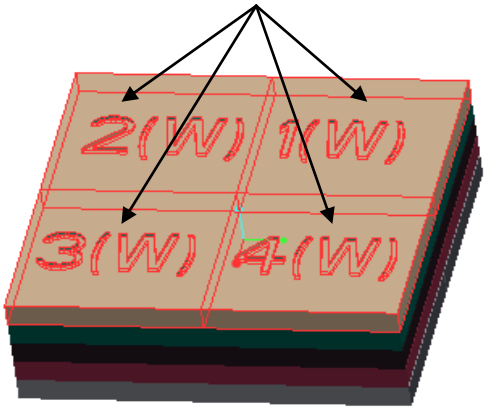

Figure 3-10 The four functional units in each layer.

We apply the procedures described in Section 3.1 to this problem by using Eq. (3-24a) and Eq. (3-24b).We also use these procedures to determine the temperature field.

Discussion of Example 3:

In this example, we use the same procedure used in Example 1.However, we also consider the effect of thermal contact resistance in this example. In ANSYS, a

professional license user may define a finite thermal contact conductance (TCC). When two surfaces touch each other, ANSYS will assume perfect thermal contact conductance between the joined members unless the user changes the contact settings for the problem. The contact region is composed of “Contact” faces on one side and “Target” faces on the other side. Heat flow is only allowed between the contact and target elements in the contact normal direction. In other words, heat can only flow if the target elements are present in the normal direction. Heat spreading between the contact and target surfaces takes place because of Fourier’s Law, and ANSYS will use the following equation to determine the heat flow between the contact elements

$$q = TCC[T_{target} - T_{contact}]$$

where T_{target} and $T_{contact}$ are the temperatures of the target and contact nodes, respectively.

In our example, we import the Pro/E model to ANSYS Workbench for steady-state thermal analysis. After successfully inputting the boundary conditions and heat flow rate of each section of the layers, we apply the TCC values at specified locations (that is, between each layer). Note that thermal contact conductance is the inverse of the contact resistance per given area.

The results are shown for the temperature contour and the heat flux in Figure 3-11 and Figure 3-12, respectively. Figure 3-13 shows the comparison between the analytical and numerical results for the selected points along the y-axis through the center of the package. Figure 3-14 depicts the temperature profile obtained analytically for the first layer, where the maximum temperature occurs.

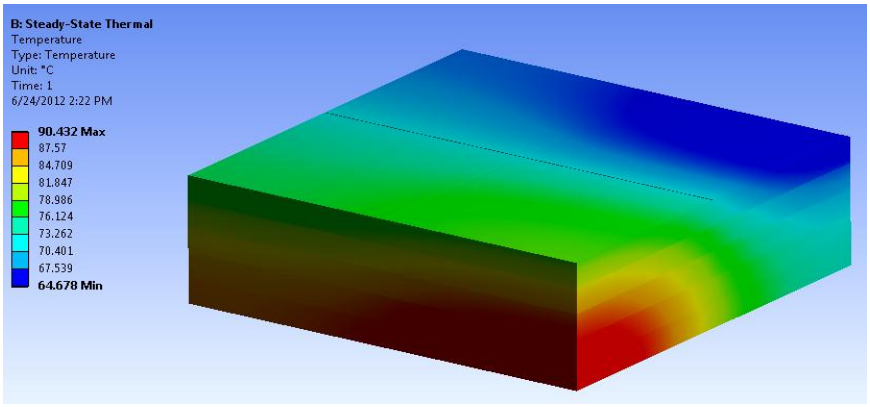

Figure 3-11 The temperature contours of the stack package.

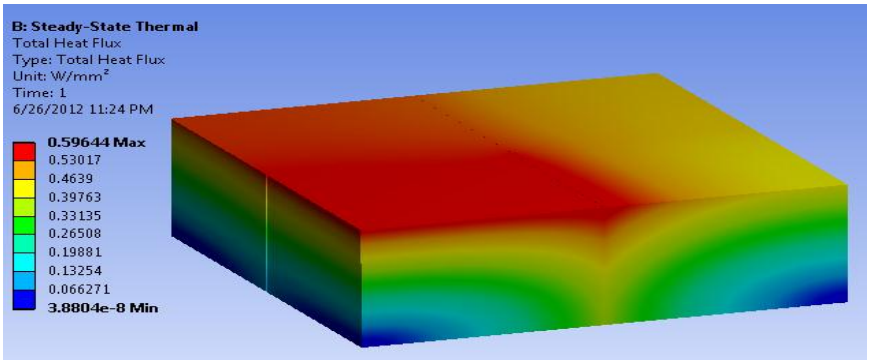

Figure 3-12 The total heat flux of the package.

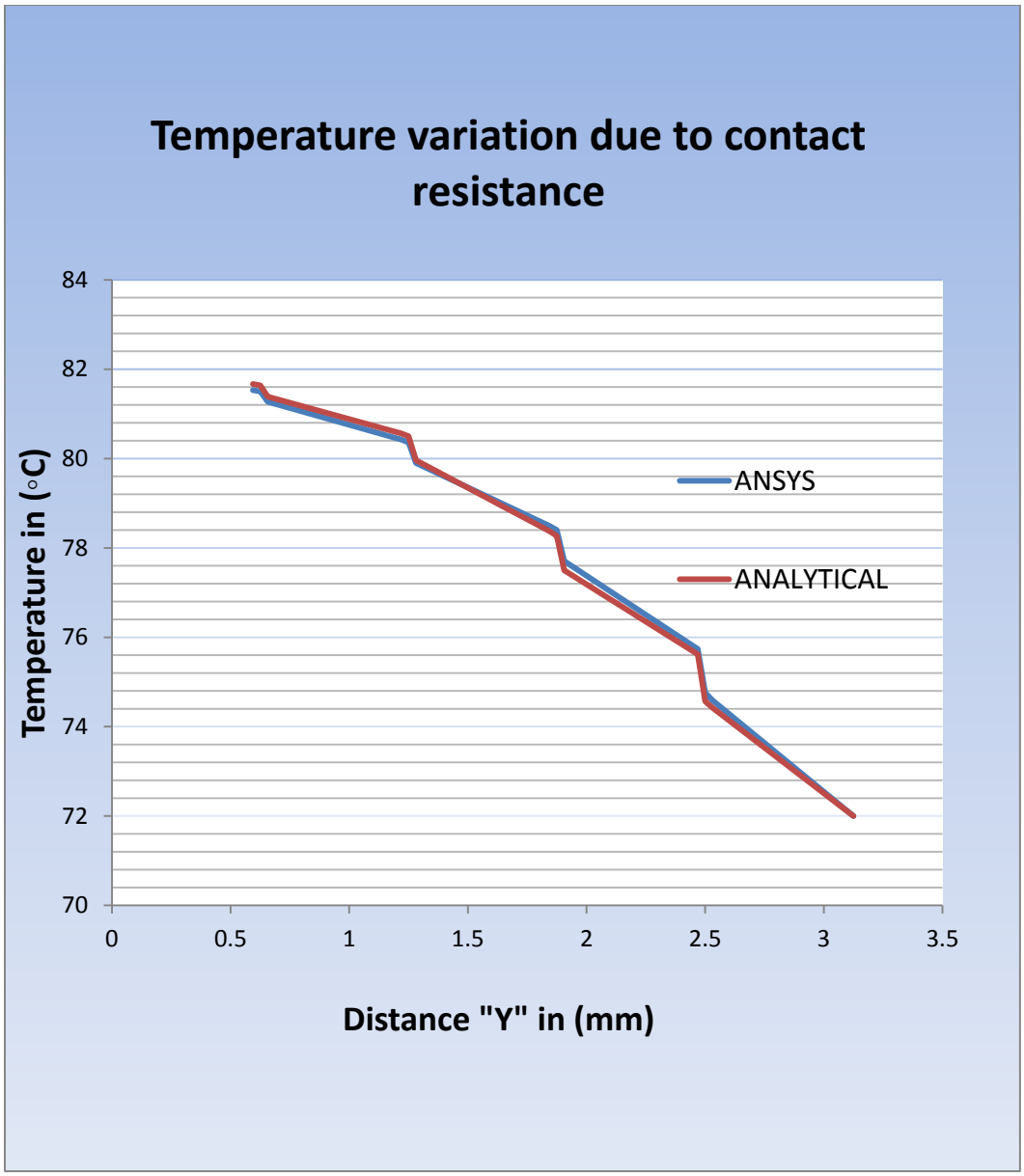

Figure 3-13 The comparison between the analytically and numerically derived results.

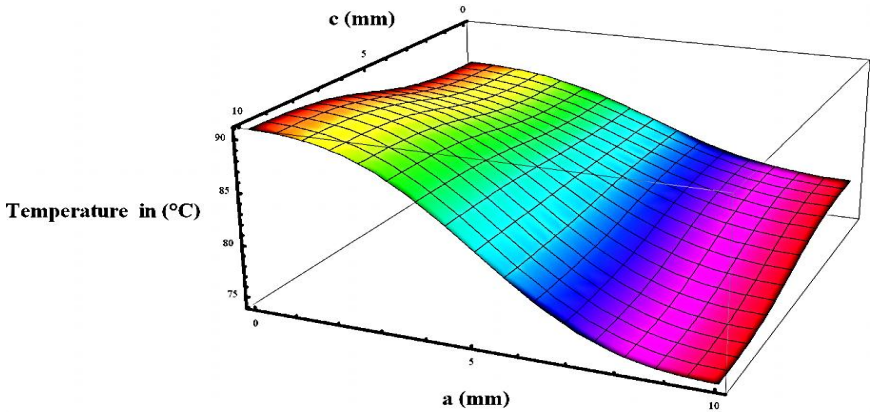

Figure 3-14 The analytically obtained temperature profile for the first layer.

3.4 Conclusion

The reported analytical solution covers a wide range of applications in electronic cooling especially in the first level packaging. The analytically derived temperature field can provide an accurate solution for the purpose of verifying a numerically acquired solution. In the second example, without the presence of any contact resistance, the numerical and analytical solutions were well matched (see Figure 3-8). The maximum temperature obtained from ANSYS in Figure 3-5(b) is 134.93ºC, and the one from the analytical solution in Figure 3-7 is 134.89ºC.

In the third example, which involves thermal contact resistance, the numerical and analytical solutions are in good agreement. The small deviation is expected because the finite element is an approximation, not an exact solution. The maximum temperature obtained analytically in Figure 3-14 is 90.7ºC; while the maximum obtained from ANSYS, shown in Figure 3-11, is approximately 90.43ºC. Both approaches show that the minimum temperature is 72ºC. In the first example, the analytical solution matched with the exact solution and verified the high accuracy of the analytical method developed in this presentation. Moreover, the analytical solutions converge with an order of magnitude faster than the computational approach.

Chapter 4

Determination of Steady State Temperature in a Two-layer Body with Different Form Factors

The determination of temperature in multi-layer bodies has been the subject of numerous studies and analytical solutions are well established [41-44]. A multi-layer body consists of plates having different thicknesses but with uniform platform areas. Also, the rectangular plates of different platform areas can be attached to each other in many engineering applications. These systems appear in different engineering applications such as in electronic cooling devices and they often do not accept closed-form analytical solutions. Information related to the use of layered materials in electronic cooling applications is in [45-49]. The study of related spread resistant is available in the literature and related information is in [50-53].

The mathematical procedure for the system under investigation also leads toward an integral equation to be solved by an inverse technique [54], which may have an analytical solution for special cases. The function specification method has often been used to solve heat conduction problems and the related methodologies are in [55-57]. Other estimation techniques are available in the literature; e.g., using a surface element technique [58], an iterative procedure [59], etc.

This presents a function-specification procedure that leads to a closed-form solution. In this study, we examine two parallel rectangular plates with different platform areas attached to each other, as shown in Figure 4-1(a). The system depicted in Figure 4-1(a) consists of two plates, one with thickness *b* and the other with thickness *d*. Plate 1 receives locally variable heat flux input at *y=b* while plate 2 serves as a heat spreader which rejects the energy received at $\eta = d$ to the environment from the surface located

at $\eta = 0$. Analytically obtained closed-form series solutions are presented for these two plates in contact. These solutions exhibit special convergence behaviors, as discussed in this presentation. The two analytical solutions are: one for Layer 1 and the other for Layer 2. These two solutions accept the imposed compatibility conditions at the contact surface where *y*=0. The two solutions, for Layers 1 and 2, are acquired analytically by functionally specifying the heat flux leaving Layer 1 at y=0 and entering Layer 2 at $\eta = d$.

4.1 Mathematical Relations

This is to study the behavior of a temperature field within a two-layer body when each layer has a different size. The schematic of the region and the coordinate systems is in Figure 4-1(a). The governing equations for steady state conduction must satisfy the Laplace equation

$$\frac{\partial^2 T_j}{\partial x^2} + \frac{\partial^2 T_j}{\partial y^2} + \frac{\partial^2 T_j}{\partial z^2} = 0 \tag{4-1}$$

with *j*=1 in region 1 and *j*=2 in region 2. This system has insulated boundaries in *x*- and *z*-directions. The subsequent mathematical presentations include solutions for two- and three-dimensional temperature fields.

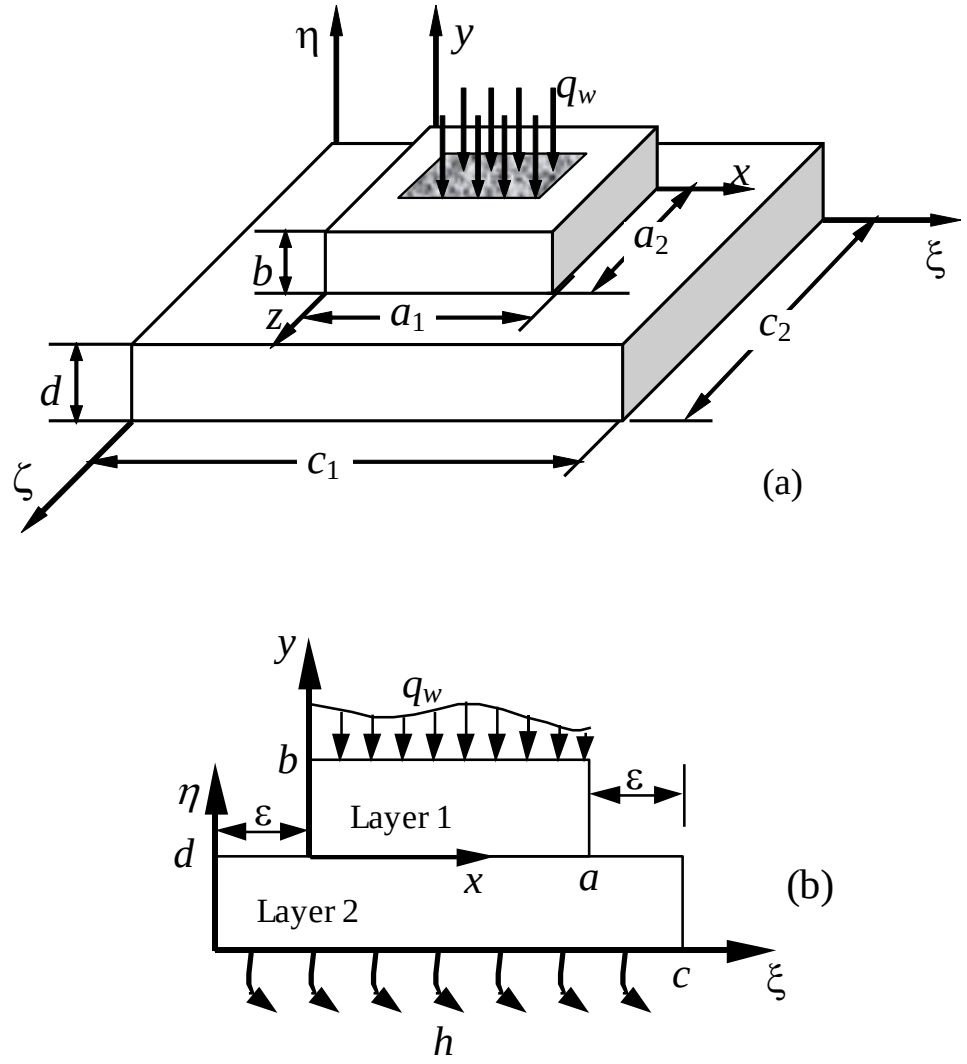

Figure 4-1 Schematic of two-layer bodies: (a) in three-dimensional apace with coordinates (x, y, z) and (ξ, η, ς), (b) in two-dimensional space with coordinates (x, y) and (ξ, η).

Next, the temperature solutions for Layer 1 and for Layer 2 are in separate sections. As stated earlier, these two solutions must satisfy the imposed boundary conditions and the compatibility conditions between the two layers.

4.2 Temperature Solution in Layer 1

The temperature in Layer 1, designated as $T_1(x, y)$, must satisfy the Laplace equation

$$\frac{\partial^2 T_1}{\partial x^2} + \frac{\partial^2 T_1}{\partial y^2} + \frac{\partial^2 T_1}{\partial z^2} = 0 \tag{4-2}$$

with boundary conditions:

(BC 1, 2) $q_1(0, y, z) = q_1(a_1, y, z) = 0$

(BC 3, 4) $q_1(x, y, 0) = q_1(x, y, a_2) = 0$

(BC 5) $T_0(x, z) - T_1(x, 0, z) = R q_1(x, 0, z)$

(BC 6) $q_1(x, b, z) = q_w(x, z)$

where the interface temperature, $T_0(x, z) = T_2(x, 0, z)$ is the unknown surface temperature. The parameter *R* in (BC 5) accounts for the effect of thermal contact resistant between these two layers. This problem has two non-homogeneous boundary conditions; therefore, it is to be decomposed into two problems $T_1(x, y, z) = T_a(x, y, z) + T_b(x, y, z)$ each having five homogeneous boundary conditions and a single non-homogeneous boundary condition. The first problem requires the solution of equation

$$\frac{\partial^2 T_a}{\partial x^2} + \frac{\partial^2 T_a}{\partial y^2} + \frac{\partial^2 T_a}{\partial z^2} = 0 \tag{4-3}$$

with boundary conditions:

(BC 1, 2) $q_a(0, y, z) = q_a(a_1, y, z) = 0$

(BC 3, 4) $q_a(x, y, 0) = q_a(x, y, a_2) = 0$

(BC 5) $T_a(x,0,z) = -Rq_a(x,0,z)$

(BC 6) $q_a(x,b,z) = q_w(x,z)$

This is a classical steady-state problem [60] and a solution that satisfies the differential equation and the homogeneous boundary conditions (BC 1-4), and (BC 6) is

$$T_a(x,y,z) = C_{00}(y + Rk_1) + \sum_{m=0}^{\infty}\sum_{n=0}^{\infty} C_{mn}(1-\delta_{0,m+n})\cos(n\pi x/a_1)\cos(n\pi z/a_2) \times[\sinh(\gamma_{mn}y) + Rk_1\gamma_{mn}\cosh(\gamma_{mn}y)] \tag{4-4a}$$

where $\delta_{0,m+n}$ is the Kronecker delta indicating $\delta_{0,m+x} = 1$ when $m+n=0$ while $\delta_{0,m+x} = 0$ when $m+n \neq 0$. Then, the use of non-homogeneous boundary condition (BC 6), followed by the application of orthogonality condition, would produces the relation

$$T_a(x,y,z) = \left(\frac{y+Rk_1}{a_1a_2}\right)\int_{z=0}^{a_2}\int_{x=0}^{a_1}\frac{-q_w(x,z)}{k_1}dxdz + \sum_{m=0}^{\infty}\sum_{n=0}^{\infty}\cos(m\pi x/a_1) \times\cos(n\pi z/a_2)\left(\frac{[\sinh(\gamma_{mn}y) + Rk_1\gamma_{mn}\cosh(\gamma_{mn}y)]}{N_mN_n\gamma_{mn}[\cosh(\gamma_{mn}b) + Rk_1\gamma_{mn}\sinh(\gamma_{mn}b)]}\right) \times(1-\delta_{0,m+n})\int_{z=0}^{a_2}\int_{x=0}^{a_1}\frac{-q_w(x,z)}{k_1}\cos(m\pi x/a_1)\cos(n\pi z/a_2)dxdz \tag{4-4b}$$

where $\gamma_{mn} = [(m\pi/a_1)^2 + (n\pi/a_2)^2]^{1/2}$. After determination of temperature field, the heat flux at *y*=0 surface is obtainable from the relation

$$q_a(x,0,z) = D_{00} + \sum_{m=0}^{\infty}\sum_{n=0}^{\infty}(1-\delta_{0,m+n})D_{mn}\cos(m\pi x/a_1)\cos(n\pi z/a_2) \tag{4-5a}$$

with

$$D_{00} = \frac{1}{a_x a_z} \int_{z=0}^{a_2} \int_{x=0}^{a_1} q_w(x,z)\,dx\,dz \tag{4-5b}$$

when *m*=0 and *n*=0, while

$$D_{mn} = \left(\frac{1}{N_m N_n [\cosh(\gamma_{mn} b) + Rk_1 \sinh(\gamma_{mn} b)]} \right) \times \int_{z=0}^{a_2} \int_{x=0}^{a_1} q_w(x,z) \cos(m\pi x / a_1) \cos(n\pi z / a_2)\,dx\,dz \tag{4-5c}$$

when $m > 0$ or $n > 0$. These coefficients have known quantities since $q_w(x)$ is the prescribed heat flux distribution over *y=b* surface.

The second problem is to solve for $T_b(x,y,z)$, which also satisfies the Laplace equation

$$\frac{\partial^2 T_b}{\partial x^2} + \frac{\partial^2 T_b}{\partial y^2} + \frac{\partial^2 T_b}{\partial z^2} = 0 \tag{4-6}$$

with boundary conditions:

(BC 1, 2) $q_b(0,y,z) = q_b(a_1,y,z) = 0$

(BC 3, 4) $q_b(x,y,0) = q_b(x,y,a_2) = 0$

(BC 5) $T_0(x,z) - T_b(x,0,z) = Rq_b(x,0,z)$

(BC 6) $q_b(x,b,z) = 0$

where the interface temperature, $T_0(x,z)$, is the unknown surface condition, to be determined from the forthcoming $T_2(\xi,\eta,\zeta)$ solution for inclusion into the compatibility condition (BC 5) at *y*=0. The separation of variables technique, using the homogeneous boundary conditions, provides the relation

$$T_b(x,y,z) = C_{00} + \sum_{m=0}^{\infty}\sum_{n=0}^{\infty} C_{mn}(1-\delta_{0,m+n}) \times \cos(m\pi x/a_1)\cos(n\pi z/a_2)\cosh[\gamma_{mn}(b-y)] \tag{4-7a}$$

Once $T_0(x,z)$ is specified, the non-homogeneous boundary condition (BC 5) produces the temperature solution $T_b(x,y,z)$ as,

$$T_b(x,y,z) = \frac{1}{a_1 a_2}\int_{z=0}^{a_2}\int_{x=0}^{a_1} T_0(x,z)dxdz + \sum_{m=0}^{\infty}\sum_{n=0}^{\infty}(1-\delta_{0,m+n}) \times \frac{\cos(m\pi x/a_1)\cos(n\pi z/a_2)\cosh[\gamma_{mn}(b-y)]}{N_m N_n[\cosh(\gamma_{mn}b) + Rk_1\gamma_{mn}\sinh(\gamma_{mn}b)]} \times \int_{z=0}^{a_2}\int_{x=0}^{a_1} T_0(x,z)\cos(m\pi x/a_1)\cos(n\pi z/a_2)d\,xdz \tag{4-7b}$$

and then the heat flux at y=0 surface becomes

$$q_b(x,0,z) = \sum_{m=0}^{\infty}\sum_{n=0}^{\infty} B_{mn}(1-\delta_{0,m+n})\cos\left(\frac{m\pi x}{a_1}\right)\cos\left(\frac{n\pi z}{a_2}\right) \tag{4-8a}$$

wherein

$$B_{mn} = \frac{\gamma_{mn}\tanh(\gamma_{mn}b)}{N_m N_n[1+Rk_1\gamma_{mn}\tanh(\gamma_{mn}b)]} \times \int_{z=0}^{a_2}\int_{x=0}^{a_1} T_0(x,z)\cos(m\pi x/a_1)\cos(n\pi z/a_2)d\,xdz \tag{4-8b}$$

while $B_{00} = 0$. Then, the specified heat flux over $y = 0$ surface, denoted as being the primary unknown within the relation $q_0(x,z) = q_1(x,0,z)$, leads to the relation $q_0(x,z) = q_a(x,0,z) + q_b(x,0,z)$. It is to be noted that $q_b(x,0,z)$ is deterministic once the function $T_0(x,z)$ is known. Therefore, one needs to produce the temperature

solution $T_2(\xi,\eta,\zeta)$ in Layer 2 and then the temperature solution $T_2(\xi,\eta,\zeta)$ in Layer 2 would yield the function $T_0(x,z)$.

4.3 Temperature Solution in Layer 2

For convenience of this presentation, a new set of coordinates is selected using $\xi = \varepsilon_x + x$, $\eta = y + d$ and $\zeta = \varepsilon_z + x$, as shown in Figure 4-1(a). The temperature solution in the second layer also satisfies the Laplace equation

$$\frac{\partial^2 T_2}{\partial \xi^2} + \frac{\partial^2 T_2}{\partial \eta^2} + \frac{\partial^2 T_2}{\partial \zeta^2} = 0 \tag{4-9}$$

where $T_2 = T_2(\xi,\eta,\zeta)$ must satisfy the boundary conditions

(BC 1, 2) $q_2(0,\eta,\zeta) = q_2(c_1,\eta,\zeta) = 0$

(BC 3, 4) $q_2(\xi,\eta,0) = q_2(\xi,\eta,c_2) = 0$

(BC 5) $\partial T_2(\xi,\eta,\zeta)/\partial\eta\big|_{\eta=0} = (h/k_2)\,T_2(\xi,0,\zeta)\big|$

(BC 6) $-k_2\partial T_2(\xi,\eta,\zeta)/\partial\eta\big|_{\eta=d} = q_2(\xi,d,\zeta)$, in which

$q_2(\xi,d,\zeta) = q_0(\xi-\varepsilon_1,\zeta-\varepsilon_2)$.

The heat flux $q_2(\xi,d,\zeta)$ has a finite value within the contact area; otherwise, it has a zero value. Similar problems with partial heating have received consideration in transient heat conduction applications [61]. The solution begins by using the classical separation technique using the homogeneous boundary conditions (BC 1-5).

$$T_2(\xi,\eta,\zeta) = C_{00}\left(\eta + k_2/h\right) + \sum_{m=0}^{\infty}\sum_{n=0}^{\infty} C_{mn}(1-\delta_{0,m+n})\cos\left(\frac{m\pi\xi}{c_1}\right)\cos\left(\frac{n\pi\zeta}{c_2}\right) \times\left[\cosh(\lambda_{mn}\eta) + \frac{h}{k_2\lambda_{mn}}\sinh(\lambda_{mn}\eta)\right] \tag{4-10a}$$

The application of the non-homogeneous boundary condition (BC 6) results in a closed form temperature solution as

$$T_2(\xi,\eta,\zeta) = \left[\int_{\varepsilon_2}^{c_2-\varepsilon_2}\int_{\varepsilon_1}^{c_1-\varepsilon_1} \frac{-q_2(\xi,d,\zeta)}{c_1c_2k_2}\,d\xi d\zeta\right]\left(\eta + k_2/h\right) + \sum_{m=0}^{\infty}\sum_{n=0}^{\infty} \frac{(1-\delta_{0,m+n})}{N_mN_n}\cos(m\pi\xi/c_1)\cos(n\pi\zeta/c_2) \times\frac{\left[\cosh(\lambda_{mn}\eta) + \frac{h}{k_2\lambda_{mn}}\sinh(\lambda_{mn}\eta)\right]}{\lambda_{mn}\sinh\left(\frac{m\pi d}{c}\right) + \frac{h}{k_2}\cosh\left(\frac{m\pi d}{c}\right)} \times\int_{\varepsilon_2}^{c_2-\varepsilon_2}\int_{\varepsilon_1}^{c_1-\varepsilon_1} \frac{-q_2(\xi,d)}{k_2}\cos(m\pi\xi/c_1)\cos(n\pi\zeta/c_2)d\xi d\zeta \tag{4-10b}$$

Then, the temperature over the contact surface becomes

$$T_0(\xi,\zeta)=\left[\int_{\varepsilon_2}^{c_2-\varepsilon_2}\int_{\varepsilon_1}^{c_1-\varepsilon_1}\frac{-q_2(\xi,d,\zeta)}{c_1c_2k_2}\,d\xi d\zeta\right](\eta+k_2/h)$$
$$+\sum_{m=0}^{\infty}\sum_{n=0}^{\infty}\frac{(1-\delta_{0,m+n})}{N_mN_n}\cos(m\pi\xi/c_1)\cos(n\pi\zeta/c_2)$$
$$\times\frac{\left[\cosh(\lambda_{mn}d)+\dfrac{h}{k_2\lambda_{mn}}\sinh(\lambda_{mn}d)\right]}{\lambda_{mn}\sinh\left(\dfrac{m\pi d}{c}\right)+\dfrac{h}{k_2}\cosh\left(\dfrac{m\pi d}{c}\right)} \qquad (4\text{-}11)$$
$$\times\int_{\varepsilon_2}^{c_2-\varepsilon_2}\int_{\varepsilon_1}^{c_1-\varepsilon_1}\frac{-q_2(\xi,d)}{k_2}\cos(m\pi\xi/c_1)\cos(n\pi\zeta/c_2)d\xi d\zeta$$

4.3 Function Specification Method

Numerous investigators have used the function specification method in the past. This procedure leads to a methodology for direct determination of $q_0(x,z)$ and $T_0(x,z)$ for this application. The following formulations are devoted to determination of the heat flux $q_0(x,z)$ over the contact area. The relation $q_0(x,z)=q_a(x,0,z)+q_b(x,0,z)$ suggests having a specified functional form for $q_0(x,z)$; that is

$$q_0(x,z)=\sum_{m=0}^{\infty}\sum_{n=0}^{\infty}A_{mn}\cos(m\pi x/a_1)\cos(n\pi z/a_2) \qquad (4\text{-}12)$$

wherein A_{mn} coefficients are the unknowns to be determined. Using Eq. (4-5a), the function $q_a(x,0,z)$ has a deterministic form

$$q_a(x,0,z)=\sum_{m=0}^{\infty}\sum_{n=0}^{\infty}D_{mn}\cos(m\pi x/a_1)\cos(n\pi z/a_2) \qquad (4\text{-}13)$$

since the coefficients, D_{mn}, have known values, as given by Equations (4-5b) and (4-5c) respectively. Furthermore, Equations (4-8a) and (4-8b) describe the functional form of $q_b(x,0,z)$. Therefore, it can be stated that $q_0(x,z) = q_a(x,0,z) + q_b(x,0,z)$ and, after substitution of their functional forms, one obtains:

$$\sum_{m=0}^{\infty}\sum_{n=0}^{\infty} A_{mn}\cos(m\pi x/a_1)\cos(n\pi z/a_2) - \sum_{m=0}^{\infty}\sum_{n=0}^{\infty} B_{mn}\cos(m\pi x/a_1)\cos(n\pi z/a_2)$$
$$= \sum_{m=0}^{\infty}\sum_{n=0}^{\infty} D_{mn}\cos(m\pi x/a_1)\cos(n\pi z/a_2) \tag{4-14a}$$

Then, according to the orthogonality condition, this equation requires to have

$$A_{mn} - B_{mn} = D_{mn}. \tag{4-14b}$$

Physically, the integration of $q_b(x,0,z)$, as given by Eq. (4-8a), over the contact area

$$\sum_{m=0}^{\infty}\sum_{n=0}^{\infty} \int_0^{a_2}\int_0^{a_1} B_{mn}\cos(m\pi x/a_1)\cos(n\pi z/a_2)dxdz = B_{00}a_1a_2 \tag{4-14c}$$

represents the total heat flux that must be equal to zero since all other surfaces are insulated and there is no volumetric heat source. Therefore, the coefficient $B_{00} = 0$ and this makes $A_{00} = D_{00}$ and A_{00} has a known value, as given by Eq. (4-5b).

These relations suggest that the determination of the unknown coefficients A_{mn} require the solution of *N* simultaneous equations. First, consideration is given to a two-dimensional system, depicted in Figure 4-1(b), and a numerical example. Then, the solution for three-dimensional problems is applied to a numerical example.

4.4 Two-Dimensional Systems

Consider a two-dimensional case wherein $a = a_1,\ c = c_1,\ \varepsilon = \varepsilon_1,\ a_2 = c_2$, and $\varepsilon_2 = 0$. Next, after needed simplification, the parameter D_m has known values and each B_m depends on all A_m parameters, which produces *N* equations for *N* unknowns; where, *N* is an arbitrarily selected number of eigenvalues for a desired accuracy. Accordingly, one can select a modified form of Eq. (8b) in two-dimensional space to get

$$\frac{B_m}{\left(\frac{2\pi k_1}{a^2}\right) m \tanh(m\pi b/a)} = \int_{x=0}^{a} T_0(x)\cos(m\pi x/a)\,dx \qquad (4\text{-}15)$$

wherein the function $T_0(x)$, as given by Eq. (4-11), takes the following form

$$T_0(x) = 2\sum_{n=0}^{\infty} \Phi_n \cos\left(\frac{n\pi(x+\varepsilon)}{c}\right) \int_{\varepsilon}^{\varepsilon+a} \frac{-q_0(\xi-\varepsilon)}{k_2} \cos\left(\frac{n\pi\xi}{c}\right) d\xi \qquad (4\text{-}16a)$$

where

$$\Phi_n = \left(\frac{d}{c} + \frac{1}{Bi}\right) \text{ when } n=0 \qquad (4\text{-}16b)$$

and

$$\Phi_n = \frac{\cosh\left(\frac{n\pi d}{c}\right) + \frac{Bi}{n\pi}\sinh\left(\frac{n\pi d}{c}\right)}{(n\pi)\sinh\left(\frac{n\pi d}{c}\right) + Bi\cosh\left(\frac{n\pi d}{c}\right)} \text{ when } n>0 \qquad (4\text{-}16c)$$

After substitution for $q_0(x)$, as given by Eq. (4-12) in Eq. (4-16a), the function $T_0(x)$ takes the form

$$T_0(x) = \frac{-2}{k_2}\sum_{n=0}^{\infty} \Phi_n \cos\left(\frac{n\pi(x+\varepsilon)}{c}\right)\sum_{j=0}^{\infty} A_j \int_{\varepsilon}^{\varepsilon+a} \cos\left(\frac{n\pi\xi}{c}\right)\cos\left(\frac{j\pi(\xi-\varepsilon)}{a}\right) d\xi \quad (4\text{-}17)$$

Now, one can define a new parameter P_{nj} as

$$\begin{aligned} P_{nj} &= \int_{\varepsilon}^{c-\varepsilon} \cos\left(\frac{n\pi\xi}{c}\right)\cos\left(\frac{j\pi(\xi-\varepsilon)}{a}\right) d\xi \\ &= \Psi\left(\frac{n\pi\xi}{c}, \frac{j\pi\xi}{a}, \varepsilon\right)\Big|_{\xi=\varepsilon}^{\varepsilon+a} \end{aligned} \quad (4\text{-}18a)$$

where the integral in this equation takes the forms

$$\Psi\left(\frac{n\pi\xi}{c}, \frac{j\pi\xi}{a}, \varepsilon\right) = \begin{cases} a & \text{when} \quad n = j = 0 \\ \dfrac{\xi\cos(\varepsilon n\pi/c)}{2} - \dfrac{c\sin[n\pi(\varepsilon-2\xi)/c]}{4n\pi} & \text{when} \quad n/c = j/a \end{cases} \quad (4\text{-}18b)$$

Otherwise,

$$\begin{aligned} \Psi\left(\frac{n\pi\xi}{c}, \frac{j\pi\xi}{a}, \varepsilon\right) = &\frac{\sin[\varepsilon j\pi/a + (n\pi/c - j\pi/a)\xi]}{2(n\pi/c - j\pi/a)} \\ &- \frac{\sin[\varepsilon j\pi/a - (n\pi/c + j\pi/a)\xi]}{2(n\pi/c + j\pi/a)} \end{aligned} \quad (4\text{-}18c)$$

This equation describes three separate solutions. Therefore, modified and simpler forms of this equation are needed when $n = j = 0$ and when $n/c = j/a$. This leads to the temperature solution at the contact surface as

$$\begin{aligned} T_0(x) &= \frac{-2}{k_2}\sum_{n=0}^{\infty} \Phi_n \cos\left(\frac{n\pi(x+\varepsilon)}{c}\right)\sum_{j=0}^{\infty} A_j P_{nj} \\ &= \frac{-2}{k_2}\sum_{j=0}^{\infty} A_j \sum_{n=0}^{\infty} \Phi_n \cos\left(\frac{n\pi(x+\varepsilon)}{c}\right) P_{nj} \end{aligned} \quad (4\text{-}19)$$

and then the coefficient B_m as given in Eq (4-15) becomes

$$B_m = \frac{-4\pi m k_1}{a^2 k_2} \tanh\left(\frac{m\pi b}{a}\right) \sum_{j=0}^{\infty} A_j \sum_{n=0}^{\infty} \Phi_n P_{nj} H_{mn} \tag{4-20}$$

wherein the function H_{mn} is determined and it becomes

$$\begin{aligned} H_{mn} &= \int_0^a \cos\left(\frac{m\pi x}{a}\right) \cos\left(\frac{n\pi(x+\varepsilon)}{c}\right) dx \\ &= \Psi\left(\frac{m\pi x}{a}, \frac{n\pi x}{c}, -e\right)\Big|_0^a \end{aligned} \tag{4-21a}$$

and

$$\Psi\left(\frac{m\pi\xi}{a}, \frac{n\pi\xi}{c}, -e\right) = \begin{cases} a & \text{when} \quad n = j = 0 \\ \dfrac{x\cos(\varepsilon m\pi/a)}{2} + \dfrac{a\sin[m\pi(\varepsilon+2x)/a]}{4m\pi} & \text{when} \quad m/a = n/c \end{cases} \tag{4-21b}$$

Otherwise,

$$\begin{aligned} \Psi\left(\frac{m\pi\xi}{a}, \frac{n\pi\xi}{c}, -e\right) &= \frac{\sin[\varepsilon n\pi/c + (n\pi/c - m\pi/a)x]}{2(n\pi/c - m\pi/a)} \\ &+ \frac{\sin[\varepsilon n\pi/c + (n\pi/c + m\pi/a)x]}{2(n\pi/c + m\pi/a)} \end{aligned} \tag{4-21c}$$

Similar to Eq. (4-18a,b), the form of this equation is modified when $m = n = 0$ and when $n/c = m/a$. Accordingly, the form of constants B_m, as given by Eq. (4-20), reduces to take the following form

$$B_m = \sum_{j=0}^{\infty} \beta_{mj} A_j \tag{4-22a}$$

where,

$$\beta_{mj} = -\frac{4\pi m k_1}{a^2 k_2} \tanh\left(\frac{m\pi b}{a}\right) \sum_{n=0}^{\infty} \Phi_n P_{nj} H_{mn} \tag{4-22b}$$

and it is analytically deterministic for *N* unknown coefficients. Additionally, the reduced form of Eq. (4-5c) yields the coefficient D_m for this application as

$$D_0 = \frac{1}{a} \int_{x=0}^{a} q_w(x) dx \text{ when } m=0 \tag{4-23a}$$

and

$$D_m = \frac{2}{a} \int_{x=0}^{a} \frac{q_w(x) \cos(m\pi x / a)}{[\cosh(n\pi b / a) + Rk_1 \sinh(n\pi b / a)]} dx \text{ when } m> \tag{4-23b}$$

As stated earlier $A_0 = D_0$ and it has a known value. Then, selecting a finite number of terms, *N*, the coefficients A_j for this two-dimensional case are needed to get the surface heat flux $q_0(x)$ as,

$$\begin{aligned} q_0(x) &= \sum_{n=0}^{N} A_m \cos(m\pi x / a_1) \\ &= D_0 + \sum_{n=1}^{N} A_m \cos(m\pi x / a_1) \end{aligned} \tag{4-24}$$

Next, Eq. (4-14b) for this two-dimensional case takes the form

$$A_m - \sum_{j=0}^{N} \beta_{mj} A_j = D_m \tag{4-25a}$$

and after setting $A_0 = D_0$, it becomes

$$A_m - \sum_{j=1}^{N} \beta_{mj} A_j = D_m + \beta_{m0} D_0 \tag{4-25b}$$

As a test case, when *N*=4, this equation for *m*=1, 2, 3, and 4 leads to four equations with four unknowns,

$$\begin{aligned} A_1 - (\beta_{11}A_1 + \beta_{12}A_2 + \beta_{13}A_3 &= D_1 + D_0\beta_{10} \quad \text{when } m=1 \\ A_2 - (\beta_{21}A_1 + \beta_{22}A_2 + \beta_{23}A_3 &= D_2 + D_0\beta_{20} \quad \text{when } m=2 \\ A_3 - (\beta_{31}A_1 + \beta_{32}A_2 + \beta_{33}A_3 &= D_3 + D_0\beta_{30} \quad \text{when } m=3 \\ A_4 - (\beta_{41}A_1 + \beta_{42}A_2 + \beta_{43}A_3 &= D_4 + D_0\beta_{40} \quad \text{when } m=4 \end{aligned} \tag{4-26a}$$

In this illustration, these equations for determination of A_m coefficients have a matrix form,

$$\left(\begin{bmatrix} 1 & 0 & 0 & 0 \\ 0 & 1 & 0 & 0 \\ 0 & 0 & 1 & 0 \\ 0 & 0 & 0 & 1 \end{bmatrix} - \begin{bmatrix} \beta_{11} & \beta_{12} & \beta_{13} & \beta_{14} \\ \beta_{21} & \beta_{22} & \beta_{23} & \beta_{24} \\ \beta_{31} & \beta_{32} & \beta_{33} & \beta_{34} \\ \beta_{41} & \beta_{42} & \beta_{43} & \beta_{44} \end{bmatrix} \right) \begin{bmatrix} A_1 \\ A_2 \\ A_3 \\ A_4 \end{bmatrix} = \begin{bmatrix} D_1 \\ D_2 \\ D_3 \\ D_4 \end{bmatrix} + D_0 \begin{bmatrix} \beta_{10} \\ \beta_{20} \\ \beta_{30} \\ \beta_{40} \end{bmatrix} \tag{4-26b}$$

The above equation takes the abbreviated form

$$([I]-[B])\cdot[A]=[D]+D_0[B_0] \tag{4-27}$$

where [I] is the identity matrix. Following a matrix inversion, a vector representing the unknown coefficients becomes

$$[A]=([I]-[B])^{-1}\cdot([D]+D_0[B_0]) \tag{4-28}$$

Once the vector [A] is known, the heat flux and then temperature values become deterministic. The value of $q_0(x)$ is readily available by using Eq. (4-12) while the value of $T_0(x)$ is obtainable from Eq. (19). Then, Eq. (7b) provides the temperature $T_b(x,y)$ for the computation of $T_1(x,y)=T_a(x,y)+T_b(x,y)$ and Eq. (4-10) yield the temperature $T_2(\xi,\eta)$ in Layer 2, by using

$$q_2(\xi,d)=\begin{cases} q_0(\xi-\varepsilon) & \text{when } \varepsilon \le \xi \le \varepsilon + a \\ 0 & \text{when } \xi < \varepsilon \text{ and } \xi > \varepsilon + a \end{cases}$$

Further details related to the method of determination of vector [A] are included in the following numerical example. Also, the data exhibit the convergence behaviors of $T_1(x, y)$ and $T_2(\xi,\eta)$ functions.

Numerical example 1. Consideration is given to a two-layer body with different form factors place so that $\varepsilon = (c-a)/2$. Having *b* as the characteristic length, the other dimension of Layer 1 is $a = 2b$. The heat flux q_w is considered to be a constant between *x*=*a*/4 to *a*/2 and between *x*=3*a*/4 to *a*. The second layer, as depicted in Figure 4-1(a), has dimensions $c = 5b$ and, $d = b$; this makes $\varepsilon = (c-a)/2 = 3b/2$. By assuming k_1 to have an arbitrarily selected value, the other properties are being selected so that $k_2 = 4k_1$ and the Biot number is $Bi = hc/k_2 = 20$. This will permit the examination of this numerical procedure and the accuracy of temperature values.

Solution. First, Equation (4-28) provides the coefficients A_n for insertion in Eq. (4-12) in order to determine the specified heat flux, $q_0(x)$. A sample of computed heat flux, $q_0(x)/q_w$, values is in Table 4-1 and a plot is in Figure 4-2. Also, the heat flux contribution $q_b(x,0)$ is plotted in the same figure and shows similar convergence. The acquired heat flux data for $N = 200$ and $N = 500$, plotted in Figure 4-2, clearly show the behaviors of these $q_0(x)/q_w$ and $q_b(x,0)/q_w$ functions. Although the data agree well graphically, their deviations are relatively large near $x = 0$ and $x = a$. This is demonstrated in Figure 4-3 that contains the differences within the computed values. The $q_0(x)/q_w$ data when $N = 200$ are subtracted from those for $N = 500$ and the difference is plotted as a solid line in Figure 4-3. The process is repeated subtracting data for $N = 100$ and they are also subtracted from those for $N = 500$; the results are plotted as a

dot-dash line in Figure 4-3. These plotted data clearly show that the error in surface heat flux is of the order of $1/N$ and it reduces as *N* increases. Furthermore, Figure 4-3 clearly shows relatively larger deviations near $x = 0$ and $x = a$.

Table 4-1 Computed specified function $q_0(x)/q_w$ along the contact surface at *y*=0.

	$q_0(x)/q_w$				
x/b	*N*=20	*N*=50	*N*=100	*N*=200	*N*=500
0.0	-0.58636	-0.67738	-0.76256	-0.86345	-1.02422
0.1	-0.45023	-0.44204	-0.44838	-0.44719	-0.44410
0.2	-0.41035	-0.42336	-0.42402	-0.42207	-0.42069
0.3	-0.40362	-0.40688	-0.41590	-0.41710	-0.41519
0.4	-0.42430	-0.42369	-0.42146	-0.42016	-0.41925
0.5	-0.42735	-0.42503	-0.42573	-0.42734	-0.42568
0.6	-0.44030	-0.43500	-0.43767	-0.43657	-0.43581
0.7	-0.43677	-0.44224	-0.44478	-0.44654	-0.44496
0.8	-0.45541	-0.45932	-0.45755	-0.45652	-0.45581
0.9	-0.46182	-0.46311	-0.46451	-0.46631	-0.46476
1.0	-0.48324	-0.47429	-0.47712	-0.47610	-0.47539
1.1	-0.48235	-0.48367	-0.48458	-0.48635	-0.48479
1.2	-0.49626	-0.50052	-0.49865	-0.49758	-0.49684
1.3	-0.49943	-0.50473	-0.50851	-0.51018	-0.50856
1.4	-0.52768	-0.52307	-0.52551	-0.52430	-0.52346
1.5	-0.54119	-0.53759	-0.53845	-0.53989	-0.53813
1.6	-0.56149	-0.56108	-0.55846	-0.55694	-0.55588
1.7	-0.55977	-0.56252	-0.57518	-0.57602	-0.5739
1.8	-0.58299	-0.60294	-0.60250	-0.60004	-0.5983
1.9	-0.64900	-0.63517	-0.64532	-0.64282	-0.63901
2.0	-0.82659	-0.94851	-1.06315	-1.19950	-1.41767

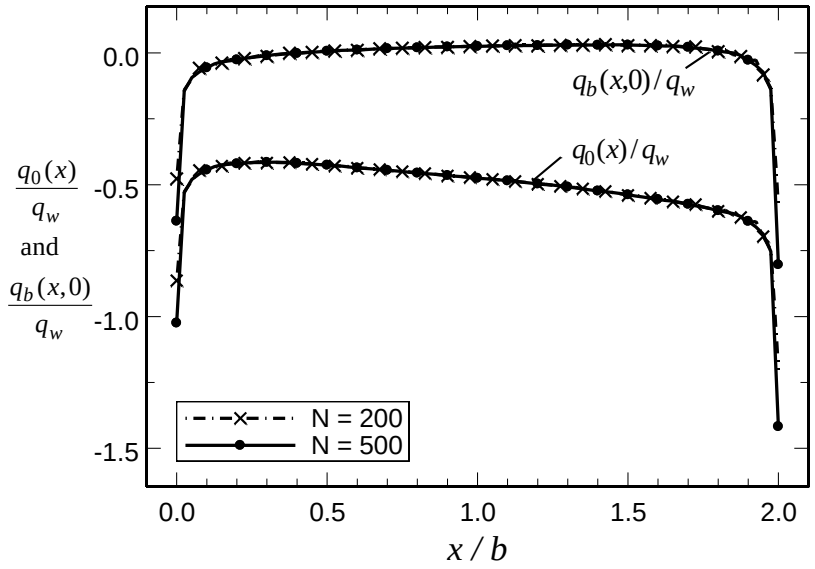

Figure 4-2 The computed specified function $q_0(x)$ using 200, and 500 eigenvalues.

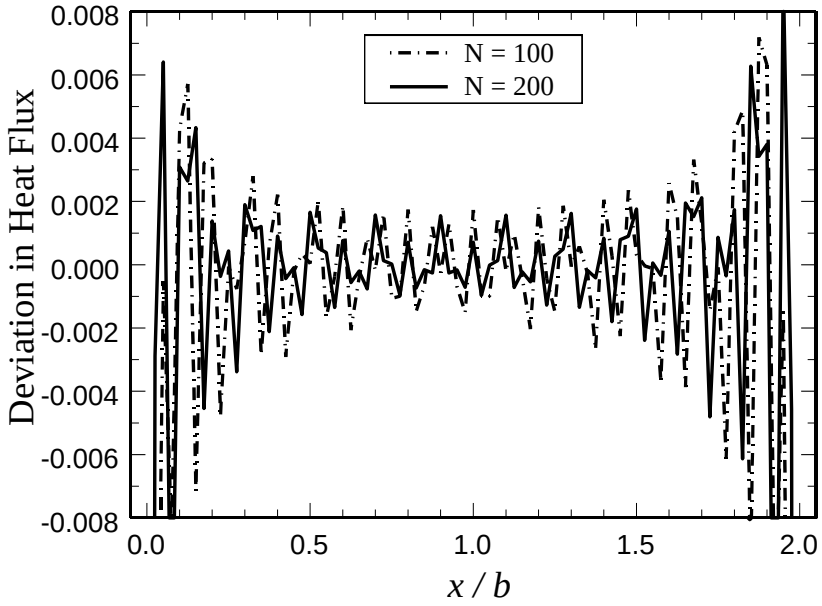

Figure 4-3 The computed deviation as the number of eigenvalues changes.

Figure 4-4 is prepared to show the computed heat flux over $\eta = d$ surface that contains the temperature values along the contacting surfaces. The plotted temperature

data are extremely well behaved. A sample of acquired data is tabulated for different *N* values in Table 4-2. They clearly show that small differences, of the order of $1/N^2$. Figure 4-5 shows the computed dimensionless temperature along *y=b* surface. As in the previous case, these plotted data are well behaved and a sample of acquired data is in Table 4-3. These data also clearly show that their deviations reduce as *N* increases and it is of the order of $1/N^2$.

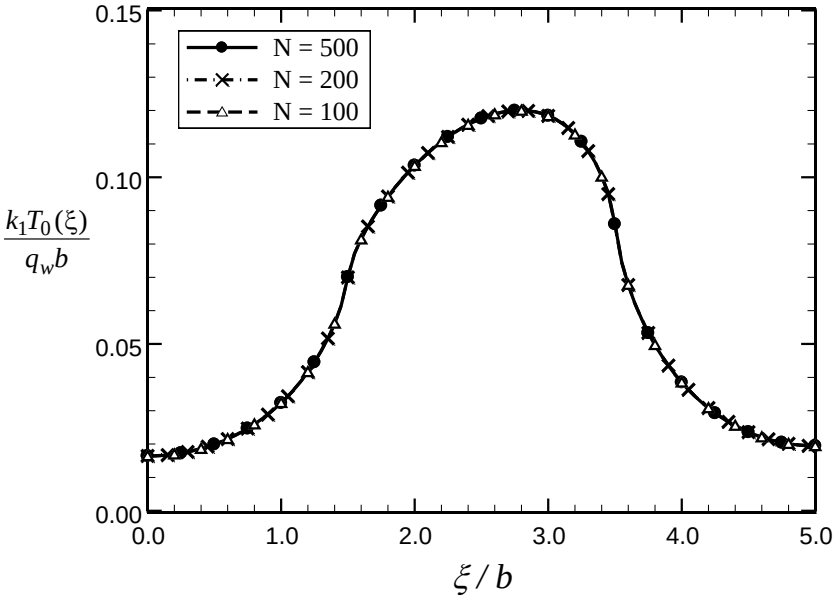

Figure 4-4 The dimensionless temperature along the contacting surfaces.

Table 4-2 Computed values of $k_1 T_2(\xi, d)/(q_w b)$ by different number of terms in series.

	$k_1 T_2(\xi, d)/(q_w b)$				
ξ/b	N=20	N=50	N=100	N=200	N=500
0.0	0.016724	0.016371	0.016446	0.016433	0.016429
0.2	0.016723	0.016909	0.016985	0.016972	0.016968
0.4	0.018782	0.018565	0.018645	0.018631	0.018626
0.6	0.021565	0.021472	0.021559	0.021544	0.021539
0.8	0.025749	0.025884	0.025984	0.025967	0.025961
1.0	0.032837	0.032253	0.032379	0.032357	0.032349
1.2	0.040837	0.041449	0.041635	0.041602	0.041590
1.4	0.057640	0.055780	0.056186	0.056106	0.056077
1.6	0.080519	0.081871	0.081443	0.081525	0.081553
1.8	0.094779	0.094373	0.094217	0.094247	0.094256
2.0	0.102977	0.103570	0.103475	0.103494	0.103500
2.2	0.110863	0.110671	0.110598	0.110614	0.110618
2.4	0.115619	0.115826	0.115760	0.115774	0.115779
2.6	0.118780	0.119019	0.118949	0.118964	0.118969
2.8	0.120336	0.120101	0.120016	0.120034	0.120039
3.0	0.117805	0.118537	0.118416	0.118440	0.118448
3.2	0.113623	0.113080	0.112871	0.112910	0.112923
3.4	0.098965	0.100854	0.100263	0.100376	0.100415
3.6	0.069896	0.067244	0.067830	0.067716	0.067674
3.8	0.048582	0.049482	0.049753	0.049705	0.049689
4.0	0.039238	0.038337	0.038522	0.038490	0.038479
4.2	0.030459	0.030697	0.030845	0.030819	0.030811
4.4	0.025598	0.025432	0.025560	0.025538	0.025531
4.6	0.022294	0.021973	0.022091	0.022070	0.022064
4.8	0.019714	0.020006	0.020118	0.020099	0.020092
5.0	0.019918	0.019367	0.019477	0.019458	0.019452

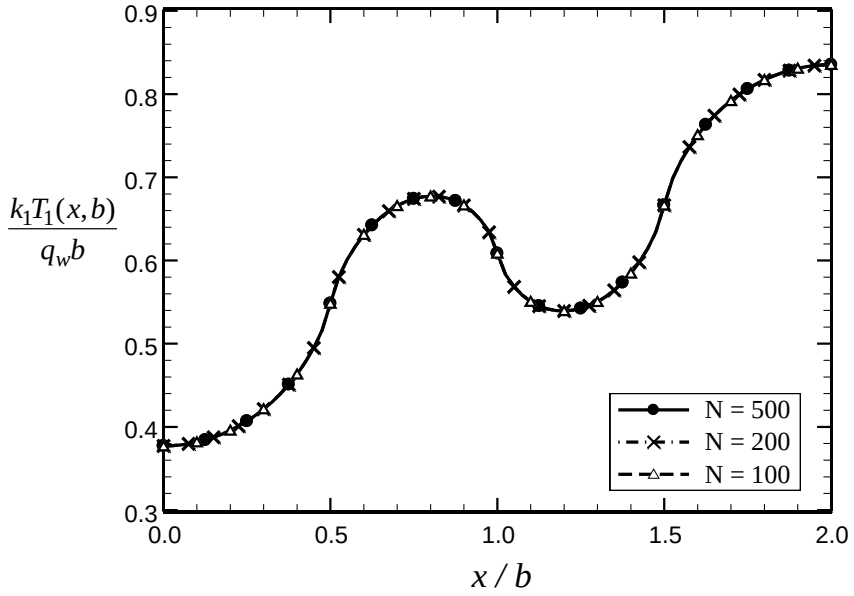

Figure 4-5 The dimensionless temperature over the heated surface of the first layer.

Table 4-3 Computed temperature at the heated locations where *y=b*.

	$k_1 T_1(x)/(q_w b)$				
x/b	*N*=20	*N*=50	*N*=100	*N*=200	*N*=500
0.0	0.37506	0.37719	0.37704	0.37713	0.37712
0.1	0.38347	0.38168	0.38174	0.38167	0.38168
0.2	0.39351	0.39568	0.39571	0.39581	0.39581
0.3	0.42379	0.42119	0.42148	0.42139	0.42139
0.4	0.45974	0.46355	0.46318	0.46339	0.46336
0.5	0.54937	0.5482	0.54834	0.54830	0.54831
0.6	0.63185	0.63069	0.63103	0.63092	0.63097
0.7	0.66566	0.66600	0.66566	0.66564	0.66567
0.8	0.67624	0.67758	0.67728	0.67731	0.67733
0.9	0.66834	0.66595	0.66643	0.66628	0.66633
1.0	0.60840	0.60851	0.60852	0.60853	0.60853
1.1	0.54836	0.55096	0.55051	0.55066	0.55063
1.2	0.54015	0.53902	0.53935	0.53933	0.53932
1.3	0.55022	0.55011	0.55048	0.55051	0.55049
1.4	0.58340	0.58479	0.58449	0.58460	0.58457
1.5	0.66516	0.66658	0.66647	0.66653	0.66653
1.6	0.75406	0.75051	0.75092	0.75072	0.75076
1.7	0.78934	0.79222	0.79196	0.79206	0.79208
1.8	0.81907	0.81719	0.81720	0.81711	0.81713
1.9	0.82876	0.83084	0.83083	0.83090	0.83092
2.0	0.83705	0.83522	0.83541	0.83533	0.83535

Numerical example 2. In this example, consideration is given to a similar two-layer body as in the previous example, having $a_1 = a_2 = a$ and $c_1 = c_2 = c$. However, the form factors are rectangular in shape and temperature has a three-dimensional solution. To acquire a three-dimensional condition, the heat sources are located as given in Example 1 except for the z-direction. Accordingly, the heating sites are extended from $z = 0 \rightarrow a$ to become within $z = a/8$ to $z = 7a/8$. Furthermore, a contact resistance $R=2b/k_1$ is added to the interface condition.

Solution. As in the 2-D case, the insertion of $T_0(x,z)$ from Eq. (4-19) into Eq. (4-8a,b) provides *N* equations for *N* unknowns. The selected parameters are the same as those in Example 1 except the applied heat flux makes the temperature solution a 3-D problem. Using 100 eigenvalues for each direction, the size of matrix becomes very large. For this reason this example is used to test the acquisition of A_{mn} coefficients by an iterative technique, as presented in [4-19]. The test was successful and it provided a rapid solution. It begins by setting $B_{mn}=0$ and using the relation $A_{nm}=B_{mn}+D_{mn}$ to calculate A_{mn}. Next, using Eq. (4-11) and Eq. (4-8b) provides a new set of B_{mn} for insertion in the relation $A_{nm}=B_{mn}+D_{mn}$ for a new set of A_{mn} values. Table 4-4 shows the first 15 A_{mn} coefficients from a relatively large number of computed values, when the indices *m* and *n* change between 0 and 50. Only three to five iterations can produce satisfactory solutions while seven and 10 iterations show accurate results. As an illustration, the computed temperature data are plotted in Figure 4-6. To show the accuracy of the acquired data, the temperature values along a line going from the point $(0,b,a/2)$ to the point $(a,b,a/2)$ are presented in Table 4-5. The computed data show very rapid convergence and only a few iteration produces highly accurate results. The last column in Table 4-5 contains numerically acquired data using ANSYS. The temperature data obtained numerically are in excellent agreement with those computed analytically, in column 6 of Table 4-5. Two contour plots of the temperature data are depicted in Figure 4-7(a,b) while the corresponding heat flux data are graphically presented in Figure 4-8.

Table 4-4 Computed A_{mn} coefficients of heat flux $q_0(x,z)$ by an iterative technique.

			A_{mn}				
m	*n*	D_{mn}	1 Iteration	3 Iterations	5 Iterations	7 Iterations	10 Iterations
0	0	-0.375	-0.375	-0.375	-0.375	-0.375	-0.375
1	0	0.0203074	0.0197024	0.0196291	0.0196283	0.0196283	0.0196283
2	0	0	-0.0033979	-0.0038378	-0.0038438	-0.0038438	-0.0038438
3	0	0.0006623	0.0007220	0.00072753	0.00072756	0.00072756	0.00072756
4	0	0	-0.0013315	-0.0015258	-0.0015290	-0.0015291	-0.0015291
0	2	0.0026746	-0.0007841	-0.0012319	-0.0012379	-0.0012380	-0.001238
1	2	-0.000883	-0.0007580	-0.0007450	-0.0007449	-0.0007449	-0.0007449
2	2	0	0.0006584	0.00072288	0.00072319	0.00072319	0.00072319
3	2	-0.00013	-0.0001416	-0.0001423	-0.0001423	-0.0001423	-0.0001423
4	2	0	0.0002309	0.00025664	0.00025685	0.00025685	0.00025685
0	4	4.382E-05	-0.0012836	-0.0014773	-0.0014806	-0.0014806	-0.0014806
1	4	-1.85E-05	3.047E-05	0.00003585	3.5898E-05	3.5899E-05	3.5899E-05
2	4	0	0.0002255	0.00025065	0.00025086	0.00025086	0.00025086
3	4	-7.58E-06	-1.271E-05	-1.313E-05	-1.313E-05	-1.313E-05	-1.313E-05
4	4	0	9.741E-05	0.00011029	0.00011046	0.00011046	0.00011046

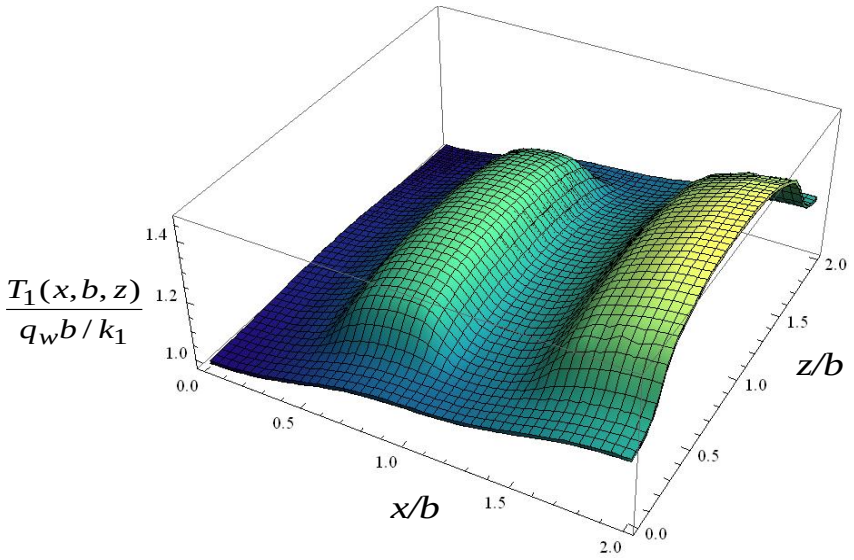

Figure 4-6 Computed temperature values over *y=b* surface as a function of *x/b* and *z/b* when Rk_1/b=2, for Example 2.

Table 4-5 Computed $k_1T_1 / q_w b$ along a line when *y*=*b* and $z = a/2$.

x/b	$k_1T_a / q_w b$	$k_1T_1 / q_w b$				
		1 Iteration	2 Iterations	3 Iterations	5 Iterations	ANSYS
0	1.01191	1.01181	1.01180	1.01180	1.01180	1.0118
0.2	1.02970	1.02961	1.02959	1.02959	1.02959	1.0296
0.4	1.09589	1.09579	1.09578	1.09577	1.09577	1.0957
0.6	1.26145	1.26135	1.26134	1.26134	1.26134	1.2614
0.8	1.30748	1.30738	1.30736	1.30736	1.30736	1.3072
1.0	1.23849	1.23839	1.23837	1.23837	1.23837	1.2385
1.2	1.16946	1.16935	1.16934	1.16934	1.16934	1.1693
1.4	1.21538	1.21527	1.21526	1.21526	1.21526	1.2152
1.6	1.38081	1.38070	1.38069	1.38068	1.38068	1.3807
1.8	1.44688	1.44677	1.44676	1.44675	1.44675	1.4466
2.0	1.46463	1.46452	1.46451	1.46451	1.46451	1.4646

Temperature Distribution Contour using ANSYS Workbench

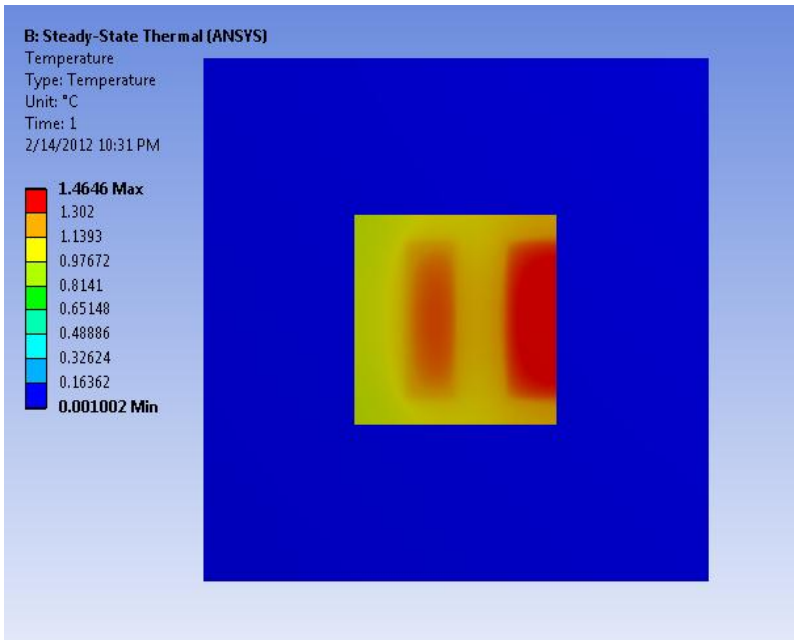

(a)

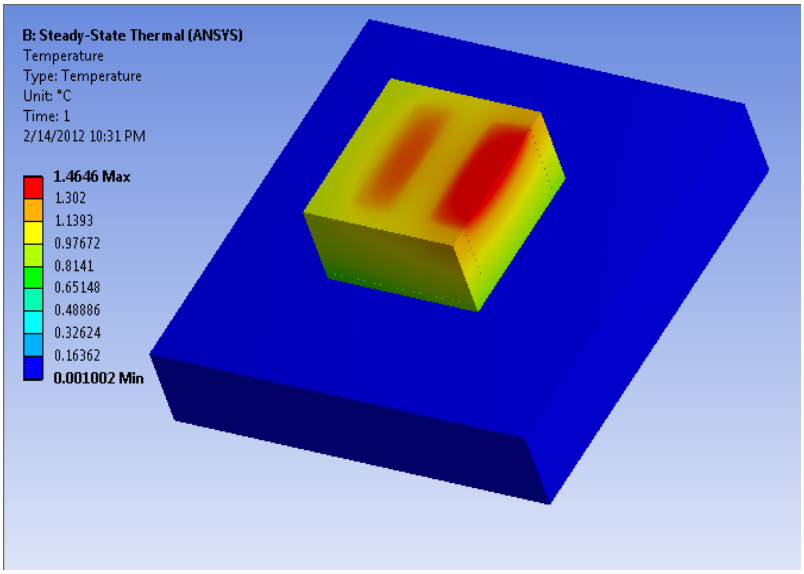

(b)

Figure 4-7 (a) Temperature distribution contour using ANSYS workbench (top view), and (b) temperature distribution contour using ANSYS workbench (isometric view).

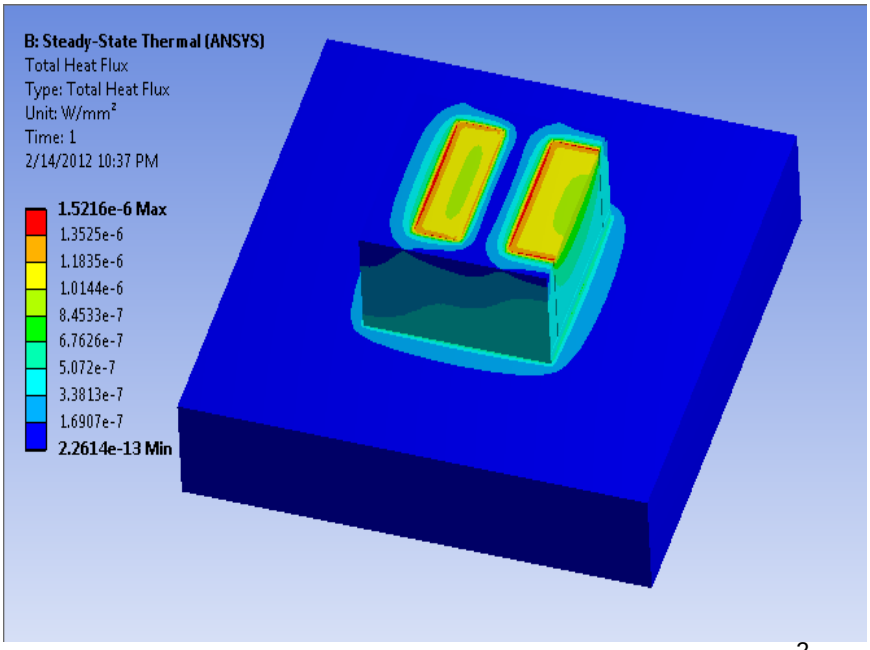

Figure 4-8 Graphical presentation of the total heat flux in W/mm^2.

4.5 Comments and Discussions

An examination of Eq. (4-5c) shows the convergence behavior of $q_a(x,0)$ that contributes to the specified function $q_0(x)$. It shows that Eq. (4-5a) converges very fast since the term $2/[a\cosh(n\pi b/a)]$ reduces exponentially. As an illustration, for *a*/*b*=2, this quantity takes the value of 3.0×10^{-7} when *n*=10 and it further reduces to become 1.2×10^{-10} when *n*=15; therefore, its convergence is not a major issue. Accordingly, the changes observed the values of $q_0(x)$ are mainly due to the uncertainty in determination $T_b(x,y)$ that is related to the function $T_0(\xi)=T_2(\xi,d)$.

The concept of this function specification method has been used for developing a numerical solution. This study presents a technique for analytical determination of the specified coefficients. If one selects the functional form of $q_0(x)$, as emerged from the

solution of $T_1(x,y) = T_a(x,y) + T_b(x,y)$, it is possible to analytically determine the coefficients A_n in Eq. (4-12). This task is accomplished using Eq. (4-22) and the computed temperature values are presented in Tables 4-2 and 4-3. The tabulated values of $T_2(\xi, d)$ in Table 4-2 and $T_1(x,b)$ in Table 4-3 show expected behaviors and it is possible to acquire reasonably accurate solutions for practical applications.

This presents a verification tool that allows the exact values of the coefficients to be obtained iteratively for related applications. It permits a view of the convergence behavior of the iterative technique that can be used for three-dimensional cases. This procedure is reasonably simple if the matrix is of a reasonable size. This is the primary reason for selecting a two-dimensional multi-layer system.

If this matrix is very large, an iterative procedure is a reasonably fast technique for determination of these coefficients. The process of determining the coefficients can be modified by developing an iterative procedure. The iterative procedure begins be selecting estimated values of B_n; e. g., by setting $B_n = 0$. Since D_n coefficients have known values, Eq. (4-14b) provides A_n for insertion in Eq. (4-20) in order to get new values for B_n. This process can be repeated by inserting this new B_n. The first iteration begins by placing B_n into Eq. (4-14b) to get a new A_n and repeat the process by using Eq. (4-20) for determination of a new set of B_n values. This process is to be repeated for second, third, and other iterations. Often, about six iterations can produce results with reasonable accuracy. Observing the behaviors of the numerically acquired data shows that one can accelerate the convergence procedure by using a relaxation factor ω and selecting the new set A_n as

$$A_n\big|_{\text{new}} = (1-\omega)A_n\big|_{\text{old}} + \omega(D_n + B_n) \tag{4-26}$$

Preliminary test shows that having ω=~0.85 can reduce the number or iteration by about 40% for a predetermined accuracy.

4.6. Conclusion

The analytically obtainable temperature field can provide an accurate solution for the purpose of verification of a numerically acquired solution. This analytical procedure is reasonably fast if the matrix size is not very large. For matrices of large size, the A_n coefficients within Eq. (4-12) are obtainable rapidly by an iterative technique with a high degree of accuracy. This procedure was tested successfully within the previous example. The iteratively determined coefficients become a reasonably fast procedure when the conduction is three-dimensional. Also, the same procedure is applicable to a system when two multi-layer blocks replace both layers, in Figure 4-1(a,b).

Chapter 5

Inverse Estimation of Temperature between Plates of Different Footprints by an Iterative Approach

In this chapter, consideration is given to a simplified model mainly to study the performance of iterative analytical/numerical solutions to non-uniform footprints problems. The analytical procedure leads to an integral equation. Then, the heat flux and temperature at the interface are computed using an iterative inverse methodology. To verify the accuracy, selected data are compared to numerically determined values. Although the presented computational procedure is for a two-dimensional solution, the methodology equally applies to three-dimensional problems.

The adequate cooling improves the performance as it improves the speed of data execution. Numerical and theoretical studies as to determination of thermal performance are available in the literature. The related information and adequate citation of the related literature are in [62-66]. The analytical determination of temperature field in a two-layer system, as shown in Figure 5-1, is the objective of this work. This type of system can appear in different engineering application such as in electronic cooling devices. Plate 1, in Figure 5-1 can be viewed as a die with non-uniform power distribution. Plate 2 can be viewed as a heat spreader connected to a heat sink. Numerical studies of the related problems are in Kaisare et al. [67] which also contains details related to these types of devices.

The objective of this study is to examine a suitable inverse procedure for a relatively accurate determination of the temperature field in a multi-layer domain as shown in Figure 5-1. In practice, each of Layers 1 and 2 may contain two or more layers. However, for convenience of the presentation of this inverse methodology, Layer 1 and 2

are selected to be single layers as depicted in Figure 5-1. Additionally, the mathematical steps are presented for a two-dimensional case. The extension to three-dimensional case requires a minor modification, although the equations become a bit lengthy. In general, the mathematical procedure leads toward an integral equation to be solved by an inverse technique. Classical description of various inverse techniques is well documented in [68-71]. As an illustration, function specification and other techniques have been used to solve transient and steady-state inverse heat conduction problems by many investigators, e.g., see [72-77]. In this presentation, an iterative inverse procedure is selected for estimation of the temperature field and this becomes equivalent to the function specification method.

5.1 Mathematical Relations

This is to study the behavior of the temperature field within a two-layer body when each layer has a different size. The schematic of the region and the coordinate systems are in Figure 5-1. The governing equations for steady-state heat conduction satisfy the Laplace equations

$$\frac{\partial^2 T_j}{\partial x^2}+\frac{\partial^2 T_j}{\partial y^2}+\frac{\partial^2 T_j}{\partial z^2}=0 \tag{5-1}$$

with *j*=1 in regin1 and *j*=2 in region 2. In subsequent analyses, the function T_j represents the reduced temperature so that $T_j=\theta_j-\theta_\infty$; where T_j is the physical temperature and θ_∞ is the temperature of surroundings. Consideration is given to insulated boundary conditions in *x*- and *z*-directions. Therefore, for convenience of properly demonstrating this presentation, a two-dimensional case is selected within the subsequent mathematical presentations.

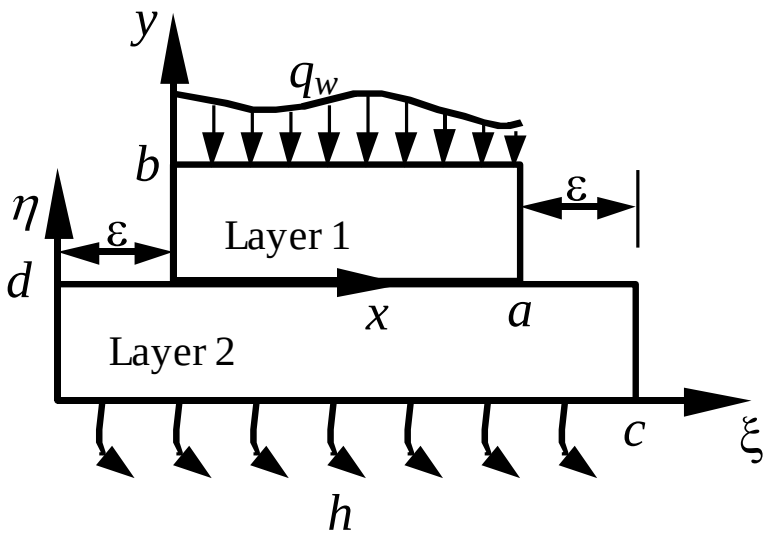

Figure 5-1 Schematic of a two-layer body and the coordinates.

Clearly, there are two temperature solutions: one for Layer 1 and the second one for Layer 2. These two solutions must satisfy the boundary conditions and the compatibility conditions between the two layers.

5.2 Temperature Solution in Layer 1

The temperature in Layer 1, designated as $T_1(x, y)$, must satisfy the Laplace equation

$$\frac{\partial^2 T_1}{\partial x^2} + \frac{\partial^2 T_1}{\partial y^2} = 0 \tag{5-2}$$

with boundary conditions:

(BC 1, 2) $q(0, y) = q(a, y) = 0$

(BC 3) $T_1(x,0) = T_0(x)$

(BC 4) $q(x, b) = q_w(x)$

This problem has two non-homogeneous boundary conditions; therefore, it is to be decomposed into two problems by selecting $T_1(x, y) = T_a(x, y) + T_b(x, y)$. Then, each of these problems has three homogeneous boundary conditions and a single non-homogeneous boundary condition.

The first problem requires the solution of equation

$$\frac{\partial^2 T_a}{\partial x^2} + \frac{\partial^2 T_a}{\partial y^2} = 0 \tag{5-3}$$

with boundary conditions:

(BC 1, 2) $q_a(0, y) = q_a(a, y) = 0$

(BC 3) $T_a(x,0) = 0$

(BC 4) $q_a(x,b) = q_w(x)$

This is a classical steady-state heat conduction problem. A solution that satisfies the differential equation and the homogeneous boundary conditions 1, 2, and 3 is

$$T(x, y) = A_0 y + \sum_{n=1}^{\infty} A_n \cos(n\pi x / a) \sinh(n\pi y / a) \tag{5-4}$$

Next, using the fourth boundary condition (BC 4), one obtains a relation

$$\begin{aligned} q_w(x) &= -k_1 [\partial T(x, y) / \partial y]_{y=b} \\ &= -k_1 \left[A_0 + \sum_{n=1}^{\infty} A_n \cos(n\pi x / a)(n\pi / a) \cosh(n\pi b / a) \right] \end{aligned} \tag{5-5}$$

Then, an application of the orthogonality condition produces

$$A_0 = \frac{1}{a} \int_{x=0}^{a} \frac{-q_w(x)}{k_1} dx \tag{5-6a}$$

and

$$A_n = \left(\frac{2}{n\pi \cosh(n\pi b/a)} \right) \int_{x=0}^{a} \frac{-q_w(x)}{k_1} \cos(n\pi x/a) dx \text{ when } n > 0 \qquad (5\text{-}6b)$$

and the temperature solution becomes

$$T_a(x,y) = \frac{y}{a} \int_{x=0}^{a} \frac{-q_w(x)}{k_1} dx + 2\sum_{n=1}^{\infty} \left(\frac{\cos(n\pi x/a)\sinh(n\pi y/a)}{n\pi \cosh(n\pi b/a)} \right) \times \int_{x=0}^{a} \frac{-q_w(x)}{k_1} \cos(n\pi x/a) dx \qquad (5\text{-}7)$$

After determination of temperature field, the heat flux at *y*=0 surface, defined as $q_a(x,0) = -k_1 \partial T_a(x,y)/\partial y|_{y=0}$, becomes

$$q_a(x,0) = \frac{1}{a} \int_{x=0}^{a} q_w(x) dx + \frac{2}{a} \sum_{n=1}^{\infty} \left(\frac{\cos(n\pi x/a)}{\cosh(n\pi b/a)} \right) \int_{x=0}^{a} q_w(x) \cos(n\pi x/a) dx \qquad (5\text{-}8)$$

The second problem is to solve for $T_b(x,y)$ that satisfies the Laplace equation

$$\frac{\partial^2 T_b}{\partial x^2} + \frac{\partial^2 T_b}{\partial y^2} = 0 \qquad (5\text{-}9)$$

with boundary conditions:

(BC 1, 2) $q_b(0,y) = q_b(a,y) = 0$

(BC 3) $T_b(x,0) = T_0(x)$

(BC 4) $q_b(x,b) = 0$

A solution that satisfies the differential equation and the non-homogeneous boundary conditions 1, 2, and 4 is

$$T_b(x,y) = \sum_{n=0}^{\infty} B_n X_n(x) \left[\frac{\cosh[\gamma_n (b-y)]}{\cosh(\gamma_n b)} \right] \tag{5-10}$$

The function $X_n(x)$ satisfies the condition $X_n''(x)/X(x) = -\gamma_n^2$ and the boundary conditions at *x*=0 and *x*=*a*. Next, the non-homogeneous boundary condition (BC 3), at y=0 obtainable from the temperature solution in the Layer 2, has the form

$$T_0(x) = \sum_{n=0}^{\infty} C_n X_{2,n}(x) \tag{5-11}$$

The needed interface temperature, $T_0(x)$, is obtainable by using the compatibility condition with Layer 2. It is expected that the temperature $X_{2,n}(x)$ acquired from the temperature solution for Layer 2 will not satisfy the conditions (BC 1, 2) for $T_b(x,y)$ solution. Therefore, modifications are needed when $X_{2,n}(x)$ does not satisfy the insulated boundary conditions at *x*=0 and *x*=*a*. In this case, it is necessary to select $X_n(x) = \cos(n\pi x/x)$ in Eq. (5-10) and then an application of the orthogonality condition produces the constants

$$B_0 = \frac{1}{a} \int_{x=0}^{a} T_0(x)dx \text{ , when } n=0 \tag{5-12a}$$

and

$$B_n = \frac{2}{a} \int_{x=0}^{a} T_0(x)\cos(n\pi x/a)dx \text{ , when } n>0 \tag{5-12b}$$

After appropriate substitutions, the temperature solution takes the form

$$T_b(x,y)=\frac{1}{a}\int_{x=0}^{a}T_0(x)dx+\frac{2}{a}\sum_{n=1}^{\infty}\frac{\cos(n\pi x/a)\cosh[n\pi(b-y)/a]}{\cosh(n\pi b/a)}\times\int_{x=0}^{a}T_0(x)\cos(n\pi x/a)dx \tag{5-13}$$

It is to be noted that the heat flux vector in *x*-*y* plane has a zero value at (*x, y*)=(0, 0) and at (*x, y*)=(*a*, 0) locations. This also suggests that the functional form for $T_0(x)$, acquired from the solution of temperature field in Layer 2, is to be recalculated in accordance with Eqs. (5-12a,b). Next, the heat flux at *y*=0 surface, using the Fourier equation is $q_b(x,0)=-k_1\partial T_b(x,y)/\partial y|_{y=0}$, and it becomes

$$q_b(x,0)=\frac{2\pi k_1}{a^2}\sum_{n=1}^{\infty}n\cos(n\pi x/a)\tanh(n\pi b/a)\int_{x=0}^{a}T_0(x)\cos(n\pi x/a)dx \tag{5-14}$$

The function $q_b(x,0)$ is the unknown to be determined by using the functional form of $T_0(x)$ acquired from the temperature solution within Layer 2. Therefore, the function $q_b(x,0)$ is the primary unknown for determination of the heat flux across the contacting surface at $x=0$, since $q_0(x)=q_a(x,0)+q_b(x,0)$ while $q_a(x,0)$ has a known value. Having the function $q_0(x)$, the functional form of $T_0(x)$ could be estimated from the temperature solution $T_2(\xi,\eta)$ in Layer 2. Furthermore, once the functional $T_0(x)$ as given by Eq. (5-11) is available, Eq. (5-13) would serve as a transformation.

5.3 Temperature Solution in Layer 2

For convenience of this presentation, a new set of coordinates is selected using $\xi = \varepsilon + x$ and $\eta = y + d$ while $\varepsilon = (c-a)/2$, as shown in Figure 5-1. The temperature solution in the second layer also satisfies the Laplace equation

$$\frac{\partial^2 T_2}{\partial \xi^2} + \frac{\partial^2 T_2}{\partial \eta^2} = 0 \tag{5-15}$$

where $T_2 = T_2(\xi, \eta)$ must satisfy the boundary conditions

(BC 1, 2) $\quad q_2(0,\eta) = q_2(c,\eta) = 0$

(BC 3) $\quad \partial T_2(\xi,\eta)/\partial\eta\big|_{\eta=0} = (h/k_2)\, T_2(\xi,\eta)$

(BC 4) $\quad -k_2 \partial T_2(\xi,\eta)/\partial\eta\big|_{\eta=d} = q_2(\xi)$ which is $q_2(\xi,d) = q_0(\xi-\varepsilon)$.

The solution begins by using the classical separation technique that produces

$$\begin{aligned} T_2(\xi,\eta) = C_0\left[Bi\left(\frac{\eta}{c}\right)+1\right] + \sum_{m=1}^{\infty} C_m \cos\left(\frac{m\pi\xi}{c}\right) \\ \times\left[\cosh\left(\frac{m\pi\eta}{c}\right) + \frac{Bi}{m\pi}\sinh\left(\frac{m\pi\eta}{c}\right)\right] \end{aligned} \tag{5-16}$$

where $Bi = hc/k_2$. The fourth boundary condition, (BC 4), leads to the relation

$$\begin{aligned} q_2(\xi,d) = -k_2 \left.\frac{\partial T_2(\xi,\eta)}{\partial\eta}\right|_{\eta=d} = -C_0 k_2\left(\frac{Bi}{c}\right) \\ - k_2 \sum_{m=0}^{\infty} C_m \cos\left(\frac{m\pi\xi}{c}\right)\left[\left(\frac{m\pi}{c}\right)\sinh\left(\frac{m\pi d}{c}\right) + \frac{Bi}{c}\cosh\left(\frac{m\pi d}{c}\right)\right] \end{aligned} \tag{5-17a}$$

Next, the orthogonality condition leads to the values of C_m; that is,

$$C_0 = \frac{1}{N_0}\int_0^c \frac{q_2(\xi,d)}{k_2}\,d\xi \tag{5-17b}$$

with $N_0 = Bi$ and, when $m > 0$,

$$C_m = \frac{2}{N_m}\int_0^c \frac{-q_2(\xi,d)}{k_2}\cos\left(\frac{m\pi\xi}{c}\right)d\xi \tag{5-17c}$$

where N_m is the dimensionless norm equal to

$$N_m = (m\pi)\sinh\left(\frac{m\pi d}{c}\right) + Bi\cosh\left(\frac{m\pi d}{c}\right)$$

After substitution for C_m, the solution for temperature in Layer 2 is

$$\begin{aligned} T_2(\xi,\eta) = &\left[\int_\varepsilon^{c-\varepsilon} \frac{-q_2(\xi,d)}{k_2}\,d\xi\right]\left(\frac{\eta}{c}+\frac{1}{Bi}\right) + 2\sum_{m=1}^{\infty}\frac{1}{N_m}\cos\left(\frac{m\pi\xi}{c}\right) \\ &\times\left[\cosh\left(\frac{m\pi\eta}{c}\right)+\frac{Bi}{m\pi}\sinh\left(\frac{m\pi\eta}{c}\right)\right]\int_\varepsilon^{c-\varepsilon}\frac{-q_2(\xi,d)}{k_2}\cos\left(\frac{m\pi\xi}{c}\right)d\xi \end{aligned} \tag{5-18}$$

where $q_2(\xi,d) = 0$ when $0 < \xi < \varepsilon$ and $\varepsilon + a < \xi < c$; otherwise, $q_2(\xi,d) = q_0(x) = q_0(\xi-\varepsilon)$.

The determination of the unknown temperature over the contact surface, as given by Eq. (5-18) lead to the relation

$$\begin{aligned} T_0(x) = &\left[\int_\varepsilon^{c-\varepsilon} \frac{-q_0(\xi-\varepsilon)}{k_2}\,d\xi\right]\left(\frac{d}{c}+\frac{1}{Bi}\right) + 2\sum_{m=1}^{\infty}\frac{1}{N_m}\cos\left(\frac{m\pi(\varepsilon+x)}{c}\right) \\ &\times\left[\cosh\left(\frac{m\pi d}{c}\right)+\frac{Bi}{m\pi}\sinh\left(\frac{m\pi d}{c}\right)\right]\int_\varepsilon^{c-\varepsilon}\frac{-q_0(\xi-\varepsilon)}{k_2}\cos\left(\frac{m\pi\xi}{c}\right)d\xi \end{aligned} \tag{5-19}$$

wherein the unknown function $q_0(\xi-\varepsilon)=q_0(x)$ is obtainable from Eq.(5-8) and Eq. (5-14), since $q_0(x)=q_a(x,0)+q_b(x,0)$, as

$$q_0(x)=\frac{1}{a}\int_{x=0}^{a} q_w(x)dx+\frac{2}{a}\sum_{n=1}^{\infty}\left(\frac{\cos(n\pi x/a)}{\cosh(n\pi b/a)}\right)\int_{x=0}^{a} q_w(x)\cos(n\pi x/a)\,dx$$
$$+\frac{2\pi k_1}{a^2}\sum_{n=1}^{\infty} n\cos(n\pi x/a)\tanh(n\pi b/a)\int_{x=0}^{a} T_0(x)\cos(n\pi x/a)\,dx \qquad (5\text{-}20)$$

5.4 Iterative Inverse Solution

There are two integral equations for determination of the unknowns $T_0(x)$ and $q_0(x)$. The substitution of $q_0(\xi-\varepsilon)=q_0(x)$ from Eq. (5-20) into Eq. (5-19) leads to a single integral equation that can be solved iteratively in order to acquire numerical values for $T_0(x)$. Alternatively, the substitution of $T_0(x)$ from Eq. (5-19) into Eq. (5-20) would lead to an alternative integral equation wherein the surface heat flux $q_0(x)$ is the unknown, to be determined. The next numerical example is selected to illustrate the inverse methodology employed for determination temperature $q_0(x)$ over the contact area.

Numerical example. The objective is to test the convergence behavior of this iterative solution using the computed temperature values. In dimensionless space for a special case, Layer 1 is selected so that $a=2b$ and having b as the characteristic length for both layers. The applied heat flux is q_w and it is selected as a constant at two different sites: one from $x=a/4$ to $a/2$ and the other from $x=3a/4$ to *a*. The dimensions of the second layer, as depicted in Figure 1, are $c=5b$ and, $d=b$; therefore, the spacing parameter becomes $\varepsilon=(c-a)/2=3b/2$. Furthermore, a thermal conductivity

$k_2 = 4k_1$ and a Biot number $Bi = hc/k_2 = 20$ are selected mainly to test this numerical procedure and the accuracy of temperature solutions.

For this case, the process begins by providing an initial estimate for $q_0(x) \approx q_a(x,0)$ in accordance with Eq. (5-8). Then, Eq. (5-19) provides the first estimated values for $T_0(x)$. The second step begins be expanding $T_0(x)$ into a secondary Fourier series solution that satisfies the homogeneous boundary conditions at $x = 0$ and $x = a$ for Layer 1. Next, the value $q_b(x,0)$, from Eq. (5-15), is to be used in order to get a new heat flux at *y*=0 from the relation $q_0(x) = q_a(x,0) + q_b(x,0)$, as the onset for the first iteration. This new $q_0(x)$ serves as a new heat flux input for Layer 2 and to repeat the process to determine a new $T_0(x)$ solution. The initial values of $k_1 T_0(x)/q_w b$ assuming $q_b(x,0) = 0$ are determined and the data are plotted in Figure 5-2. They are compared with the computed dimensionless temperature data from this first iteration, also plotted in Figure 5-2. The process is repeated for a second through a fourth iteration. The acquired data, plotted in Figures 5-3, compares the results from the first and the second iterations. There is reasonably good agreement, and this agreement improves when the third and fourth iterations are compared in Figure 5-4. Additionally, Figure 5-5 shows the deviation of $k_1 T_0(x)/q_w b$ for a given iteration from the previously determined values. This plotted data show that there is a relatively larger deviation between the initial guess and the first iteration, while the difference between data from the fourth and the third iteration is very small. A sample of numerical data plotted in Figure 5-2 is in Table 5-1. Column 9 in Table 5-1 shows small differences between the third and the fourth iterations and attests to a reasonably good convergence rate. It is to be noted that 31 eigenvalues (including zero) were used for determination of data

presented in this example. The process was repeated for larger numbers of eigenvalues and they all show similar behavior due to the number of iterations.

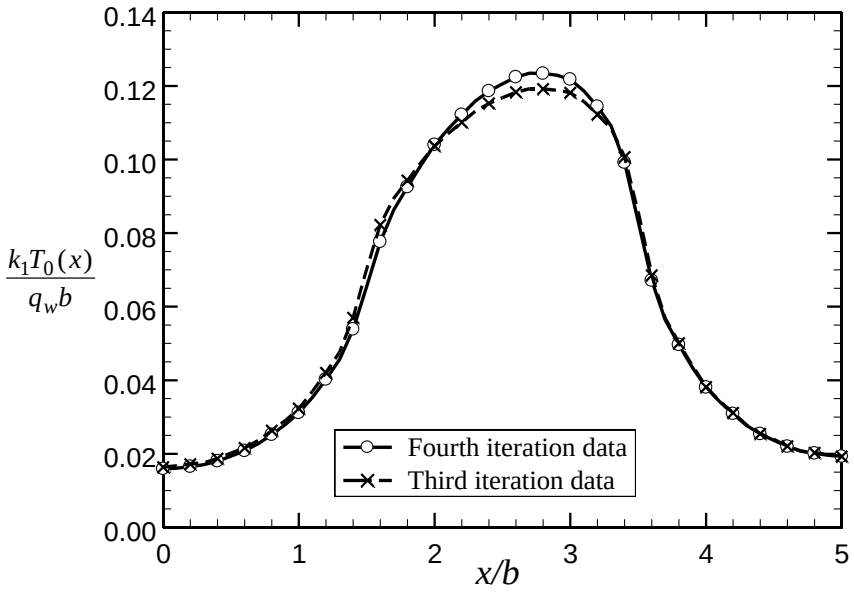

Figure 5-2 A comparison of computed $T_0(x)$ values after the 1st iteration with the initial guess.

Table 5-1 Computed values of $k_1 T_0(x)/(q_w b)$ for the first four iterations.

x/b	Initial	Diff.	1st	Diff.	2nd	Diff.	3rd	Diff.	4th
	$\frac{k_1 T_0(x)}{q_w b}$	$\frac{k_1 \Delta T_0(x)}{q_w b}$	$\frac{k_1 T_0(x)}{q_w b}$	$\frac{k_1 \Delta T_0(x)}{q_w b}$	$\frac{k_1 T_0(x)}{q_w b}$	$\frac{k_1 \Delta T_0(x)}{q_w b}$	$\frac{k_1 T_0(x)}{q_w b}$	$\frac{k_1 \Delta T_0(x)}{q_w b}$	$\frac{k_1 T_0(x)}{q_w b}$
0.0	0.01586	0.0005	0.01637	-1E-04	0.01627	2E-05	0.01629	-4E-06	0.01629
0.2	0.01649	0.0007	0.01718	-1E-04	0.01707	2E-05	0.01709	-3E-06	0.01708
0.4	0.01803	0.0007	0.01870	-1E-04	0.01859	2E-05	0.01861	-4E-06	0.01861
0.6	0.02083	0.0007	0.02156	-1E-04	0.02143	3E-05	0.02146	-5E-06	0.02145
0.8	0.02522	0.0011	0.02631	-2E-04	0.02614	3E-05	0.02617	-5E-06	0.02616
1.0	0.03113	0.0012	0.03229	-2E-04	0.03208	4E-05	0.03212	-8E-06	0.03212
1.2	0.04022	0.0018	0.04202	-3E-04	0.04171	6E-05	0.04177	-1E-05	0.04176
1.4	0.05383	0.0031	0.05696	-5E-04	0.05649	8E-05	0.05657	-1E-05	0.05655
1.6	0.07764	0.0046	0.08223	-9E-04	0.08135	0.0002	0.08152	-4E-05	0.08149
1.8	0.09251	0.0018	0.09428	-4E-04	0.09389	9E-05	0.09398	-2E-05	0.09396
2.0	0.10401	-3E-04	0.10367	2E-05	0.10368	3E-06	0.10369	-2E-06	0.10369
2.2	0.11218	-0.002	0.11009	0.0004	0.11052	-9E-05	0.11043	2E-05	0.11045
2.4	0.11860	-0.003	0.11525	0.0007	0.11592	-1E-04	0.11578	3E-05	0.11581
2.6	0.12241	-0.004	0.11830	0.0008	0.11912	-2E-04	0.11895	4E-05	0.11899
2.8	0.12335	-0.004	0.11915	0.0009	0.12000	-2E-04	0.11982	4E-05	0.11986
3.0	0.12178	-0.004	0.11813	0.0007	0.11879	-1E-04	0.11866	3E-05	0.11869
3.2	0.11439	-0.002	0.11223	0.0004	0.11258	-6E-05	0.11252	1E-05	0.11253
3.4	0.09919	0.0015	0.10066	-4E-04	0.10023	0.0001	0.10034	-3E-05	0.10031
3.6	0.06713	0.0014	0.06851	-2E-04	0.06828	4E-05	0.06833	-9E-06	0.06832
3.8	0.04961	0.0004	0.05006	-1E-04	0.04994	3E-05	0.04997	-6E-06	0.04996
4.0	0.03803	0.0001	0.03816	-4E-05	0.03812	1E-05	0.03813	-3E-06	0.03813
4.2	0.03087	0.0003	0.03116	-6E-05	0.03110	1E-05	0.03111	-2E-06	0.03111
4.4	0.02538	5E-05	0.02543	-3E-05	0.02540	9E-06	0.02541	-2E-06	0.02541
4.6	0.02195	1E-04	0.02205	-2E-05	0.02202	6E-06	0.02203	-2E-06	0.02203
4.8	0.02015	0.0002	0.02030	-3E-05	0.02026	7E-06	0.02027	-1E-06	0.02027
5.0	0.01925	-6E-06	0.01925	-1E-05	0.01924	6E-06	0.01924	-2E-06	0.01924

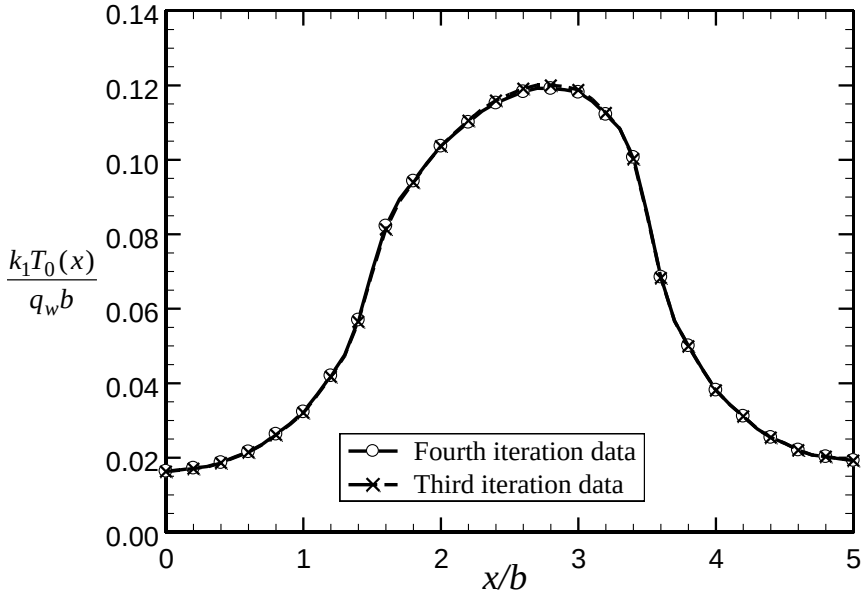

Figure 5-3 A comparison of computed $T_0(x)$ values after the 1st iteration and after the 2nd iteration.

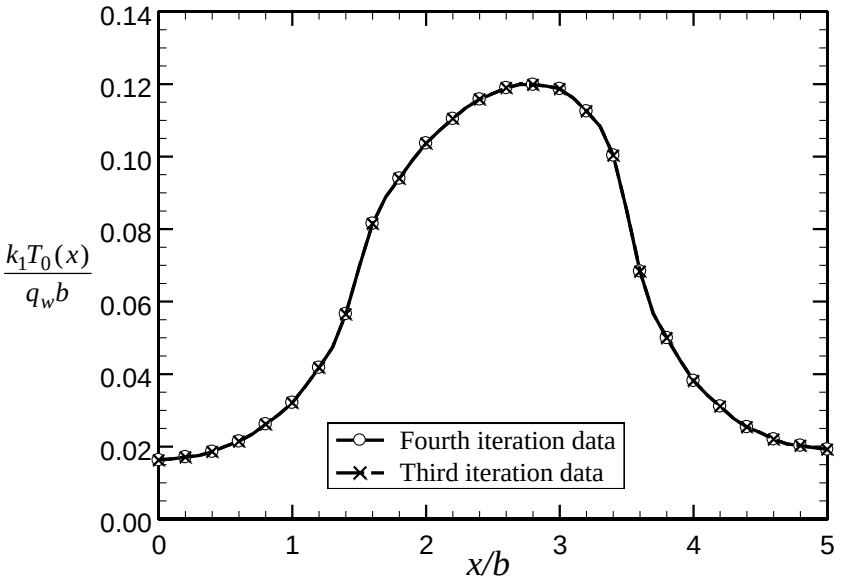

Figure 5-4 A comparison of the computed $T_0(x)$ values from 3rd and 4th iterations.

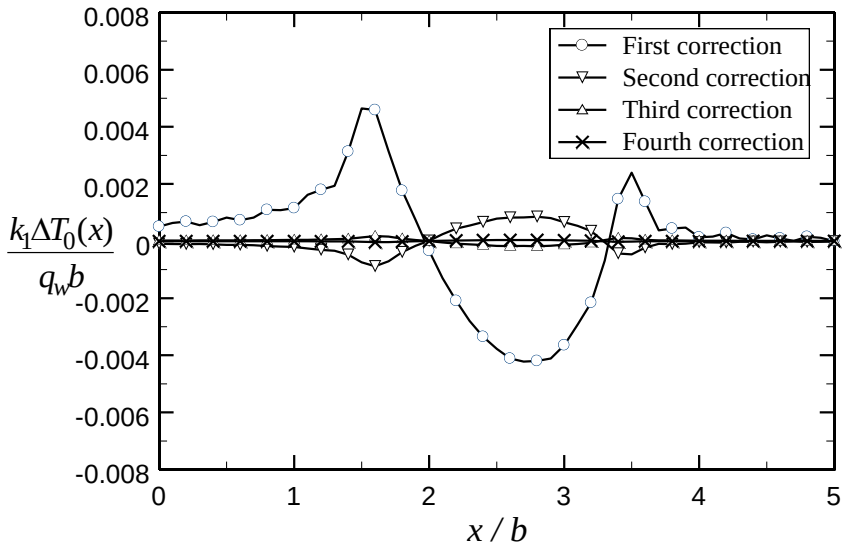

Figure 5-5 The deviations of $T_0(x)$ from the previously determined values, for each iteration.

The determination of temperature data at *y=b*, where the heaters are located, is important to the design and manufacturing of the devices where temperature assumes its maximum values. Table 5-2 is prepared to show the computed temperature values at *y=b* for all four sets of iterations. It is remarkable that the data for the first iteration are well behaved and they agree with subsequent iterations. Column 6 of Table 5-2 contains the numerically acquired data using ANSYS. The CFD model was developed so that it was not mesh sensitive. The data in Column 6 agree reasonably well with those in Column 7 of Table 5-2, which contains a set of computed temperatures using 500 eigenvalues followed by a sufficient number of iterations. The data in Column 7 should represent the exact values since they are accurate to all digits appearing in Table 5-2. These data show mixed agreements with those from the fourth iteration and the CFD data. The last column in Table 5-2 contains the percent deviation between the data in columns 5 and 6 of this table. Figure 5-6 shows the plotted temperature values for the fourth iteration and

the CFD data, as presented in Table 5-2. This figure illustrate that 30 eigenvalues provide data that they agree well with the numerically acquired information.

Table 5-2 Computed values of $T(x,b)$ and their comparison $/(q_w b)$ with numerically determined values

x/b	$k_1 T_1(x,b)\ /(q_w b)$						Percent difference
	1st Set	2nd Set	3rd Set	4th Set	by CFD	Exact	
0.0	0.37734	0.37719	0.37721	0.37721	0.37715	0.37712	0.015
0.1	0.38183	0.38165	0.38167	0.38167	0.38170	0.38168	0.008
0.2	0.39575	0.39551	0.39555	0.39554	0.39583	0.39581	0.074
0.3	0.42113	0.42078	0.42083	0.42082	0.42141	0.42139	0.140
0.4	0.46353	0.46304	0.46312	0.46310	0.46350	0.46336	0.085
0.5	0.54857	0.54791	0.54803	0.54800	0.54893	0.54831	0.169
0.6	0.63165	0.63081	0.63096	0.63093	0.63093	0.63097	8E-04
0.7	0.66731	0.66629	0.66647	0.66644	0.66575	0.66567	0.104
0.8	0.67889	0.67770	0.67792	0.67787	0.67740	0.67733	0.069
0.9	0.66717	0.66581	0.66606	0.66601	0.66629	0.66633	0.041
1.0	0.60971	0.60821	0.60849	0.60843	0.60915	0.60853	0.117
1.1	0.55212	0.55051	0.55081	0.55075	0.55079	0.55063	0.007
1.2	0.54002	0.53833	0.53863	0.53858	0.53936	0.53932	0.146
1.3	0.55101	0.54927	0.54958	0.54952	0.55052	0.55049	0.183
1.4	0.58592	0.58414	0.58446	0.58440	0.58472	0.58457	0.055
1.5	0.66815	0.66636	0.66668	0.66662	0.66717	0.66653	0.083
1.6	0.75232	0.75054	0.75085	0.75079	0.75073	0.75076	0.008
1.7	0.79392	0.79217	0.79247	0.79241	0.79217	0.79208	0.031
1.8	0.81866	0.81692	0.81722	0.81716	0.81721	0.81713	0.006
1.9	0.83217	0.83044	0.83074	0.83068	0.83100	0.83092	0.039
2.0	0.83651	0.83479	0.83508	0.83503	0.83543	0.83535	0.048

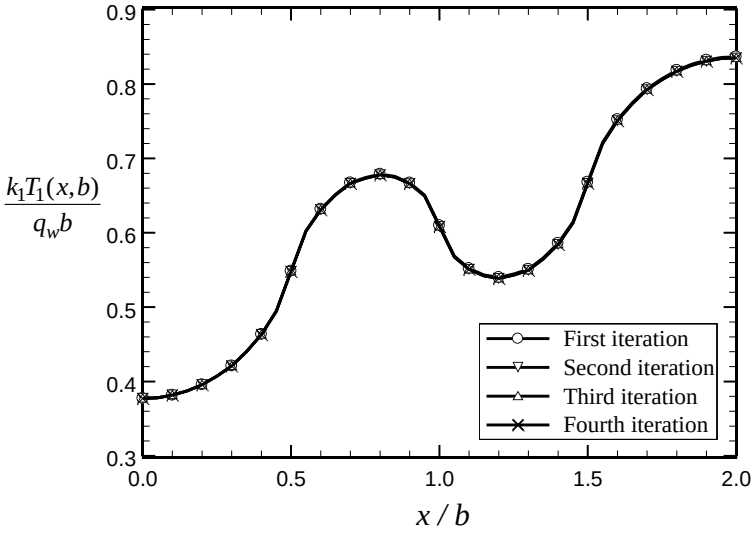

Figure 5-6 The temperature distribution over the heated surface as described by four successive iterations.

Figure 5-7 shows the plotted temperature values for the fourth iteration and the ANSYS data, as presented in Table 5-2. This figure illustrates that 30 eigenvalues provide data that agree well with the numerically acquired information.

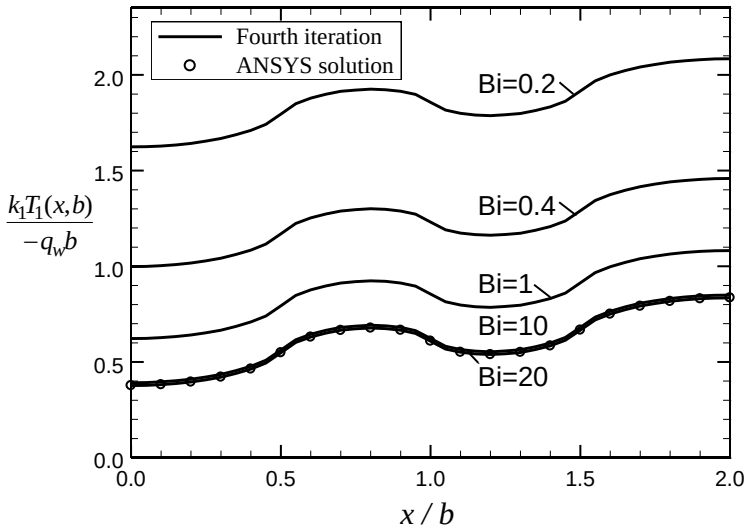

Figure 5-7 Temperature distribution over the heated surface after the 4th iteration for different *Bi* and the numerically computed data by ANSYS for *Bi*=20.

5.5 Comments and Discussions

This iterative procedure begins by properly selecting a function $q_0(x)$. This function is to be used in order to determine $T_2(\xi, d)$ using Eq. (5-19) and then obtain $T_0(x)$ from Eqs. (5-11) and (5-12a,b). No iteration becomes necessary if the function $q_b(x,0)$ obtained from Eq. (5-14) is the same as the original heat flux function $q_0(x)$. The first iteration begins if these two quantities are different using the relation $q_0(x) = q_a(x,0) + q_b(x,0)$, as it emerged from the solution of $T_1(x,y) = T_a(x,y) + T_b(x,y)$. The data acquired and presented in Table 5-1 show that, for a fixed number of terms in the series solution, only a few iterations are needed in order to get a relatively accurate solution. An alternative test shows that using a relaxation factor ω=0.82 to 0.88 and selecting the new $q_0(x)$ as

$$q_0(x)\big|_{\text{new}} = (1-\omega) q_0(x)\big|_{\text{old}} + \omega[q_a(x,0) + q_b(x,0)] \qquad (5\text{-}21)$$

can improve the convergence rate.

The prepared computer program permits one to increase the number of iterations until a solution is obtained with a desired convergence for a fixed number of terms, *N*. Then, the temperature is computed with a high number of iterations using *N*=30 terms. Selecting the data obtained from this solution as the reference values, the convergence due to the number of iterations was tested. With a relaxation factor of ω=1, the data over *y*=b surface converged with deviations below 5×10^{-7} after 6 iterations. However, with a relaxation factor of $\omega = 0.85$, only 4 iterations were needed in order to get alternative numerical results with deviations less than 1.5×10^{-7}.

5.6 Conclusion

The information presented earlier attests that the objectives of this study were accomplished. It was demonstrated that only a few iterations were needed to achieve satisfactory convergence and faster convergence was realized with a properly selected relaxation factor. Furthermore, the convergence related to the number of eigenvalues was tested and it is a classical Fourier series issue.

This tested inverse procedure is equally applicable to three-dimensional cases as the inclusion of *z*-axes can be accommodated with ease, similar to that for the *x*-axes. Furthermore, this opens a path for future application of this inverse methodology to multi-layer bodies that are commonly used in electronic cooling applications. As an illustration, each of the two layers in Figure 5-1 is to be replaced by a block of layers with uniform footprints. The methodology for determination of temperature in each block is in [78].

Chapter 6

Determination of Effective Thermal Conductivity in Heterogenous Material (TSV Technology)

A key 3D packaging technology is electrical packaging technology, which means that it is vital to connecting stacked chips electrically. Conventional 3D packaging technology uses wire bonding with metal lead wires. Recently, novel technologies have been developed to replace wire bonding. Through silicon via interconnects are emerging to serve a wide range of 3D packaging applications and 3D IC architectures that demand higher levels of performance and silicon integration with lower power consumption. As an illustration a comparison of wire bonding and TSV technologies can be depicted in Figure 6-1.

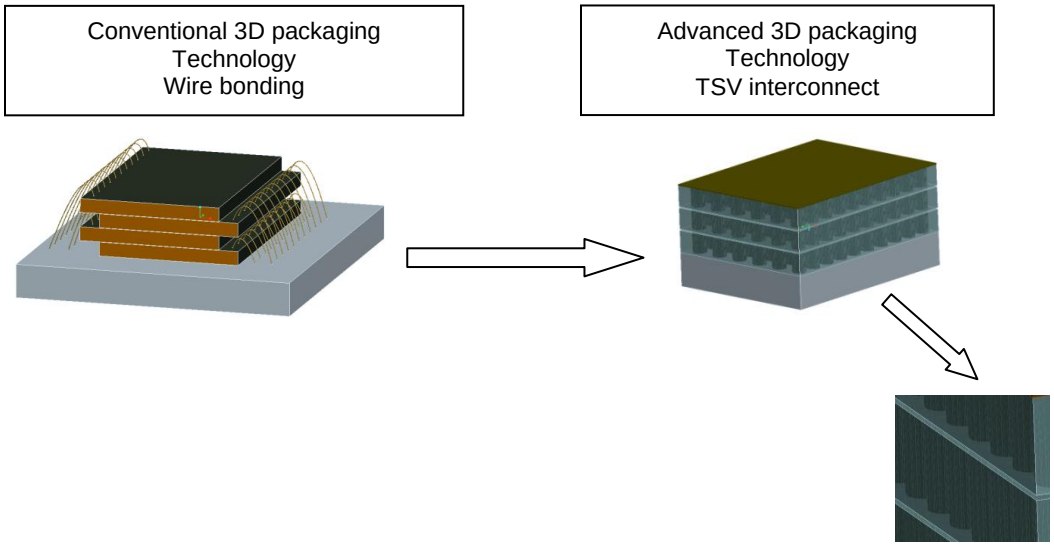

Figure 6-1 Comparison of conventional and TSV technology in 3D packaging

Predicting the temperature solutions of heterogeneous materials has been the subject of extensive research in the electronic packaging industry.

With analytical solutions being almost impossible to obtain for such open-ended problems, and numerical techniques being computationally expensive, semi-analytical methods are highly valuable to both chip makers and design engineers. There have been numerous publications on how to obtain the analytical or numerical solutions of steady state or transient heat conduction in homogeneous multilayer bodies.

With recent evolution in 3D stack packaging technology and introduction of TSVs, one cannot rely on previous work alone. The addition of TSVs in the silicon die matrix imposes new challenges. To start off, thermal stresses caused by CTE (coefficient of thermal expansion) mismatch. During the operation, chips generate non-uniform heat dissipation which in turn produces excessive forces in TSV connection and finally results in reliability degradation and failure. Thus, the study of heat conduction and obtaining the temperature solution for such systems are the subject of investigation in this chapter. In microelectronic devices, materials used often have different thermophysical and mechanical properties. However, there are many situations when the assumption of isotropy in a single layer is used mainly to simplify the thermal analyses. For example, if there are many layers and all layers actively participate in the heat transfer process, an approximate computation of the temperature distribution may be based on average thermophysical properties. However, this assumption may not be valid, especially when there are substantial differences between the physical properties of the constituents of the model under investigation.

The objective of this work is to provide an effective thermal conductivity (K_{eff}) for the matrix of silicon die and TSV inclusions. Once K_{eff} is calculated, the temperature solutions of steady-state heat conduction in conjunction with previous work (chapters 1-5) become deterministic. Galerkin-based numerical approximation is used for determination of effective coefficient of thermal conductivity.

For a multidimensional body the numerical evaluation of the effective thermal conductivity is difficult. Therefore, the 2D analysis of the system in question will be studied first. Then with the use of parallel resistance theory in heat transfer, the system in a 3D domain can be modeled and analyzed.

6.1 Galerkin Approximation Method

The Ritz variational principle in the form of the B.G. Galerkin method usually provides approximate solutions to various engineering problems. A relatively high degree of accuracy in numerical results is the interesting characteristic of these methods. Often, the accuracy of the solution far exceeds the application demand. The method of B. G. Galerkin, simply referred to as the Galerkin method, is used for fundamental problems in solid mechanics, fluid mechanics, and heat transfer. Generally, ordinary and partial differential equations describe physical phenomena such as transfer of heat, wave motion, stress distribution in solids, etc. The finite element method and Galerkin-type solutions provide capabilities to solve these differential equations in complex-shaped bodies when the exact solution either is not available or is too cumbersome for practical applications. In other words, the numerical solutions deal effectively with simple or difficult problems and have been widely used in recent technological advancement.

Variational calculus is a powerful mathematical tool with important applications. It is basic to the finite element method and Galerkin-type solution techniques. The Galerkin method provides closed-form solutions. The finite element method is a discretized form of the Galerkin method that produces numerical values at preselected nodal points. The goal is to show the application of the Galerkin method to selected engineering applications such as the TSV system in electronic packaging as described earlier.

In this chapter, the Galerkin-based integral (GBI) method is extended to solve a heterogeneous system. The purpose is to fill the gap that currently exists, to

accommodate a difficult conduction problem that is mathematically challenging and cumbersome, and to solve those for which the use of discretization methods are very time-consuming.

The developed procedure could be readily applied to both heterogeneous as well as homogenous medium. The major difference lies between how to select the basis functions for each model to satisfy imposed natural and homogeneous boundary conditions associated with each case

6.2 Galerkin Mathematical Form

The Galerkin method is a broad generalization of the Ritz method and is used primarily for the approximate solution of variational and boundary value problems, including problems that do not reduce to variational problems. The basic idea behind the Galerkin method is as follows. Suppose the requirement to find a solution, defined in some domain *D*, of the differential equation

$$L[U] = 0 \tag{6-1}$$

(here, *L* is a differential operator, for example, an operator in two variables) where the solution satisfies at the boundary *S* of *D* the homogeneous boundary conditions

$$U = 0 \tag{6-2}$$

If the function *u* is a solution of equation (6-1) in *D*, then *L[u]* is identically equal to zero in this domain and, consequently, is orthogonal to any function in *D.* The approximate solution of equation (6-1) is sought in the form

$$u_n(x,y) = \sum_{i=1}^{n} a_i \psi_i(x,y) \tag{6-3}$$

where $\psi_i(x,y)$ (i = 1, 2, …, n) are linearly independent functions that satisfy the boundary conditions (6-2) and are the first n functions of some system of functions $\psi_1(x,y)$, $\psi_2(x,y)$, …, $\psi_n(x,y)$ that is complete in the given domain. The constant coefficients

a_i are chosen so that $L[u_n]$ is orthogonal in *D* to the first *n* functions of the system $\psi_i(x,y)$:

$$\iint_D L[u_n(x,y)\psi_i(x,y)dxdy = \iint_D L[\sum_{k-1}^{n} a_k\psi_k(x,y)]\psi_i(x,y)dxdy = 0 \quad (6\text{-}4)$$

$$i = 1,2,\dots\dots\dots,n$$

The Galerkin method is used in solving a broad class of problems. Its most general formulation is given in terms of functional analysis for the solution of equations of the form *Au - f* = 0, where *A* is a linear operator defined on a linear space that is dense in some Hilbert space *H, u* is the unknown, and *f* is a specified element of *H.* The method came into use after it was described in a paper by B. G. Galerkin in 1915. The advantage of this method is the higher accuracy and faster computation time in comparison with discretized numerical methods. Although the method of analysis is the same as the Galerkin finite element method, unlike the standard finite element method, it maintains the continuity of heat flux throughout the domain.

6.3 Mathematical Procedure

Prior to any derivation, it is essential to understand the concept of effective thermal conductivity (K_{eff}). Consider a solid layer of silicon bulk material that consists of many cylindrical copper interconnects, namely TSVs. If one of the surfaces of the silicon layer is subjected to a Dirichlet boundary condition, the other end of the solid block will receive the same amount of energy based on thermodynamics. The consideration is given to an equivalent homogeneous solid material that is identical in shape to the original body and subjected to the same boundary conditions. Under steady-state conditions the heat exchange between the modeled body and its surroundings is same as the actual body. Thus, the equivalent thermal conductivity of the modeled body will be the one we seek as it represents the overall thermal conductivity of the solid with inclusions. For one-dimensional heat transfer, when one surface is subjected to a

constant temperature and opposite side of the block is maintained at some fixed temperature, the following relation will hold,

$$q_{in} = q_{out} = \frac{|\Delta T|}{C/K_{eff}} \tag{6-5}$$

where $|\Delta T|$ is the difference in temperature across the actual body and the equivalent solid. Similarly, q_{in} and q_{out} remain the same for both the actual body and equivalent solid and they are equal to average heat flux, $|q_{ave}|$. This definition for the effective thermal conductivity, k_{eff}, will be used throughout this paper.

In order to obtain a temperature and heat flux solution, it is necessary to solve the diffusion equation given below known as a Laplace equation over the entire domain of matrix and inclusion.

$$\nabla.(K\nabla T) = 0 \tag{6-6}$$

The external surfaces of the body could take any type of the boundary condition. The assumption is that the thermal conductivity is independent of the temperature and therefore, a Galerkin-based integral method could be applied to obtain an accurate closed-form solution. A Galerkin solution that uses heat-flux conserving basis functions (Haji-Sheikh, 1988) conserves the continuity of temperature and heat flux across the phase boundaries. Moreover, it can deal accurately with a temperature jump in the presence of an imperfect contact.

The Galerkin method uses a set of basis functions that are usually non-orthogonal and chosen in a manner to satisfy the homogeneous boundary conditions. There are many methods proposed as to how to select the basis functions required for each case; however, there is not an exact way to describe the procedure. The method of selecting the basis functions for boundary conditions of the first kind is available in many literatures (Kantorovich and Krylov, 1960; Ozisik, 1980; Haji-Sheikh, 1987). In 1992, Beck

et al. came up with a method of selecting these basis functions for different types of boundary conditions. However, the obtained basis functions needs to be modified to accommodate the presence of inclusion in the main domain at the boundary of the two constituents and to account for the compatibility condition between the inclusion and matrix at the boundaries. Once the basis functions are developed, the Galerkin method is applied and the matrix produced by Galerkin method will be deterministic. The derivation of getting such a matrix is shown by (Beck et al., 1992) and leads to,

$$a_{ij} = \int_V f_i \nabla.\left(K\nabla f_j\right)dV \tag{6-7}$$

$$b_{ij} = \int_V f_i f_j \, dV \tag{6-8}$$

Once a_{ij} and b_{ij} are known the matrix can be solved for unknown coefficients. $f_i \; and \; f_j$ are described in numerical examples in future sections. Depending on the number of the terms, we will have N equations and N unknown.

$$A.C = \psi \tag{6-9}$$

$$C = A^{-1}.\psi \tag{6-10}$$

There are two steps to determine the basis functions. The first step is in the homogeneous domain, where there is no inclusion. The basis function denoted by $f_{m,j}$, implies to main domain and described as

$$f_j = f_{j,m} \tag{6-11}$$

The next step is very important, that is to modify the basis function obtained to accommodate the presence of inclusion bounded by the surfaces $\emptyset_e = 0$ using the relationship described by (Beck, et al. 1992) it will lead to the following relations,

$$f_j = f_{j,e} \tag{6-12}$$

$$f_{j,e} = f_{j,m} + U_e + \emptyset_e H_e \tag{6-13}$$

where the function $f_{j,e}$ is the modified basis function sought and will be used in the inclusion domain. One could see that if $U_e = 0, and\ \emptyset_e = 0$, then the boundary condition at the interface of the inclusion and matrix is satisfied since $f_{j,m} = f_{j,e}$.

In order to comply with the interface condition between the inclusion and the matrix, the use of the compatibility condition must be regarded, that is

$$K_m \frac{\partial f_{j,m}}{\partial n_e} = K_e \frac{\partial f_{j,e}}{\partial n_e} \tag{6-14}$$

The jump condition is defined as,

$$f_{j,e} = f_{j,m} - \left(\frac{K_m}{C}\right)\left(\frac{\partial f_{j,m}}{\partial n}\right) \tag{6-15}$$

In the absence of thermal conductance $U_e = 0$ and the substitution of f_j into the compatibility condition, equation (6-15) described above yields,

$$[H_e]_{\emptyset_{e=0}} = -\frac{\left[\left(\frac{K_m}{K_e}-1\right)\frac{\partial f_{j,e}}{\partial n_e}\right]_{\emptyset_{e=0}}}{\left(\frac{\partial \emptyset_e}{\partial n_e}\right)_{\emptyset_{e=0}}} \tag{6-16}$$

$$[H_e]_{\emptyset_{e=0}} = -\frac{\left[\left(\frac{K_m}{K_e}-1\right)\nabla f_{j,m}.\nabla \emptyset_e\right]_{\emptyset_{e=0}}}{(\nabla \emptyset_e.\nabla \emptyset_e)_{\emptyset_{e=0}}} \tag{6-17}$$

The derivation for equation (6-16) and (6-17) is presented in Appendix B. The equation (6-17) is used when there is no resistance between the constituents in the model; however, the effect of thermal contact conductance should not be omitted and can be implemented using the interfacial jump condition defined as follows by rearranging equation (6-15),

$$K_m \frac{\partial f_{j,m}}{\partial n_e} = C(f_{j,m} - f_{j,e}) \tag{6-18}$$

Next, the values obtained for f_{mj} and f_{ej} will be substituted in the above equation. Simplifying the equation and regarding that $\emptyset_e = 0$ at the interface of inclusion and matrix, it will yield

$$U = -\left(\frac{K_m}{C}\right)(\partial f_{j,m}/\partial n)|_{\emptyset_e=0} \quad (6\text{-}19)$$

Thus, the H_e can be computed using the following equation

$$H_e = \frac{\left(\frac{K_m}{K_e}-1\right)\nabla f_{j,m}.\nabla\emptyset - \nabla U_e.\nabla\emptyset_e}{(\nabla\emptyset_e.\nabla\emptyset_e)_{\emptyset_{e=0}}} \quad (6\text{-}20)$$

Now, with Eqs. (6-19) and (6-20) in hand, U and H_e are defined and one can obtain the basis functions for inclusions. Once the basis functions are all calculated, the temperature solution can be obtained. For cylindrical inclusion, the denominator of the above equation is a constant and not a function. However, for odd-shape geometry the denominator of equation (6-20) could be a function.

Subsequently, the average mean heat flux can be calculated and the effective thermal conductivity will be deterministic using the following equation for one-dimensional conduction

$$q_{av} = -K_{eff}\frac{dT}{dx} \quad (6\text{-}21)$$

6.3.1 Numerical Example:

Consider a TSV copper being embedded into a Silicon matrix as shown in Figure 6-2.

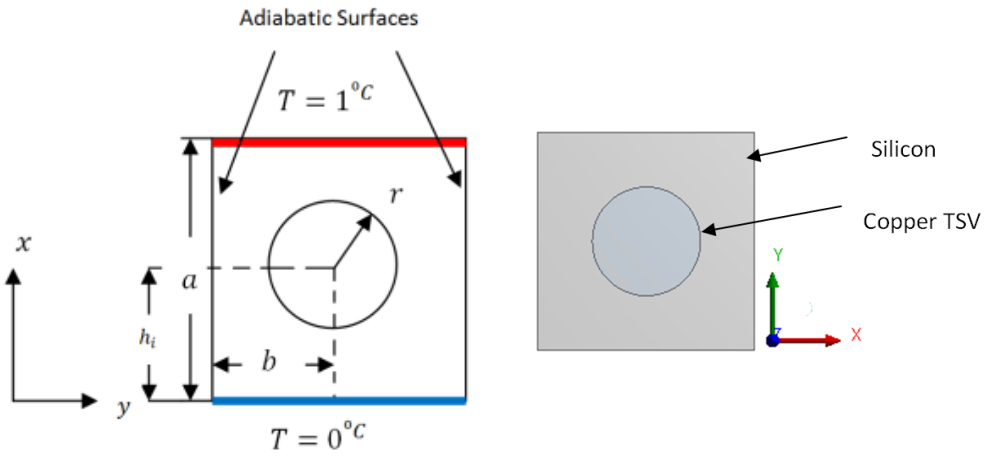

(a) (b)

Figure 6-2(a) Copper embedded in a silicon matrix, and (b) copper embedded in a silicon matrix (side view)

As was mentioned before, we are seeking solutions to the Laplace equation, $\nabla^2 T = 0$

$$\nabla.(K\nabla T) = 0 \tag{6-22}$$

Using the transformation of T to satisfy the non-homogeneous boundary condition at x=a where the boundary condition of the first kind is prescribed to obtain the temperature solution, results in

$$\theta_m = T + \frac{x}{a} \text{ in the main domain and,} \tag{6-23}$$

$$\theta_e = T + f_e \text{ in the inclusion} \tag{6-24}$$

Therefore,

$$\nabla.(K_m \nabla \theta_m) = 0 \text{ for the main domain} \tag{6-25}$$

$$\nabla.(K_e \nabla \theta_e + K_e \nabla f_e) = 0 \text{ for the inclusion} \tag{6-26}$$

Now, multiplying the above equation and integrating over the domain will lead to the following relation,

(6-27)

$$\int_{V_m} \nabla\ (K_m \nabla\ \theta_m) f_m dV + \int_{V_e} \nabla\ (K_e \nabla\ \theta_e) f_e dV = -K_e \int_V f_{ej} \cdot \nabla^2 f_{ei} dV$$

Since, the consideration is given to a 2D analysis, we obtain the following,

$$\theta = \sum_{j=1}^{N} C_m f_m$$

(6-28)

Thus,

$$\sum C_m \left[\int_m K_m \left(\nabla^2 . f_{mj}\right) f_{mi} dA + \int_e K_e \left(\nabla^2 . f_{ej}\right) f_{ei} dA\right] = -K_e \int_e \nabla^2 f_{ej} f_{ei} dA$$

(6-29)

Therefore, by inspection one could rewrite the above equation in matrix form as follows,

$$[C][A] = [\psi] \quad (6\text{-}30)$$

where, the matrix element [A] is defined as,

$$a_{ij} = \int_m K_m \left(\nabla^2 . f_{mj}\right) f_{mi} dA + \int_e K_e \left(\nabla^2 . f_{ej}\right) f_{ei} dA \quad (6\text{-}31)$$

and the [ψ] defined as,

$$[\psi] = -K_e \int_e \nabla^2 f_{ej} f_{ei} dA \quad (6\text{-}32)$$

therefore, the coefficient matrix [C] will become deterministic.

$$[C] = [A]^{-1}[\psi] \quad (6\text{-}33)$$

For illustration purposes, for a three-term solution we obtain a 3X3 matrix as depicted below,

$$\begin{aligned} c1 \int_V f_1 \nabla^2 f_1 dV + c2 \int_V f_1 \nabla^2 f_2 dV + c3 \int_V f_1 \nabla^2 f_3 dV &= \int_V \left(\frac{g}{K}\right) f_1 dV \\ c1 \int_V f_2 \nabla^2 f_1 dV + c2 \int_V f_2 \nabla^2 f_2 dV + c3 \int_V f_2 \nabla^2 f_3 dV &= \int_V \left(\frac{g}{K}\right) f_2 dV \\ c1 \int_V f_3 \nabla^2 f_1 dV + c2 \int_V f_3 \nabla^2 f_2 dV + c3 \int_V f_3 \nabla^2 f_3 dV &= \int_V \left(\frac{g}{K}\right) f_3 dV \end{aligned} \quad (6\text{-}24)$$

$$c1a_{11} + c2a_{12} + c3a_{13} = \psi_1$$

$$c1a_{21} + c2a_{22} + c3a_{23} = \psi_2 \quad (6\text{-}35)$$

$$c1a_{31} + c2a_{32} + c3a_{33} = \psi_3$$

Where $\int_V f_1 \nabla^2 f_2 dV = \int_{Vm} f_{m1} \nabla^2 f_{m2} dV + \int_{Ve} f_{e1} \nabla^2 f_{e2} dV$ (6-36)

6.4 Determination of Basis Function for a Silicon Matrix:

Basis functions for localized domains, or heterogeneous materials, are discussed in previous the previous section (6.3). Kantrorovich and Krylov (1960) defined basis functions as a set of linear independent functions that satisfy the homogeneous boundary conditions. There are literature sources that present basis functions for orthogonal bodies and include works by Kantrorovich and Krylov (1960), Carslaw and Jaeger (1959), Shih (1984), Beck et al. (1992), and Cotta (1993). The most complete basis functions is in Beck et al. (1992), in which basis functions in Cartesian, cylindrical, and spherical coordinate systems are presented. Lee and Haji-Sheikh (1991) and Beck et al. (1992) have presented procedures for defining basis functions in nonorthogonal bodies.

The procedure for finding basis functions is not unique and any properly defined set of basis functions are acceptable as long as they satisfy the homogenous boundary conditions. The basis functions presented will include the basis functions that satisfy the boundary conditions of the first kind (prescribed temperature, $f_j = 0$), the second kind (prescribed heat flux, $\frac{\partial f_j}{\partial n} = 0$), or the third kind (convection, $-K\frac{\partial f_j}{\partial n} = hf_j$).

Computation of effective thermal conductivity K_{eff} requires the global basis functions of the first kind, since we have prescribed temperature on the top surface of the matrix as shown in Figure 6-1(a).

When a multi-dimensional body has a regular shape, the basis function describing that body is a product of one-dimensional basis functions. To obtain a

reasonably accurate solution for irregular multi-dimensional bodies, the number of basis functions is usually greater than 2. Numerical matrix operation becomes necessary when dealing with complex multi-dimensional problem.

The method in which the basis functions are selected for the boundary conditions of the first kind is available in literature (Kantrorovich and Krylov 1960; Carslaw and Jaeger 1959; Ozisik, 1980; Haji-Sheikh and Mashena, 1987).

If a region is bounded by N surfaces, $\phi_1, \phi_2, \phi_3, \ldots \phi_N$, then the first member of the set of the basis functions is

$$f_1(r) = \emptyset_1\, \emptyset_2\, \emptyset_3 \ldots\ldots\ldots\ldots\ \emptyset_N \tag{6-37}$$

Each subsequent member of the set of basis functions is obtained by multiplying $f_1(r)$ by an element of a complete set, for example, in a Cartesian coordinate system

$$\begin{aligned} f_2(r) &= f_1(r)x \\ f_3(r) &= f_1(r)y \\ f_4(r) &= f_1(r)x^2 \\ f_5(r) &= f_1(r)xy \\ f_6(r) &= f_1(r)y^2 \end{aligned} \tag{6-38}$$

Each basis function is required to vanish only over the exterior boundaries. Some, but not all, basis functions may become zero at the interior point. This can be ensured if $f_1(r)$ is not zero within the region. This method produces accurate results except in a domain with inside corners. Whenever all basis functions vanish at the interior point, the region can be subdivided into many different subregions. The basis functions are constructed for each subregion and matched at the common boundary of each subregion (Kantrorovich and Krylov 1960). Lee and Haji-Sheikh (1991) showed procedures for selecting such basis functions for domains with inside corners.

In our model as shown in Figure 6-1(a) we have T=1 at top and T=0 at the bottom. Remember that the sides are all adiabatic. The basis function for the model excluding the inclusion was chosen as,

$$f_{mj} = \left[1 - \left(\frac{j}{j+1}\right)\right]\left(\frac{y}{b}\right)^2 \left(\frac{x}{a} - \frac{i+1}{i+2}\right)\left(\left(\frac{x}{a}\right) - \frac{i+1}{i+2}\right)\left(\frac{x}{a}\right)^2\left(\frac{x}{a}\right)^i\left(\frac{y}{b}\right)^{2j} \quad (6\text{-}39)$$

It was mentioned that the basis functions obtained for a matrix without inclusion must be modified to allow compatibility between the constituents in the model. The use of equation (6-9) allows the computation of basis functions for the inclusion.

Upon successful computation of effective thermal conductivity in x and y direction, one needs to determine the effective thermal conductivity in a lateral direction. In the following section, the determination of effective thermal conductivity in z direction will be discussed.

6.5 Determination of Effective Thermal Conductivity in a Lateral Direction

Once the effective thermal conductivity in 2-D is known, in order to develop a 3-D model the effective thermal conductivity in a lateral direction should also be determined. The analytical calculation of the effective thermal conductivity in 3-D is very difficult and time-consuming. In this research, the goal is to simplify the analysis and use the parallel resistors theorem of heat transfer to find the effective thermal conductivity in Z-direction. In order to comprehend the analogy, consider the figure shown below,

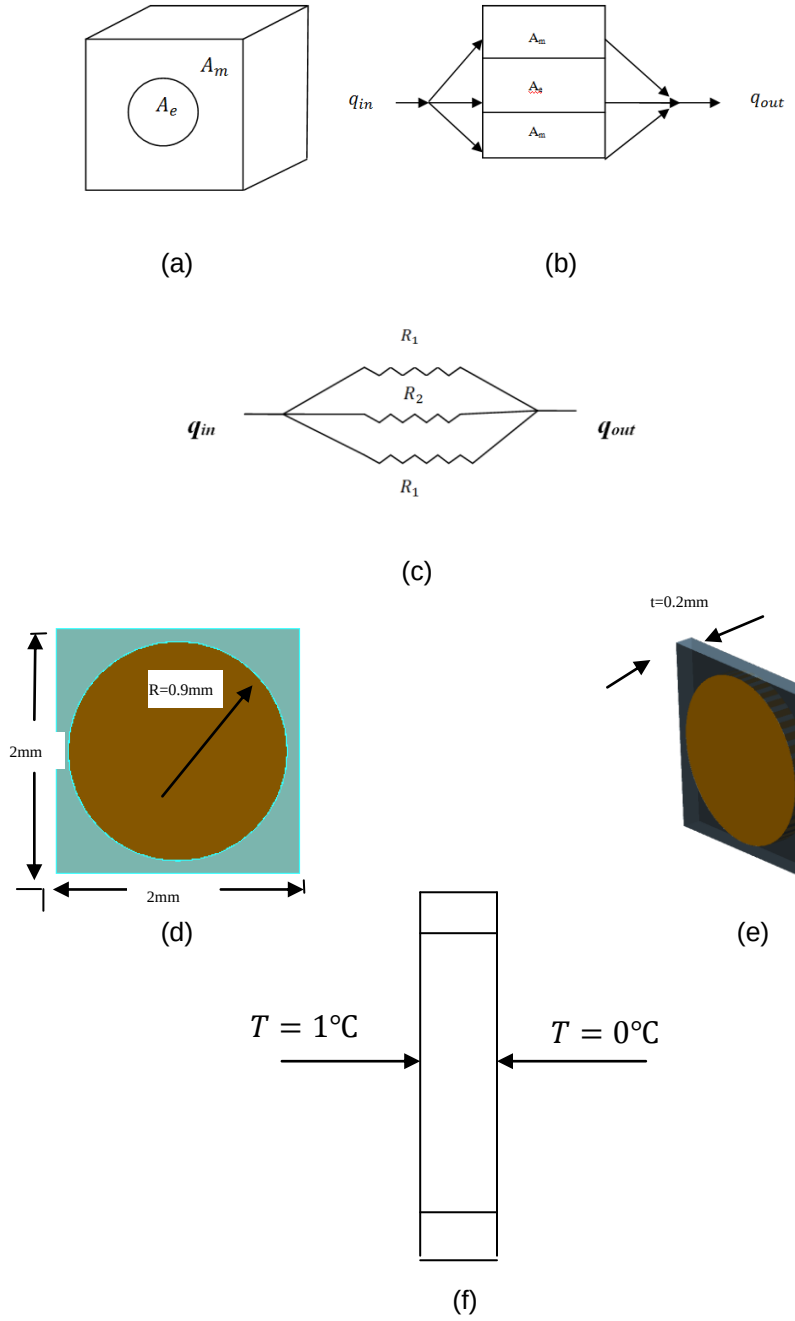

Figure 6-3 (a) Isometric view of TSV and silicon, (b) side view of the TSV and silicon, and (c) parallel network resistance diagram; (d, e, f) schematic and boundary conditions on the model

Here A_m and A_e are the areas of the silicon main domain and copper TSV respectively.

If the parallel resistance theory is applied as shown in Figure 6-3(b), one could drive the total resistance by means of equations (6-24, 6-25).

$$\frac{1}{R_1}+\frac{1}{R_2}+\frac{1}{R_1}=\frac{1}{R_{total}} \tag{6-40}$$

$$R_{total}=\frac{R_1R_2}{2R_2+R_1} \tag{6-41}$$

Consider a cylindrical copper embedded into a silicon matrix as shown in Figure 6-3(d) and Figure 6-3(e); they are subjected to the temperature conditions depicted in Figure 6-3(f). The effective thermal conductivity in a lateral direction is the unknown. Based on the methodology described above, essentially, the effective thermal conductivity would be based on volume proportion and the analytical results are compared with FEM analysis and depicted in Table (6-1). The temperature and heat flux using ANSYS are shown in Figure (6-4) and Figure (6-5) respectively.

Table 6-1 Comparison of effective thermal conductivity between analytical and FEA

k_{Copper}	$400\ (^{W}/_{m.K})$
$k_{Silicon}$	$180\ (^{W}/_{m.K})$
$Analytical\ (k_{eff})$	$320\ (^{W}/_{m.K})$
$Numerical\ (k_{eff})$	$320\ (^{W}/_{m.K})$
$\%Error$	0%

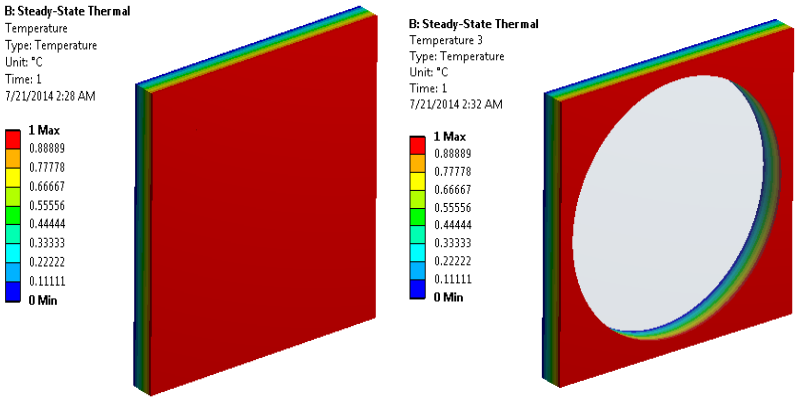

Figure 6-4 Temperature contour for copper and silicon

In the following section of this study, the analytical solution for the effective thermal conductivity of the TSV system is obtained and compared with FEA analysis of the same model using ANSYS Workbench as a tool for verification purpose. Keep in mind that the actual diameter of a TSV is around $1-5(\mu m)$. However, for better visualization purpose, the diameters of the TSVs are chosen much larger than their actual size.

6.6 Numerical Examples of TSV Systems

6.6.1 Setting a Benchmark for Our Analysis in the Forthcoming Examples

Consider a single copper inclusion in a silicon matrix with perfect contact as shown in Figure 6-1(a).

The copper and silicon have the thermal conductivity of $400(\frac{W}{m.K})$ and $180\left(\frac{W}{m.K}\right)$ respectively.

The block dimensions are $a = 2(mm)$ and $b = 1(mm)$.

The copper inclusion has radius of $r = 0.5(mm)$. The initial height is $h_i = 1(mm)$.

The top surface of the silicon matrix is subjected to a constant temperature $T = 1℃$ while the bottom surface is maintained at $T = 0℃$.

Solution;

After successful determination of basis function as described previously, the basis function was carefully chosen to satisfy the homogenous boundary conditions imposed by external surfaces of the model. That is the temperatures at x=a has to be $T|_{x=a} = 1$ and the temperature at x=0, is $T|_{x=0} = 0$.

Applying the Galerkin procedure as described earlier, the effective thermal conductivity of the matrix and inclusion is found to be $K_{eff} = 208.920\ (\frac{W}{mK})$.

The same model was analyzed using FEA techniques and results in an effective thermal conductivity of $K_{eff} = 208.902\ (\frac{W}{mK})$. Note that the average heat flux was used in FEA for determination of K_{eff}. Table 6-2 shows the results using both techniques, while Figure 6-5 shows results from ANSYS.

Table 6-2 Comparison of effective thermal conductivity between analytical and FEA without resistance

Number of Terms (J_{max})	1	2	3	4	5	6	7
K_{eff}(W/m.k)	218.950	209.523	209.426	209.100	208.964	208.958	208.920
FEA(Grid independent) #elements~1.2 Million	208.902	208.902	208.902	208.902	208.902	208.902	208.902
%Error							0.0086%

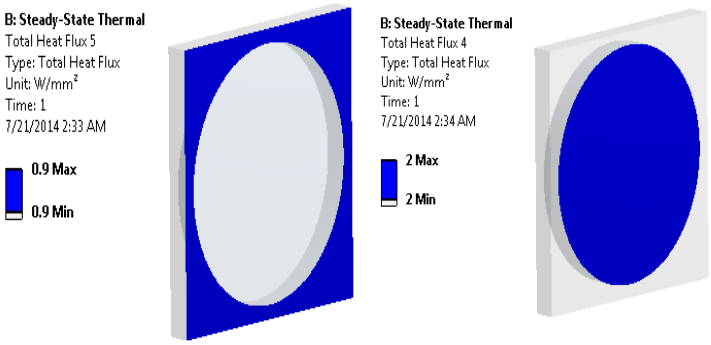

Figure 6-5 Heat flux contour for copper and silicon

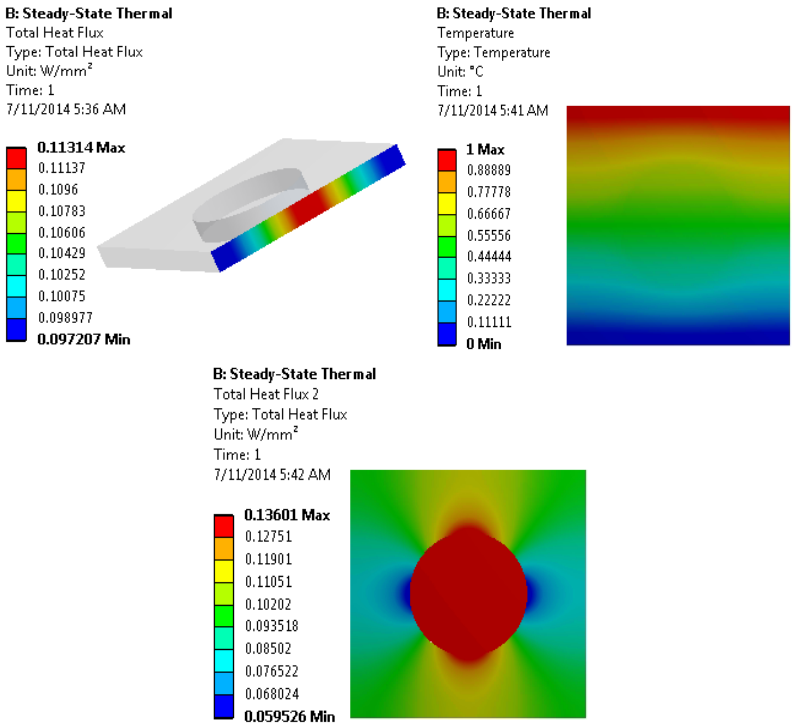

Figure 6-6 Heat flux contour and temperature distribution for perfect contact

6.6.2 Contribution of Thermal Resistance

In the next example, the contribution of thermal resistance was considered and for demonstration purpose the resistance of R=100 mm^2-K/ W applied between TSV and Copper. See Table 6-2 and Figure 6-5 for the results.

Table 6-3 Comparison of effective thermal conductivity between analytical and FEA with resistance

Number of Terms (J_{max})	2	3	4	5	6	7
$K_{eff}(\frac{W}{m.K})$, Analytical	159.035	131.902	126.040	124.642	124.051	123.69 ✓
$K_{eff}\left(\frac{W}{m.K}\right)$, FEA (Grid independent) #elements~1.2Million	123.701	123.701	123.701	123.701	123.701	123.701 ✓
%Error						0.00889%

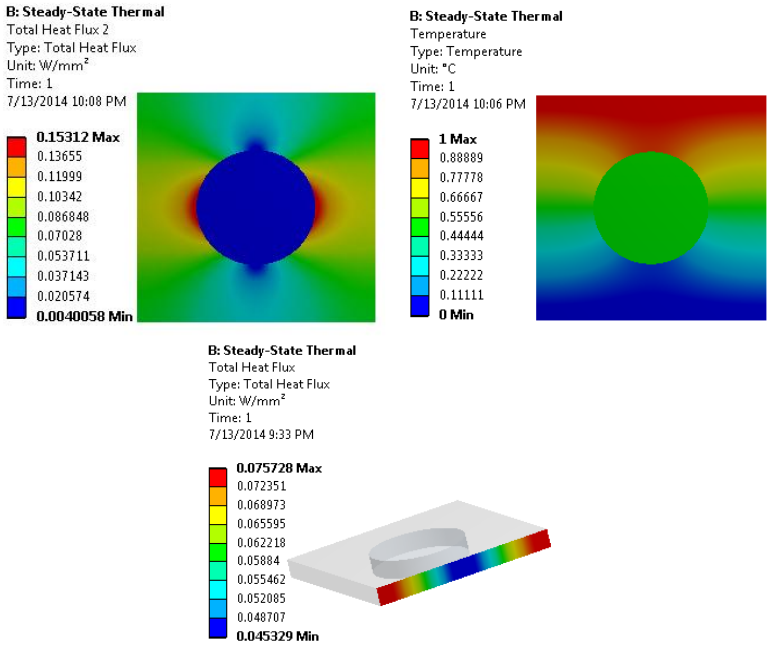

Figure 6-7 Heat flux contour and temperature distribution with contact resistance

Consideration is given to a layer of matrix that consists of many inclusions as shown in Figure 6-6 and the effective thermal conductivity is the unknown sought for. This could be considered a die layer with TSV interconnects and subjected to a known temperature boundary conditions. Thermal conductivity of silicon and copper is the same as the one discussed in the first example. However, in this example the diameters of TSVs' are variable and ranging from 0.006(mm) to 0.192(mm). This exercise was carried out with or without contact resistance. The results are depicted in Figures 6-7(a, b, c) and Figures 6-8(a, b, c) for perfect contact and with contact resistance respectively. The contact resistance of R=100 mm^2-K/ W used when computing the case with thermal resistance. Also, the results for variation in TSV's diameter versus effective thermal conductivity for both cases can be seen on Figure 6-9 and Figure 6-10.

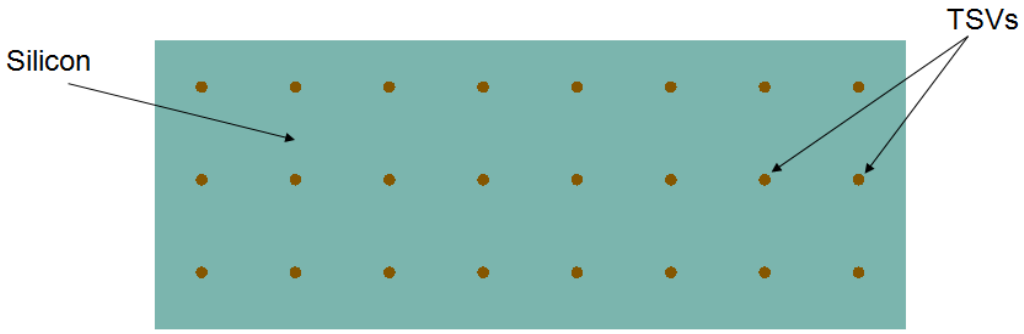

Figure 6-8 A Silicon die layer with TSV inclusions

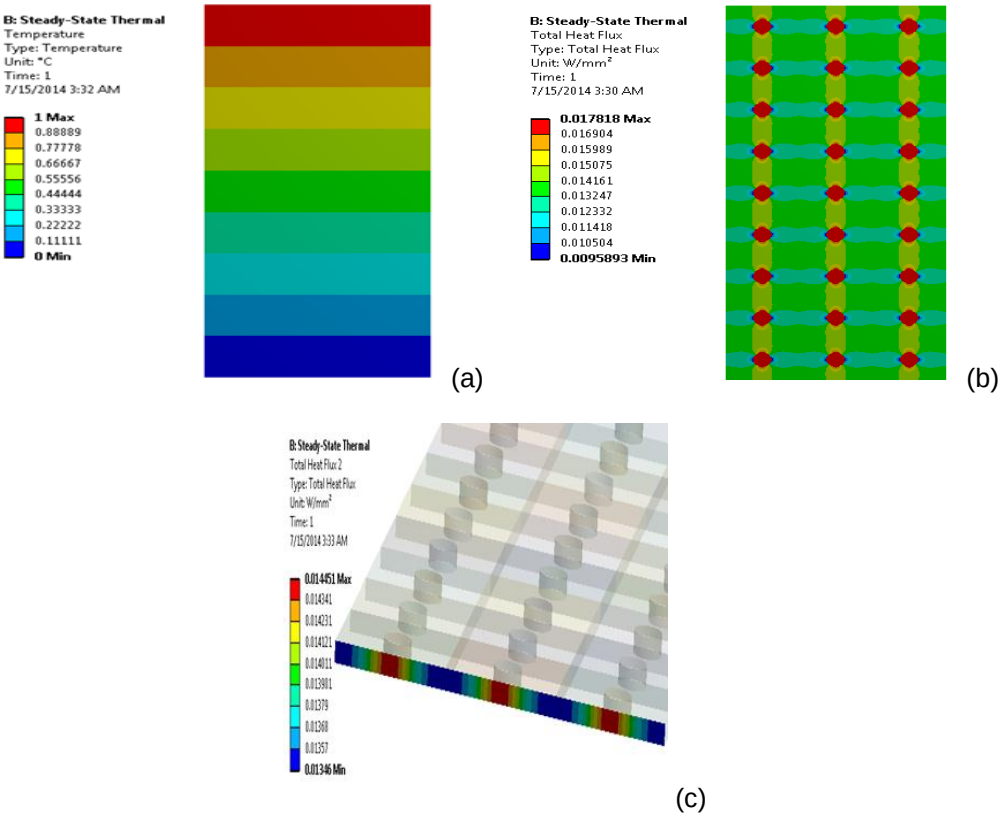

Figure 6-9 Temperature contour for multiple TSVs embedded in silicon without contact resistance, (b) total heat flux contour for multiple TSVs embedded in silicon without contact resistance, and (c) total heat flux contour at the bottom wall without contact resistance

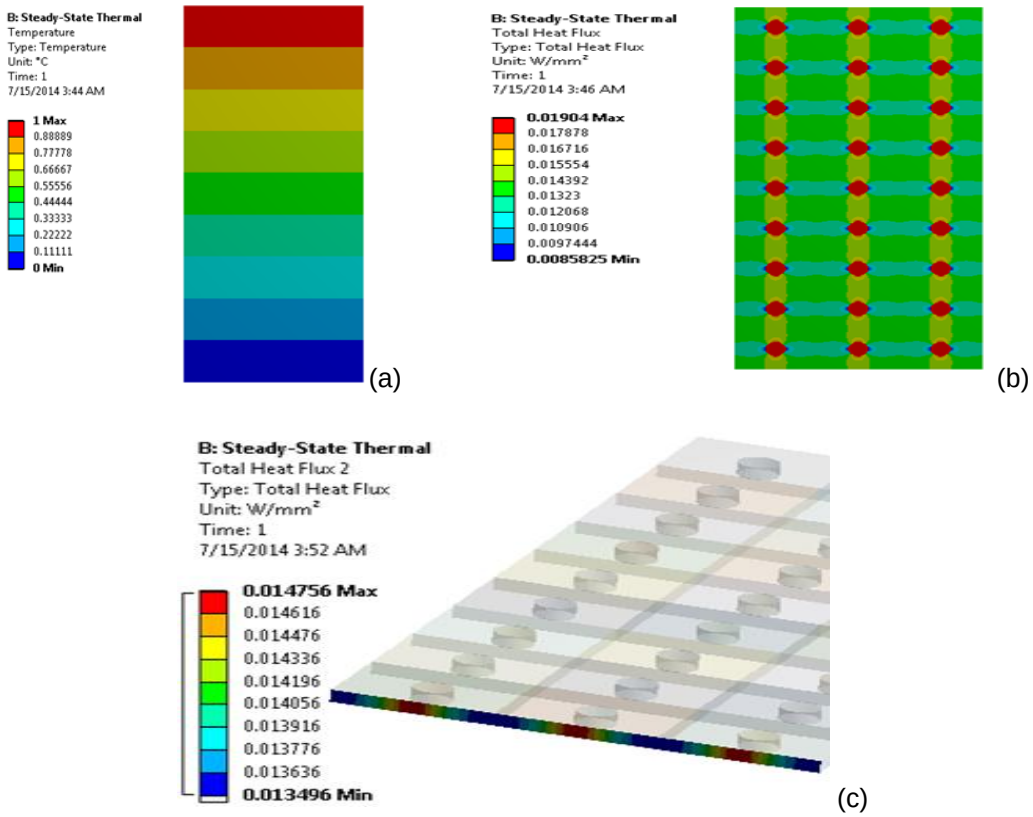

Figure 6-10 (a): Temperature contour for multiple TSVs embedded in silicon with contact resistance, (b) total heat flux contour for multiple TSVs embedded in silicon with contact resistance, and (c): total heat flux contour at the bottom wall with contact resistance

Table 6-4 Analytical and FEA comparison of K_{eff} with perfect contact

Number of Terms (J_{max})	7
$K_{eff}(\frac{W}{m.K})$, Analytical	189.128
$K_{eff}\left(\frac{W}{m.K}\right)$, FEA (Grid independent) #elements~1.2Million	189.385
%Error	0.13%

Table 6-5 Analytical and FEA comparison of K_{eff} with contact resistance

Number of Terms (J_{max})	7
$K_{eff}(\frac{W}{m.K})$, Analytical	187.087
$K_{eff}\left(\frac{W}{m.K}\right)$, FEA (Grid independent) #elements~1.2Million	187.271
%Error	0.098%

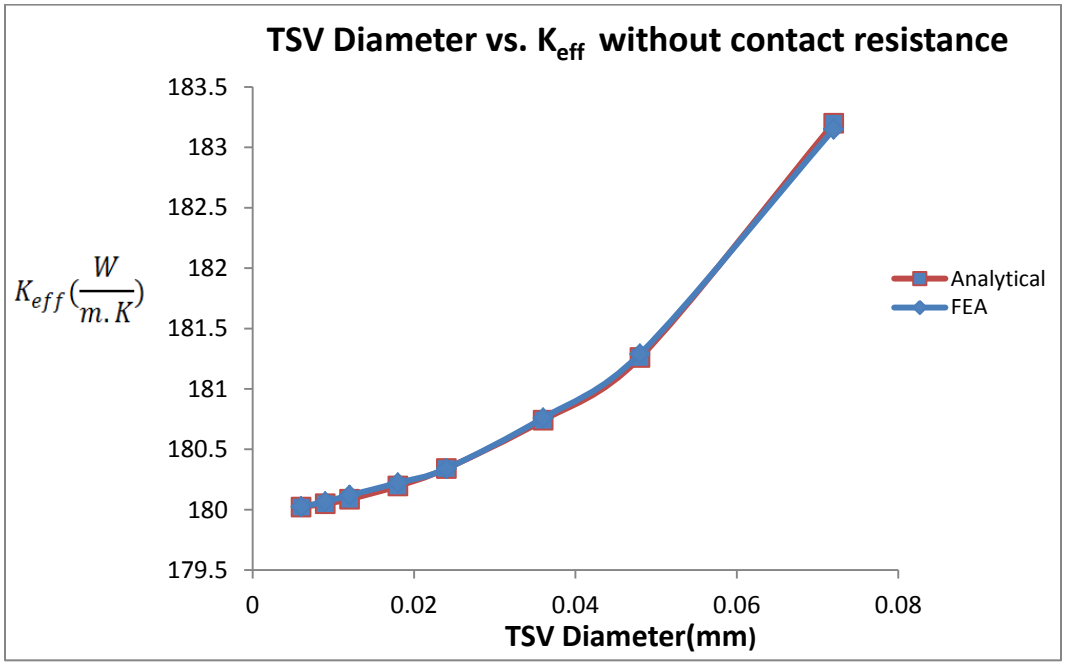

Figure 6-11 Variation of TSV's diameter vs. K_{eff} for perfect contact in the silicon layer

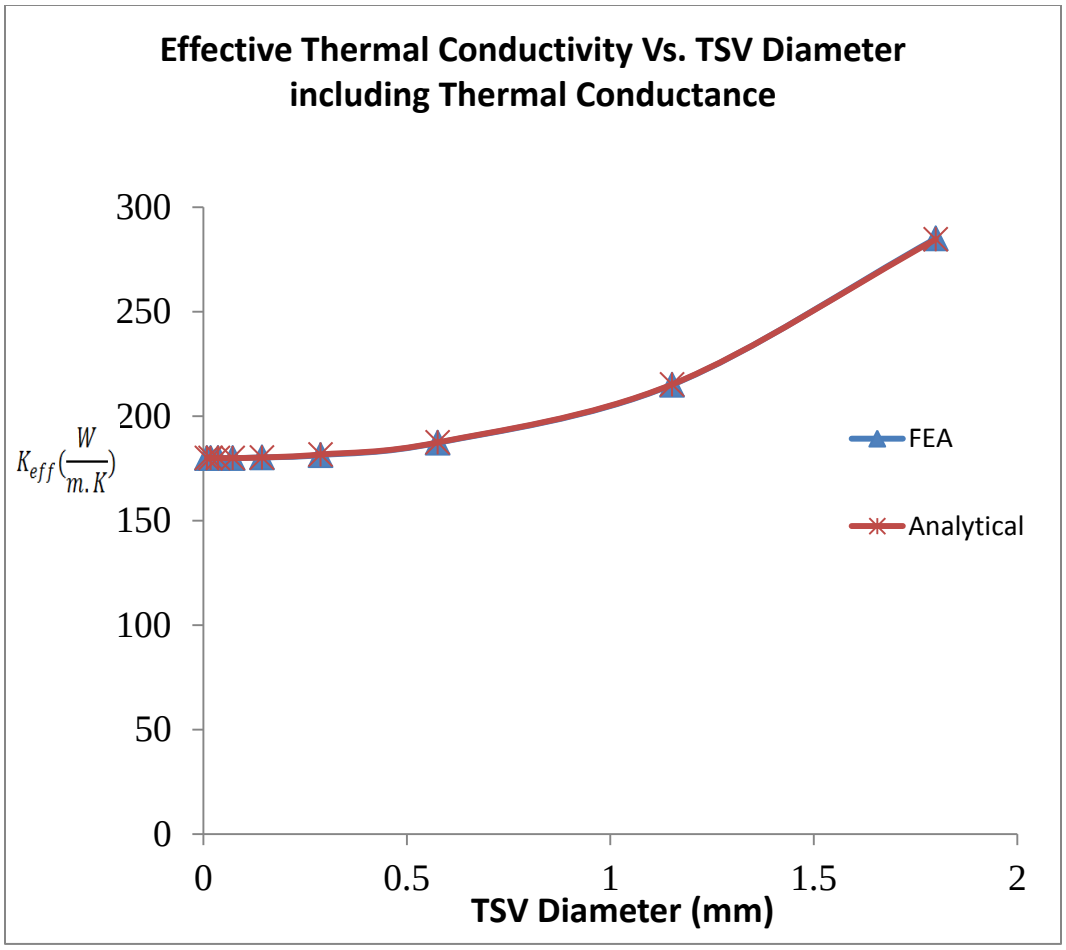

Figure 6-12 Variation of TSV's diameter vs. K_{eff} with contact resistance in silicon layer

6.7 Comments/Discussions:

The analysis shows the effectiveness of the analytically obtained results is in good agreement with Finite Element Analysis. The Galerkin-based integral approximation is very accurate and fast-converging compared to FEA. Depending on the accuracy required for specific application, the convergence of fewer terms is fairly quick and in a matter of minutes. The numerical integrations are generally slow to solve, however, it was noticed for the smaller number of terms $J_{max}<8$ that the convergence is very quick.

Changes in the analytical results are in the 4^{th} and 5^{th} decimal places for greater number of terms.

The results from Figure 6-9 and Figure 6-10 reveals that as the diameter of the TSVs gets larger, their impact in overall heat transfer would be higher. However, for actual size of the TSVs in the 1-5μm range, the effect of thermal impact to overall temperature distribution is negligible, particularly if the contact resistance is relatively small.

Chapter 7

Conclusions and Comments

Analytical methods for finding temperature solutions of steady-state heat conduction in multi-layer bodies for 3D electronic packaging were presented. Problems of this type are encountered in many engineering disciplines and different industries. As cooling problems related to device protection have emerged in many electronic devices, these analytical heat conduction solutions become an important verification tool for numerically-based solutions for thermal design engineers. Analytical solutions can provide insight into the behavior of temperature and heat flux distribution in many engineering fields from mechanical and aerospace to civil engineering. An accurate steady-state temperature solution in multi-layer bodies is an invaluable tool for determination of heat spreaders in electronic cooling applications. This includes isotropic or orthotropic multi-layer, with or without contact conductance. Steady-state solutions can provide relatively accurate results away from boundary conditions and it can improve computation time for transient problems by imposing the non-homogeneous boundary conditions from transient to steady-state solution.

During the course of this study, the semi-analytical or analytical solutions were validated with the FEM solutions to check for consistency in the solution profiles. It was also observed that the analytical and the purely numerical solutions were in excellent agreement with each other. So, a question that surfaces is why use a semi-analytical method, when a reasonable solution can be obtained using FEM? Firstly, for a heterogeneous system that contains multiple inclusions, purely numerical methods can turn out to be a computationally-expensive enterprise. In addition, if the heterogeneous medium contains very small inclusions, finite element meshing can be a bottleneck.

However, the semi-analytical approach can be conveniently extended to solve multiple inclusion problems as well as limiting cases, wherein the size of the inclusions is infinitesimally small. For example, it was observed that for very small diameter TSVs, the number of mesh increased by 40 times in comparison to a larger one. This could be very time consuming when one uses an FEA approach.

The ease of variations in the Galerkin-based functions is such that many configurations can be evaluated in a relatively short time frame. The effective thermophysical properties can be changed readily without grid-independent evaluation to ensure the stability criteria, as one must do when employing finite element method.

As was mentioned earlier, many industries other than electronics can benefit from this mathematically developed procedure. This procedure can be used in fluid applications by minor modification to allow for fluid to take place as opposed to solid. The application for this could be in fluid cooling channels in the aerospace industry for the protection of composite material skin of high-temperature, high-speed air vehicles, or infrared signal suppression on military vehicles and many more.

The material presented in this research paves the way for solving far more complex geometries and boundary conditions than is possible utilizing the finite element method, in a shorter time frame, and without the high computational costs associated with the FEA. These methods are also effectively translatable to other applications, increasing their utility.

Appendix A

Derivation of Orthogonality Condition in the Lateral Direction

The development of the orthogonality condition begins with the relations

$$-\gamma_m^2 k_y(y) Y_m(y) = \frac{\partial}{\partial y}\left[k_y(y) \frac{\partial Y_m(y)}{\partial y} \right] \tag{A1}$$

and

$$-\gamma_n^2 k_y(y) Y_n(y) = \frac{\partial}{\partial y}\left[k_y(y) \frac{\partial Y_n(y)}{\partial y} \right] \tag{A2}$$

After multiplying the first relation by $Y_n(y)$ and the second relation by $Y_m(y)$, we subtract the resulting equations and integrate both sides over *y* from 0 to *b*:

$$\int_{y=0}^{b} (\gamma_n^2 - \gamma_m^2) k_y(y) Y_m(y) Y_n(y) dy$$

$$= \sum_{j=1}^{N} \int_{y=b_{j-1}}^{b_j} \frac{\partial}{\partial y}\left\{ Y_{j,m}(y)\left[k_{j,y}(y) \frac{\partial Y_{j,m}(y)}{\partial y} \right] \right.$$

$$\left. - Y_{j,m}(y)\left[k_{j,y}(y) \frac{\partial Y_n(y)}{\partial y} \right] \right\} dy \tag{A3}$$

After integrating the right side, we can write this equation as

$$\int_{y=0}^{b} (\gamma_n^2 - \gamma_m^2) k_y(y) Y_m(y) Y_n(y) dy$$

$$= \sum_{j=1}^{N} \left\{ Y_{j,m}(y)\left[k_{j,y}(y) \frac{\partial Y_{j,m}(y)}{\partial y} \right] - Y_{j,m}(y)\left[k_{j,y}(y) \frac{\partial Y_n(y)}{\partial y} \right] \right\} \Bigg|_{b_{j-1}}^{b_j} \tag{A4}$$

Clearly, because of the external boundary conditions, the right side vanishes when *j* = 1 and $y = b_0 = 0$. Additionally, it vanishes when *j* = *N* and $y = b_N = b$. Moreover, one can show that these quantities on the right side have the same values over the contact surfaces but have the opposite signs.

For layer *j*, using the compatibility conditions for the upper limit, we can write the following term as

$$\left\{ Y_{j,n}(y)\left[k_{j,y}(y)\frac{\partial Y_{j,m}(y)}{\partial y} \right] - Y_{j,m}(y)\left[k_{j,y}(y)\frac{\partial Y_{j,n}(y)}{\partial y} \right] \right\}\Bigg|_{y=b_j}$$
$$= Y_{j,n}(b_j)\left[Y_{j+1,m}(b_j) - Y_{j,m}(b_j) \right] / R_j - Y_{j,m}(b_j)\left[Y_{j+1,n}(b_j) - Y_{j,n}(b_j) \right] / R_j$$
$$= \left[Y_{j,n}(b_j)Y_{j+1,m}(b_j) - Y_{j,m}(b_j)Y_{j+1,n}(b_j) \right] / R_j \tag{A5}$$

This process is repeated for the lower limit for layer *j*+1 to obtain

$$\left\{ Y_{j+1,n}(y)\left[k_{j+1,y}(y)\frac{\partial Y_{j+1,m}(y)}{\partial y} \right] - Y_{j+1,m}(y)\left[k_{j+1,y}(y)\frac{\partial Y_{j+1,n}(y)}{\partial y} \right] \right\}\Bigg|_{y=b_j}$$
$$= Y_{j+1,n}(b_j)\left[Y_{j+1,m}(b_j) - Y_{j,m}(b_j) \right] / R_j - Y_{j+1,m}(b_j)\left[Y_{j+1,n}(b_j) - Y_{j,n}(b_j) \right] / R_j$$
$$= \left[Y_{j,n}(b_j)Y_{j+1,m}(b_j) - Y_{j,m}(b_j)Y_{j+1,n}(b_j) \right] / R_j \tag{A6}$$

These two values are the same but have opposite signs at $y = b_j$ within the orthogonality relation. Therefore, the orthogonality for the y-direction is

$$(\gamma_n^2 - \gamma_m^2)\int_{y=0}^{b} k_y(y)Y_m(y)Y_n(y)dy = 0 \tag{A7}$$

This can be written as

$$\sum_{j=1}^{N} \int_{b_{j-1}}^{b_j} k_y(y)Y_{j,m}(y)Y_{j,n}(y)dy = \begin{cases} 0 & \text{when } m \neq n \\ N_m & \text{when } m = n \end{cases} \tag{A8}$$

where

$$N_m = \sum_{j=1}^{N} \int_{b_{j-1}}^{b_j} k_y(y)\left[Y_{j,m}(y) \right]^2 dy \tag{A9}$$

Appendix B

Derivation of Auxiliary Function H

$$f_{ej} = f_{mj} + U + \emptyset_e H$$ For inclusion

$$f_{je} = f_{jm} - \left(\frac{K_m}{C}\right)\left(\frac{\partial f_{mj}}{\partial n}\right)$$ jump condition

$$K_m \frac{\partial f_{mj}}{\partial n} = K_e \frac{\partial f_{ej}}{\partial n}$$ Interface flux compatibility

$$K_m \frac{\partial f_{mj}}{\partial n} = K_e \frac{\partial [f_{mj} + U + \emptyset_e H]}{\partial n}$$

$$(-K_m/K_e)\frac{\partial f_{mj}}{\partial n} = -\frac{\partial f_{mj}}{\partial n} - \frac{\partial U}{\partial n} - H\frac{\partial \emptyset_e}{\partial n}$$

$$H = \frac{\left(\frac{K_m}{K_e} - 1\right)\frac{\partial f_{mj}}{\partial n} - \frac{\partial U}{\partial n}}{\frac{\partial \emptyset_e}{\partial n}}$$

$$\emptyset_e = r^2 - (x - h_i)^2 - y^2$$

$$\frac{\partial f_{mj}}{\partial n} = |\nabla f_{mj} . \nabla \emptyset|_{\emptyset=0}$$

$$\boxed{H_e = -\frac{\left[\left(\frac{K_m}{K_e} - 1\right)\nabla f_{mj} . \nabla \emptyset_e\right]_{\emptyset_e=0}}{(\nabla \emptyset_e . \nabla \emptyset_e)_{\emptyset_e=0}}}$$

References

[1] Kuroda Lab., Keio University from

http://www.kuroda.elec.keio.ac.jp/publication/paper_and_lecture/2009 html

[2] Iwata, A. and Yokoyama, S., 2008, “Problems and Prospect of 3D Integration using Wireless and Optical Interconnection Technologies,” IEICE Technical Paper, 108(140) ICD2008-53, pp 89-94.

[3] Hirose, Z., Yamanishi, M., Osaka, Y., AE, T., Ichikawa, T., Yoshida, N. and Suemune, I., 1986, “Shared Memory Integrated Device of Three-Dimensional Photo Coupling,” Japanese Patent JP61003450

[4] Yamada, T., “Laminated Chip” Japanese Pat. Publ. No. 2010-016238

[5] Bonkohara, M., Takahashi, K. and Ishino, M., 2005, “Trends and Opportunities of System-in-a-Package and Three-Dimensional Integration,” Invited paper, *IEICE TRANSACTIONS on Electronics*, 88(10), pp. 37-49

[6] Knickerbocker, J. U., Andry, P. S., Buchwalter, L. P., Deutsch, A., Horton, R. R., Jenkins, K. A., Kwark, Y. H., McVicker, G., Patel, C. S., Polastre, R. J., Schuster, C. D., Sharma, A., Sri-Jayantha, S. M., Surovic, C. W., Tsang, C. K., Webb, B. C., Wright, S. L., McKnight, S. R., Sprogis, E. J. and Dang, B., 2005, “Development of Next-Generation System-on-Package (SOP) Technology Based on Silicon Carriers with Fine-Pitch Chip Interconnection,” IBM J Res. & Dev., 49(4-5), pp. 725-753.

[7] Ramm, P., 2007, “European Activities in 3D System Integration - The e-Cubes Project,” *12th Annual Pan Pacific Microelectronics Symposium*, Maui, Hawaii

[8] “Toshiba to enhance competitiveness in image sensor business by bringing manufacturing of CMOS camera modules for mobile phones in-house,” October 1, 2007,

Toshiba Corp. press release from
http://www.toshiba.co.jp/about/press/2007_10/pr0101.htm
[9] Denda, S., 2007, “The State of Development of Through Silicon Via for Three Dimensional Silicon Chip Stacking,” *J Surface Finishing Soc. Jpn.*, 58(12), pp. 712-718
[10] Dowding, K. J., Beck, J. V. and Blackwell, B. F., 1996, “Estimation of Directional-Dependent Thermal Properties in a Carbon–Carbon Composite,” Int. J. Heat Mass Trans. 39(15), pp. 3157–3164.
[11] Aviles-Ramos, C., Haji-Sheikh, A. and Beck, J.V., 1998, “Exact Solution of Heat Conduction in Composites and Application to Inverse Problems,” ASME J. Heat Transf., 120(3), pp. 592–599.
[12] Haji-Sheikh, A. and Beck, J. V., 2000, “An Efficient Method of Computing Eigenvalues in Heat Conduction,” Numer. Heat Transfer, B 38(2), pp. 133–156.
[13] Beck, J. V., Cole, K., Haji-Sheikh, A. and Litkouhi, B., 1992, “Heat Conduction Using Green’s Functions,” Taylor & Francis, Washington DC.
[14] Dowding, K. J., Beck, J. V. and Blackwell, B. F., 1996, “Estimation of Directional-Dependent Thermal Properties in a Carbon–Carbon Composite,” Int. J. Heat Mass Trans., 39(16), pp. 3157–3164.
[15] McMasters, R. L., Dowding, K. J., Beck, J. V. and Yen, D. H. Y., 2002, “Methodology to Generate Accurate Solutions for Verification in Transient Three-Dimensional Heat Conduction,” Numer. Heat Transfer (B), 41(6), pp. 521–541.
[16] Cole, K. D. and Yen, D. H. Y., 2001, “Green’s Functions, Temperature and Heat Flux in a Rectangle,” Int. J. Heat Mass Trans, 44(20), 3883–3894.
[17] Yen, D. H. Y., Beck, J. V., McMasters, R. L. and Amos, D. E., 2002, “Solution of an Initial-Boundary Value Problem for Heat Conduction in a Parallelepiped by Time Partitioning,” Int. J. Heat Mass Trans. 45(21), pp. 4267–4279.

[18] Haji-Sheikh, A., Beck, J. V. and Agonafer, D., 2003, “Steady State Heat Conduction in Multi-Layer Bodies,” Int. J. Heat Mass Trans., 46(13), pp. 2363-2379.

[19] Ghalambor, S., Agonafer, D. and Haji-Sheikh, A., 2013, “Analytical Thermal Solution to a Nonuniformly Powered Stack Package with Contact Resistance”; J. Heat Trans. 135(11), 111015, (9 pages).

[20] Kaisare, A., Agonafer, D., Haji-Sheikh, A., Chrysler, G. and Mahajan, R., 2009, “Development of an Analytical Model to a Temperature Distribution of First Level Package with a Non-Uniformly Powered Die,” J. Electron. Packag., 31, 011005-(1-7).

[21] Yovanovich, M. M., Tien, C. H. and Schneider, G. E., 1980, “General Solution of Constriction Resistance within a Compound Disk,” Heat Transfer, Thermal Control and Heat Pipes, *AIAA Progress in Astronautics and Aeronautics*, 70.

[22] Zuzovski, M. and Brenner, H., 1977, "Effective Conductivities of Composite Materials Composed of Cubic Arrangements of Spherical Particles Embedded in an Isotropic Matrix," *Zeitschrift fur angewandte Mathematik und Physik,* 28(6), pp. 979-992.

[23] Sangani, A. S. and Acrivos, A., 1983, "The Effective Conductivity of a Periodic Array of Spheres," *Proc. R. Soc. Lond. A*, 386, pp. 263-275.

[24] Ballah, T. K., Middya, T. R. and Basu, A. N., 1988, "A Multiple Scattering Theoretical Approach to the Effective Thermal Conductivity of Disordered Solids and Its Dependence on Phase Geometry," J Phys. D: Appl. Phys., 21(4), pp. 567-573.

[25] Hatta, H. and Taya, M., 1985, "Effective Thermal Conductivity of a Misoriented Short Fiber Composite," J. Appl. Phys., 58(7), pp. 2478-2486.

[26] Hashin, Z., 1983, "Analysis of Composite Materials - A Survey,” J. Appl. Mech., 50(3), pp. 481-505.

[27] Lee, Y. M. and Haji-Sheikh, A., 1991,"Temperature Field in Heterogeneous Bodies: A Non-Orthogonal Solution," *Proceedings of the National Heat Transfer Conference*, eds.. Imber, M. and Yovanovich, M. M., ASME HTD, 173, Fundamentals of Conduction, pp.1-9

[28] Tittle, C. W., 1965, "Boundary Value Problems in Composite Media," J. Appl. Phys., 36, pp. 1486-1488.

[29] Padovan, J., 1974, "Generalized Sturm-Liouville Procedure for Composite Domain Anisotropic Transient Heat Conduction Problems," AIAA J.,12(8), pp. 1158-1160.

[30] Salt, H., 1983, "Transient Conduction in a Two-Dimensional composite Slab-I. Theoretical Development of Temperature Modes," Int. J. Heat Mass Tran., 26(11), pp. 1611-1616.

[31] Salt, H., 1983, "Transient Conduction in Two-Dimensional Composite Slab-II. Physical Interpretation of Temperature Modes," Int. J. Heat Mass Tran., 26(11), pp. 1617-1623.

[32] Mikhailov, M. D. and Ozisik, M. N., 1986, "Transient Conduction in a Three-Dimensional Composite Slab," Int. J. Heat Mass Tran., 29(2), pp. 340-342.

[33] de Monte, F., 2000, "Transient Heat Conduction in One-Dimensional Composite Slab. A 'Natural' Analytical Approach," Int. J. Heat Mass Tran., 43(19), pp. 3607-3616.

[34] Aviles-Ramos, C., Haji-Sheikh, A. and Beck, J. V., 1998, "Exact Solution of Heat Conduction in Composites and Application to Inverse Problems," J. Heat Trans., 120(3), pp. 592-599.

[35] Haji-Sheikh, A. and Beck, J. V., 2002, "Temperature Solution in Multi-Dimensional Multi-Layer Bodies," Int. J. Heat Mass Tran., 45(9), pp. 1865-1877.

[36] Haji-Sheikh, A., Beck, J. V. and Agonafer, D., 2003, "Steady State Heat Conduction in Multi-Layer Bodies," Int. J. Heat Mass Tran., 46(13), pp. 2363-2379.

[37] Haji-Sheikh, A. and Beck, J. V., 2000, “An Efficient Method of Computing Eigenvalues in Heat Conduction,” Numer. Heat Transfer (B), 38(2), pp. 133-156.

[38] Ghalambor, S., Agonafer, D. and Haji-Sheikh, A., 2012, “Determination of Steady State Temperature in a Two-Layer Body with Different Form Factors,” Int. J. Heat Mass Tran., 55(25-26), pp. 7434-7443.

[39] Kaisare, A., Agonafer, D., Haji-Sheikh, A., Chrysler, G. and Mahajan, R., 2009, “Development of an Analytical Model to a Temperature Distribution of First Level Package with a Non-Uniformly Powered Die,” J. Electron. Packag., 31, 011005-(1-7).

[40] de Monte, F., 2004, “Traverse Eigenproblem of Steady-State Heat Conduction for Multi-Dimensional Two-Layer Slabs with Automatic Computation of Eigenvalues,” Int. J. Heat Mass Tran., 47, pp. 191-201.

[41] Tittle, C. W., 1965, “Boundary Value Problems in Composite Media,” J. Appl. Phys., 36, pp. 1486-1488.

[42] de Monte, F., 2000, “Transient Heat Conduction in One-Dimensional Composite Slab. A ‘Natural’ Analytical Approach,” Int. J. Heat Mass Tran., 43(19), pp. 3607-3616.

[43] Haji-Sheikh, A. and Beck, J. V., 2002, “Temperature Solution in Multi-dimensional Multi-layer Bodies,” Int. J. Heat Mass Tran., 45(9), pp. 1865-1877.

[44] Aviles-Ramos, C., Haji-Sheikh, A. and Beck J. V., 1998, “Exact Solution of Heat Conduction in Composites and Application to Inverse Problems,” J. Heat Trans., 120(3), pp. 592-599.

[45] Goh, T.J., 2002, “Thermal Methodology for Evaluating the Performance of Microelectronic Devices with Nonuniform Power Dissipation,” *4th Electronics Packaging Technology Conference*, pp. 312-317.

[46] Sikka, K. K., 2005, “An Analytical Temperature Prediction Method for a Chip Power Map,” *Semiconductor Thermal Measurement and Management Symposium*, pp. 161-166.

[47] June, M.S. and Sikka, K. K., 2002, “Using Cap-Integral Standoffs to Reduce Chip Hot-Spot Temperatures in Electronic Packages,” Thermal and Thermomechanical Phenomena in Electronic Systems, pp. 173-178.

[48] Zhiping, Y., Yergeau, D., Dutton, R. W., Nakagawa, S. and Deeney, J., 2001, “Fast Placement-Dependent Full Chip Thermal Simulation,” *VLSI Technology, Systems, and Applications*, pp. 249-252.

[49]. Mahajan, R., Nair, R. and Wakharkar, V., 2002, “Emerging Directions for Packaging Technologies,” Intel Technol. J., 6(2), pp. 62.

[50] Lee, S., Song, S., Au, V. and Moran, K. P., 1995, “Constriction/Spreading Resistance Model for Electronic Packaging,” *Proceedings of the 4th ASME/JSME Thermal Engineering Joint Conference*, 4, pp. 199-206.

[51] Kennedy, D. P., 1960, “Spreading Resistance in Cylindrical Semiconductor Devices,” J. Appl. Phys., 31, pp. 1490-1497.

[52] Lee, S., Song, S., Au, V. and Moran, K. P., 1995, “Constriction/Spreading Resistance Model for Electronic Packaging,” *Proceedings of the 4th ASME/JSME Thermal Engineering Joint Conference*, 4, pp. 199-206.

[53] Kaisare, A., Agonafer, D., Haji-Sheikh, A., Chrysler, G. and Mahajan, R., 2009, “Development of an Analytical Model to a Temperature Distribution of First Level Package with a Non-Uniformly Powered Die,” J. Electron. Packag., 131(1), 011005-(1-7).

[54] Beck, J. V., Blackwell, B. and St Clair Jr., C., 1985, *Inverse Heat Conduction: Ill-Posed Problems*, John Wiley, New York, NY.

[55] Beck, J. V., Blackwell, B. and Haji-Sheikh, A., 1996, “Comparison of Some Inverse Heat Conduction Methods Using Experimental Data,” Int. J. Heat Mass Tran., 39(17), pp. 3649-3657.

[56] Ling, X., Cheruturi, H. P. and Keanini, R. G., 2005, “A Modified Sequential Function Specification Finite Element-Based Method for Parabolic Inverse Heat Conduction Problems,” Comput. Mech., 36(2), pp. 117-128.

[57] Murio, D. A. and Beck, J. V., 1988, “Combined Function Specification-Regularization Procedure for Solution of Inverse Heat Conduction Problems,” AIAA J., 24(1), pp. 180-185.

[58] de Monte, F., Beck, J. V. and Amos, D. E., 2011, “A Heat-Flux Based ‘‘Building Block’’ Approach for Solving Heat Conduction Problems,” Int. J. Heat Mass Tran., 54(13-14), pp. 2789-2800.

[59] Haji-Sheikh, Ghalambor, A. S. and Agonafer, D., 2012, “Estimation of Temperature between Plates of Different Footprints by an Iterative Approach,” Inverse Probl. Sci. Eng., 20(6), pp. 841-855.

[60] Cole, K. D., Beck, J. V., Haji-Sheikh, A. and Litkouhi, B., 2011, *Heat Conduction Using Green's Functions*, 2nd ed., CRC Press, Taylor & Francis, Boca Raton, Florida.

[61] Beck, J. V., 2011, “Transient Three-Dimensional Heat Conduction Problems with Partial Heating,” Int. J. Heat Mass Tran., 54(11-12) 2479-2489.

[62] Goh, T. J., 2002, “Thermal Methodology for Evaluating the Performance of Microelectronic Devices with Nonuniform Power Dissipation,” *4th Electronics Packaging Technology Conference*, pp. 312-317.

[63] Sikka, K. K., 2005, “An Analytical Temperature Prediction Method for a Chip Power Map,” *Semiconductor Thermal Measurement and Management Symposium*, pp. 161-166.

[64] June, M. S. and Sikka, K. K., 2002, “Using Cap-Integral Standoffs to Reduce Chip Hot-Spot Temperatures in Electronic Packages,” *Thermal and Thermomechanical Phenomena in Electronic Systems*, pp. 173-178.

[65] Zhiping, Y., Yergeau, D., Dutton, R. W., Nakagawa, S. and Deeney, J., 2001, “Fast Placement-Dependent Full Chip Thermal Simulation,” *VLSI Technology, Systems, and Applications*, pp. 249-252.

[66]. Mahajan, R., Nair, R. and Wakharkar, V., 2002, “Emerging Directions for Packaging Technologies,” Intel Technol. J., 6(2), p. 62.

[67] Kaisare, A., Agonafer, D., Haji-Sheikh, A., Chrysler, G. and Mahajan, R., 2009, “Development of an Analytical Model to a Temperature Distribution of First Level Package with a Non-Uniformly Powered Die,” J. Electron. Packaging, 31(1), pp. 011005-(1-7).

[68] Beck, J. V., Blackwell, B. and St Clair Jr., C., 1985, *Inverse Heat Conduction: Ill-Posed Problems*, John Wiley, New York, NY.

[69] Alifanov, O. M. and Nenarokomov, A.V., 1999, “Three-Dimensional Boundary Inverse Heat Conduction Problem for Regular Coordinate Systems,” Inverse Probl. in Eng., 7(4), pp. 335-362.

[70] Alifanov, O. M. and Nenarokomov, A.V., 2001, “Boundary, Inverse Heat Conduction Problem: Algorithm and Error Analysis,” Inverse Probl. Eng., 9(6), pp. 619-644.

[71] Silva, P. M. P., Orlande, H. R. B., Colaço, M. J., Shiakolas, P. S. and Dulikravich, G. S., 2007, “Identification and Design of Source Term in a Two-Region Heat Conduction Problem,” Inverse Probl. Sci. En., 15(7), pp. 661-677.

[72] Beck, J. V., Blackwell, B. and Haji-Sheikh, A., 1996, “Comparison of Some Inverse Heat Conduction Methods Using Experimental Data,” Int. J. Heat Mass Tran., 39(17), pp. 3649-3657.

[73] Beck, J. V. and Murio, D. A., 1986, “Combined Function Specification-Regularization Procedure for Solution of Inverse Heat Conduction Problems,” AIAA J., 24(1), pp. 180-185.

[74] Scheuing, J. E. and Tortorelli, D. A., 1996, “Inverse Heat Conduction Problem Solutions via Second-Order Design Sensitivities and Newton's Method,” Inverse Probl. Eng., 2(3), pp. 227-262.

[75] Hào, D. N. and Reinhardt, H.-J., 1998, “Gradient Methods for Inverse Heat Conduction Problems,” Inverse Probl. Eng., 6(3), pp. 177-211.

[76] Zhou, D. and Wei, T., 2008, “The Method of Fundamental Solutions for Solving a Cauchy Problem of Laplace's Equation in a Multi-Connected Domain,” Inverse Probl. Sci. En., 16(3), pp. 389-411.

[77] Ling, X., Cheruturi, H. P. and Keanini, R. G., 2005, “A Modified Sequential Function Specification Finite Element-Based Method for Parabolic Inverse Heat Conduction Problems,” Comput. Mech., 36(2), pp. 117-128.

[78] Haji-Sheikh, A., Beck, J. V. and Agonafer, D., 2003, “Steady State Heat Conduction in Multi-Layer Bodies,” Int. J. Heat Mass Tran., 46(13), pp. 2363-2379.

Biographical Information

The author has completed his Ph.D. in mechanical engineering from the University of Texas at Arlington. He received his M.Sc. from the University of Texas at San Antonio and his B.Sc. from Ryerson University in Canada.

His research topics include, but are not limited to, analytical and numerical solutions of heat transfer to multi-layer bodies. His research includes cooling solutions to electronic 3D stacks.

The author has worked on numerous FEA/CFD projects related to thermal cycling and structural integrity of multi-layer stack packages.

He wishes to continue his research in the area of heat and mass transfer and to develop cooling techniques for 3D integrated circuits in the semi-conductor industry.